Synthesis and characterization of rGO/Ag nanocomposite using cinnamon plant bark extract for methylene blue dye removal from aqueous solution

Bekele Yirga Mamo

A Thesis Submitted to Department of Applied Chemistry
School of Applied Natural Science
In Partial Fulfillment of the Requirement for the Master of Science Degree in Applied Chemistry (Inorganic Chemistry)

Office of Graduate Studies
Adama Science and Technology University

June 2022

Adama, Ethiopia

Synthesis and characterization of rGO/Ag nanocomposite using cinnamon plant bark extract for methylene blue dye removal from aqueous solution

Bekele Yirga Mamo

Advisor;- Dr. Tegene Desalegn (Ph.D.)

A Thesis Submitted to Department of Applied Chemistry
School of Applied Natural Science
In Partial Fulfillment of the Requirement for the Master of Science Degree in Applied Chemistry (Inorganic Chemistry)

Office of Graduate Studies
Adama Science and Technology University

June 2022

Adama, Ethiopia

Declaration

I hereby declare that this Master Thesis entitled ‘‘**Synthesis and characterization of rGO/Ag nanocomposite using cinnamon plant bark extract for methylene blue dye removal from aqueous solution**” is my original work. That is, it has not been submitted for the award of any academic degree, diploma, or certificate in any other university. All sources of materials that are used for this thesis have been duly acknowledged through citation.

Name of Student	Signature	Date

Recommendation

I, the advisor of this thesis, hereby certify that I have read the thesis entitled "**Synthesis and characterization of rGO/Ag nanocomposite using cinnamon plant bark extract for methylene blue dye removal from aqueous solution**" prepared under my guidance by Bekele Yirga Mamo submitted in partial fulfillment of the requirements for the degree of Master of Science in Applied Chemistry (Inorganic Chemistry).

Therefore, I recommend the submission of the thesis to the department following the applicable procedures.

_____	_____	_____
Major Advisor	Signature	Date

Approval Sheet

I, the advisor of the thesis entitled **''Synthesis and characterization of rGO/Ag nanocomposite using cinnamon plant bark extract for methylene blue dye removal from aqueous solution''** and developed by Bekele Yirga Mamo, hereby certify that the recommendation and suggestions made by the board of examiners are appropriately incorporated into the final version of the thesis.

Major Advisor	Signature	Date

We, the undersigned, members of the Board of Examiners of the thesis by Bekele Yirga Mamo have read and evaluated the thesis entitled ''**Synthesis and characterization of rGO/Ag NCs using cinnamon plant bark extract for methylene blue dye removal from aqueous solution**" and examined the candidate during the open defense. This is, therefore, to certify that the thesis is accepted for partial fulfillment of the requirement of th e degree of Master of Science in Applied Chemistry (Inorganic Chemistry).

Chairperson	Signature	Date
Internal Examiner	Signature	Date
External Examiner	Signature	Date

Final approval and acceptance of the thesis are contingent upon the submission of its final copy to the Office of Postgraduate Studies (OPGS) through the Department Graduate Council (DGC) and School Graduate Committee (SGC).

Department Head	Signature	Date
School Dean	Signature	Date
Office of Postgraduate Studies, Dean	Signature	Date

ACKNOWLEDGEMENT

First and foremost, I would like to thank the Almighty God and his mother St. Marry for giving me the health, strength, wisdom, and patience to complete this thesis.

Second, I would like to express my deepest gratitude and thanks to my advisor Dr. Tegene Desalegn (Ph.D.) for his cooperation, suggestions, supervision and remarks, appreciable encouragement, fatherly consultation, and taking his time to read and correct my document, starting from the proposal writing to the completion of this thesis.

I would also like to thank my family for continuous financial and moral support from the starting to the end of my work.

I would like to appreciate my colleagues, Analytical Chemistry Laboratory Technicians, Applied Chemistry Department, Applied Biology Department, Material Engineering Department, and all individuals who supported me by sharing ideas or offering materials support which is an input for this work.

I would like to transfer also my special thanks to Wolkite University, Chemistry Department, for UV-Vis analysis in adsorption experiment, and Addis Ababa Sciences and Technology University, Central Laboratory-, for FT-IR and UV-DRS analysis.

I would like to acknowledge Adama Science and Technology University for providing me the financial support and sponsorship opportunity to continue my post-graduate study.

TABLE OF CONTENTS

CONTENTS **PAGES**

LIST OF TABLE

LIST OF FIGURE

LIST OF ABBREVIATIONS

AFM	Atomic force microscopy
BET	Brunauer Emmett teller
CVD	Chemical vapor deposition
FTIR	Fourier transform infrared
GICs	Graphite interaction compounds
GO	Graphene Oxide
HNTs	Halloysite nanotubes
HQ	Hydroquinone
HOPG	Highly oriented pyrolytic graphite
IUPAC	International union of pure and applied chemistry
MB	Methylene blue
NCs	Nanocomposite
NPs	Nanoparticle
OD	Optical density
rGO	Reduced graphene oxide
PAA	Polyacrylic acid
SEM	Scanning electron microscopy
UV-DRS	Ultraviolet-diffuse reflectance spectroscopy

Abstract

In this study, green synthesis of a reduced graphene oxide silver nanoparticle hybrid nanocomposite (rGO/Ag) was carried out using an aqueous extract of cinnamon plant bark. Graphene oxide, and silver ions simultaneously reduced by cinnamon extract, then Methylene Blue dye removal capacity and efficiency of the resulting nanoparticles and nan ocomposite were also evaluated. The synthesized nanoparticle and nanocomposite were ch aracterized by using UV-DRS, SEM, P-XRD, and FTIR spectroscopy. The XRD results sho wed that the average particle sizes were 29.9 nm, 0.67 nm, and 13.35 nm for Ag NPs, rGO, and rGO/Ag NPs nanocomposite respectively. The UV-DRS analysis result showed that rGO/Ag nanocomposite exhibited two absorbance peaks at 272 & 334 nm which corresponds to rGO and Ag NPs respectively. The functional group information obtained from the FTIR spectral was in good agreement with the expected Phytochemicals in the plant extract for all synthesized samples and rGO functional groups exist in rGO/Ag nanocomposite. The surface morphology result obtained indicated that Ag NPs showed non-homogeneity and different shapes, rGO had thin flat layer sheet morphology and in the rGO/Ag nanocomposite, Ag NPs were found to be embedded on the surface of reduced graphene oxide nanosheets. The performance of Ag NPs adsorbent was found to be best at the optimum pH 10, adsorbent dose 80 mg, contact time 50 min, and initial concentration 10mg/l with a removal efficiency of 90.03%, for rGO nanosheets the optimized parameters adsorbent were at pH 2, adsorbent dose 80 mg, contact time 50 min, and initial concentration 10 mg/l with removal efficiency 96.97% and while the rGO/Ag NPs nanocomposite showed highest removal efficiency 99.98% at optimum pH 2, adsorbent dose 80 mg, contact time 50 min and initial concentration of 10 mg/l. The Adsorption isotherms results have well fitted to Langmuir isotherm than Freundlich isotherm for all three synthesized adsorbents. The adsorption kinetics results were best fitted to the pseudo-second-order model. The study has revealed that green synthesized nanocomposite has the potential to act as an adsorbent agent and cyclic use more than five times showed that the nanocomposite has a good efficiency in adsorbing dye and has a promising effect as an environmentally friendly wastewater treatment application.

Keywords: *rGO/Ag NPs, nanocomposite, cinnamon bark, adsorbent, methylene blue, green synthesis*

CHAPTER ONE

INTRODUCTION

1.1 Background of the study

Environmental pollutants are known to cause major problems worldwide. Natural water co nservation plays a vital role in protecting the land and saving it for future generations. Industries;- such as textiles, papermaking, cosmetics, food, and leather release wastewaters into the environment (Crini *et al.,* 2020). Among these, the textile industry is one of the major industries' largest water consumers and wastewater sources. Wastewater from the textile industry contains chemicals, suspended solids, toxic compounds, and dyestuff, which are among the major pollutants in wastewater. As a result of the rapid development of textile industries, wastewaters containing dyes that are directly or indirectly discharged into the environment are increasing, especially in developing countries. Addis Ababa is one of the main cities in which industrialization is highly expanded in Ethiopia. Most of the medium and large-scale industries in Ethiopia (more than 65%) are located in Addis Ababa and the nearby town of Akaki. As a result, industrial wastewater and its impact on the environment are widely prevalent in Addis Ababa compared to other parts of the country. This contaminated water is very toxic to humans and animals (Jemal *et al.,* 2020).

Industrial wastewater contains various contaminants, and synthetic dyes are one of the most substantial pollutants in wastewater for their widespread use (Konicki *et al.* 2017). Due to their non-degradability, carcinogenicity, and mutagenicity, eliminating dyes from discharged water is of great concern. Different techniques were used to the removal of these pollutants from contaminated water (Aboubaraka *et al.,* 2017; Aboelfetoh *et al*., 2018). Adsorption is regarded to be the most popular, effective, and economic method used for the expulsion of various contaminants from water (Gemeay *et al.,* 2017; A boelfetoh *et al.* 2018).

The selection of adsorbent is essential for adsorption processes. Usually, a good adsorbent candidate should meet three standards: high specific surface area, pore volume accessible for the adsorbate molecules, and easy regeneration. Recently, the use of graphene as an adsorbent to solve environmental pollution problems has received considerable attention due to its high specific surface area and unique 2D structure for

composite material designing. Several theoretical calculations and experimental measurements were conducted for using graphene as an adsorbent to remove hazardous pollutants from aqueous solutions (Fu & Fu, 2015). Recent literature suggests that graphene based composites showed excellent performances for hazardous pollutants removal. For example, synthesized reduced graphene oxide (rGO-MnO_2) composites for removing Hg (II), (Sreeprasad et al., 2011), $ZnFe_2O_4$/rGO (Fei et al., 2013) composite for methylene blue dye removal from water. The composites showed enhanced removal capability compared to the parent material. In water treatment plants, the application of nanomaterials has attracted significant attention because of their large surface areas and more active functionalized sites (Konicki *et al.,* 2017). Currently, there is an incredible interest in graphene oxide due to its accessibility for mass production, ease of functionalization, and high dispersal in water, besides the layered structure with a very large particular surface area (Haldorai *et al*., 2014). Graphene oxide (GO) nanosheets bear various surface groups, for example, carboxyl, hydroxyl, epoxide, and carbonyl. These groups permit GO nanosheets to be all around scattered in water to yield a colloidal stable solution (Shao *et al.,* 2015).

Metal nanoparticles are among important adsorbents that have drawn considerable attention in recent years because of their (Choi et al., 2007) appropriate catalytic performance, surface to volume ratio, and considerable controlled porosity (Lu et al., 2007). Today, numerous studies have been done about metal nanoparticle biosynthesis and their application in the removal of polluting dyes from wastewaters. For instance, previous studies have different research attempts about the removal of organic dyes using silver nanoparticles (Vidhu & Philip, 2014) and the removal of Rhodamine B using silver nanoparticles, (Azeez et al., 2018). These particular preferences make it appealing to various applications (Kumar et al. 2013).

Considering the superior individual properties of GO and Ag NPs, the combination of GO and Ag NPs could yield incredible characteristics. Some approaches have been reported to synthesize nanocomposites of metallic nanoparticles and GO by depositing metallic NPs on GO nanosheets through physical adsorption or by *in situ* reductions of metallic salts on GO nanosheets (Huang *et al.,* 2016). Unfortunately, various synthesis techniques are heavily dependent on the use of organic solvents, harmful reducing agents, and stabilizers that pose ecological and biological risks (Hebeish *et al.,* 2010). However,

this research focuses on preparing new adsorbents with high adsorption capacity through an eco-friendly approach. We assessed the use of cinnamon plant bark (*Cinnamomum Verum*) aqueous extract as a reductant and safe capping agent in an *in situ* reduction procedure for synthesizing Ag NPs on rGO nanosheets. Cinnamon is widely used as a condiment and flavoring agent in cooking (Nabavi*et al.,* 2015). Due to its abundant applications, the commercial production of cinnamon powder is quite high, exhibiting a broader availability for the synthesis of Ag NPs as a biomaterial, rGO, and rGO/Ag nanocomposites with variable sizes.

The advantages of this nanocomposite are;- it keeps the Ag NPs well dispersed; when a suspension is composed of only Ag NPs, the NPs aggregate and precipitate. Additionally, the graphene increased the surface area, thereby lowering the toxicity of the metal. Currently, the development of green chemistry approaches, which use biomaterials in the synthesis of various nanostructures, has attracted a considerable amount of attention (Azizi-Lalabadi *et al.,* 2020). The present study was conducted to employ green synthesis to develop an eco-friendly process without any toxic chemicals for the preparation of Ag NPs, rGO, and rGO/Ag NCs and investigate the capacity as well as efficiency of these nanomaterials for methylene blue dye removal from aqueous solution.

1.2 Statement of the problem

Currently, the world is facing a dramatically increasing impact of water pollution by effluents from various industries. Among those, dyes that are released from the textile industry are the major pollutants. The world production of dyes per year is approximately 7 $\times 10^5$ Metric tons, and around 10 to 15% of the dyes used are dumped in wastewater. Synthetic dyes are more difficult to remove than natural dyes and this is due to their complex aromatic structure, which gives them stability against air and light. They can easily transport within the aqueous environment due to their high solubility in water. They affect the aquatic autotrophy by restricting their photosynthetic efficiency because only limited sunlight is allowed to penetrate due to their color; their toxic effect spreads along the food chain, and they are conserved for long periods deteriorating animals and humans health (Nimkar, 2018).

Water is an important necessity for the survival of human beings. Treating wastewater is a vital issue to decrease environmental contaminants and problems. In addition to this,

wastewater recycling and reuse are very important to meet the water requirements for irrigation, industry, and domestic uses due to the increase in population and development in many parts of the world. Industrial wastes and their impact on the environment are widely prevalent in Ethiopia, like Addis Ababa and Bahir Dar compared to other parts of the country. Almost all industries in the city are located in the vicinity of the watercourse and among them; about 90% simply discharge their effluent into the nearby river. In addition, improper management of wastes generated by various industrial activities and the absence of proper wastewater treatment plants intensified environmental problems in the country. This leads to a major impact on the environment, due to toxic substances like heavy metals and dyes discharged into water bodies ("Industrial Wastes and Their Management Challenges in Ethiopia," 2019) Methylene blue (MB) dye is a cationic dye with broad applications such as dye for paper, hair, and cotton and filters for medical surgery among others. It is a pollutant not only deteriorates water quality but also significantly affects the environment and human health. It has been shown that, in humans, it causes vomiting, lightheadedness, cyanosis, jaundice, tissue necrosis, increased heart rate, vomiting, shock, and tetraplegia (Guarín *et al.*, 2018)

However, there is a need to eliminate this dye present in wastewater or industrial effluents to ensure a safer environment. This and the other dyes are difficult to degrade biologically, so this studies aimed at removing these contaminants present in aqueous solution are important and must be carried out to reduce environmental damage and human health. Various technologies, including adsorption, flocculation, membrane filtration, electrolysis, biological treatments, oxidation, sedimentation, membrane separation, reverse osmosis, and photocatalytic degradation (Guarín *et al.*, 2018) have been adopted to remove dyes from sewage water. Among the mentioned treatments, adsorption has some advantages because the adsorbents are inexpensive, are available, simple to use, and have high efficiency and their design is simple. Various adsorbents such as silica gel, activated c arbon, zeolites etc. have been employed to remove dyes but these adsorbents are not efficie nt as expected.

Therefore, composite based nanomaterials are gaining attention as an adsorbent in water treatment. As dyes are difficult to degrade biologically, so this study aims at removing these contaminants present in aqueous solutions using reduced graphene oxide silver nanocomposite by a new green reductant cinnamon bark extract to reduce environmental

damage and risk to human health. In this work, we used the adsorbent silver-reduced graphene oxide nanocomposite (rGO/Ag NP) synthesized using an aqueous extract of cinnamon plant bark, for the removal of methylene blue dye from aqueous solution.

1.3 Objective

1.3.1 General Objective

The general objective of the study was to investigate the green synthesis of rGO/Ag NCs using cinnamon plant bark extract for methylene blue dye removal from an aqueous solution.

1.3.2 Specific Objective

The specific objective of the study includes:-

- ✓ To synthesize & characterize the adsorbent Ag NPs, rGO, & rGO/Ag NCs by using cinnamon bark extract and using XRD, UV-DRS, SEM, & FTIR respectively
- ✓ To optimize the effects of parameters like pH, adsorbent dose, contact time, & initial concentration of adsorbate on the adsorption process.
- ✓ To evaluate the removal efficiency of methylene blue dye from an aqueous soluti on by Ag NPs, rGO, & rGO/Ag NPs.
- ✓ To describe the adsorption process using adsorption isotherm & adsorption kinetic models.

1.4 Significance of the study

The results of this study have various advantages in terms of providing information and data that supplement mechanisms or methods to minimize water pollution and simultaneously protect the environment, particularly the aquatic environment, and avoid human diseases that result due to the depletion of the aquatic environment by providing rGO/Ag NCs as biosorbent for removing dyes from a textile, tannery, and paper industry dye effluents.

Hence, this study work has the following significance

- ✓ Provided method for green synthesis of eco-friendly adsorbent for the removal of methylene blue dyes from different industry effluents using locally available cinnamon plant bark extract mediated rGO-Ag NCs.
- ✓ It helps to strengthen the knowledge in the area of adsorption study using green synthesized NCs.
- ✓ Offers baseline information regarding removal of methylene blue dye.

- ✓ It helps as a reference for additional research to be conducted on the removal of dyes using NCs.

1.5 The scope of the study

The scope of this study was limited to the synthesis of Ag NPs, rGO, and rGO/Ag NPs hybrid nanocomposite using cinnamon plant bark extract. The synthesized nanoparticles and nanocomposites are characterized by using UV-DRS, XRD, ATR-FTIR, SEM, and evaluation of the effectiveness of the removal of methylene blue using the synthesized nanoparticles and nanocomposites.

CHAPTER TWO

LITERATURE REVIEW

2.1 Graphene

Graphene, which consists of one to a few graphitic layered sp^2 bonded 2D carbon allotropes, has become a unique material due to its extraordinary properties like electrical and thermal conductivity, high charge carrier density, carrier mobility, optical conductivity, and mechanical property. The basic building blocks of all the carbon nanostructures are a single graphitic layer that is covalently functionalized sp^2 bonded carbon atoms in a hexagonal honeycomb lattice, which forms 3D bulk graphite when the layers of single honeycomb graphitic lattices are stacked and bound by a weak van der Waals force (Choi *et al*., 2010). When the single graphite layer forms a sphere, it is well known as zero-dimensional fullerenes; when it is rolled up with respect to its axis, it forms a one-dimensional cylindrical structure called a *carbon nanotube*; and when it exhibits the planar 2D structure from one to a few layers stacked; it is called *graphene* (Fig. 2.1).

One graphitic layer is well known as monoatomic or single-layer graphene and two and three graphitic layers are known as bilayer and trilayer graphene, respectively. More than 5-layer up to 10-layer graphene is generally called *few-layer graphene*, and ~20- to 30-layer graphene is referred to as multilayer graphene, thick graphene, or nanocrystalline thin graphite.

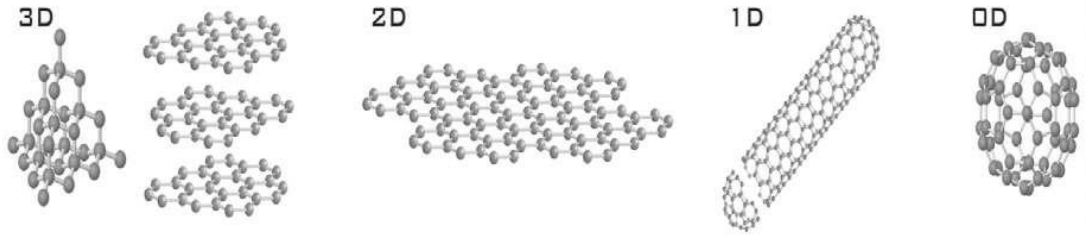

Figure: 2.1: Crystal structures of the different allotropes of carbon.

The theory of graphene was first explored by P. R. Wallace in 1947 as a starting point for understanding the electronic properties of 3D graphite. The term ‘graphene’ was introduced by Hanns-Peter Boehm and first appeared in 1987 to describe single sheets of graphite as a constituent of graphite intercalation compounds (GICs). However, the credit for the true discovery of graphene belongs to A. Geim and K. Novoselov who extracted

single sheet graphene from 3D graphite using the micromechanical cleavage technique in 2004 and received the Noble prize in physics in 2010 for this breakthrough discovery (Dresselhaus & Araujo, 2010).

2.2 Overview of Graphene Synthesis

Several techniques have been established for graphene synthesis. However, mechanical cleaving (exfoliation), chemical exfoliation, chemical synthesis, and thermal chemical vapor deposition (CVD) synthesis are the most commonly used methods today (Bhuyan *et al.,* 2016). Some other techniques are also reported such as unzipping nanotube and microwave synthesis (Jiao *et al*., 2010) however; those techniques need to be explored more extensively.

2.2.1 Mechanical Exfoliation

Mechanical exfoliation is the first recognized method of graphene synthesis. This is a top-down technique in nanotechnology, by which longitudinal or transverse stress is generated on the surface of the layered structure materials using simple scotch tape or AFM tip to slice a single layer or a few layers from the material onto a substrate. Graphite is formed when mono-atomic graphene layers are stacked together by weak van der Waals forces. The interlayer distance and interlayer bond energies are 3.34 Å and 2 eV/nm^2, respectively. For mechanical cleaving, ~300 $nN/\mu m^2$ external force is required to separate one mono-atomic layer from graphite (Zhou *et al.,* 2019). In the year 1999, Ruoff first proposed the mechanical exfoliation technique of plasma-etched pillared HOPG using an AFM tip to fabricate graphene (Ruoff, 1999). The advantage of this technique is that the individual graphene sheet prepared by this technique has high quality, while the disadvantage is that this technique is not suitable for large-scale production.

2.2.2 Chemical Exfoliation

Like mechanical exfoliation, chemical exfoliation is one of the established methods for fabricating graphene. Chemical exfoliation is a process by which alkali metals are intercalated with the graphite structure to isolate few-layer graphene dispersed in solution. Alkali metals are the materials in the periodic table that can easily form graphite-intercalated structures with various stoichiometry ratios of graphite to alkali metals. One of the major advantages of alkali metals is their ionic radii, which are smaller than the graphite interlayer spacing; hence they fit easily in the interlayer spacing. The process is versatile because it is a low-cost solution-phase method, is scalable, and would be capable

of depositing graphene on a wide variety of substrates, which is not possible using other processes like cleavage or thermal deposition (Pénicaud & Drummond, 2012)

2.2.3 Chemical Synthesis: Graphene from Reduced Graphene Oxide

Chemical synthesis is a top-down indirect graphene synthesis method and is the first method that demonstrated graphene synthesis by a chemical route. The method involves the synthesis of graphite oxide (GO) by oxidation of graphite, dispersing the flakes by sonication, and reducing it back to graphene. There are three popular methods available for GO synthesis: the Brodie method (Gleditsch, 1923), the Staudenmaier method (Poh *et al*., 2012), and the Hummers and Offeman method (Hummers & Offeman, 1958). All three methods involve the oxidation of graphite using strong acids and oxidants. The degree of oxidation can be varied by the reaction conditions (e.g., temperature, pressure, etc.), stoichiometry, and the type of precursor graphite used as a starting material.

GO was first prepared (Gleditsch, 1923), by mixing graphite with potassium chlorate and nitric acid. However, the process contains several steps that are time-consuming, unsafe, and hazardous. To overcome those problems, Hummers (Hummers & Offeman, 1958) developed a method for fabricating graphite oxide by mixing graphite with sodium nitrite, sulfuric acid, and potassium permanganate, well known as the Hummers method. To improve the preparation procedure of GO, Tour and coworkers reported a new recipe for the preparation of GO in 2010. They excluded sodium nitrate ($NaNO_3$) from the reaction, increased the amount of potassium permanganate ($KMnO_4$), and introduced phosphoric acid (H_3PO_4) into the reaction in a 9:1 mixture of H_2SO_4/H_3PO_4.

It is believed GO prepared by this method has a higher level of oxidation with more intact graphitic basal planes compared to GO prepared by Hummer's method. When graphite flakes are oxidized by using strong oxidizing agents, the carbon atoms' layer of graphite is decorated by oxygen-functional groups to form graphite oxide (Chen *et al.*, 2019). These oxygen-functional groups can expand the interlayer space of graphite planes from 0.34 nm to 0.8 nm and make the planes hydrophilic. As a result, graphite oxide can be easily dispersed and exfoliated in water by using moderate sonication or stirring for a long time. After exfoliation, the solution contains monolayer; bilayer, or few-layer sheets of carbon atoms, which are named graphene oxide (GO).

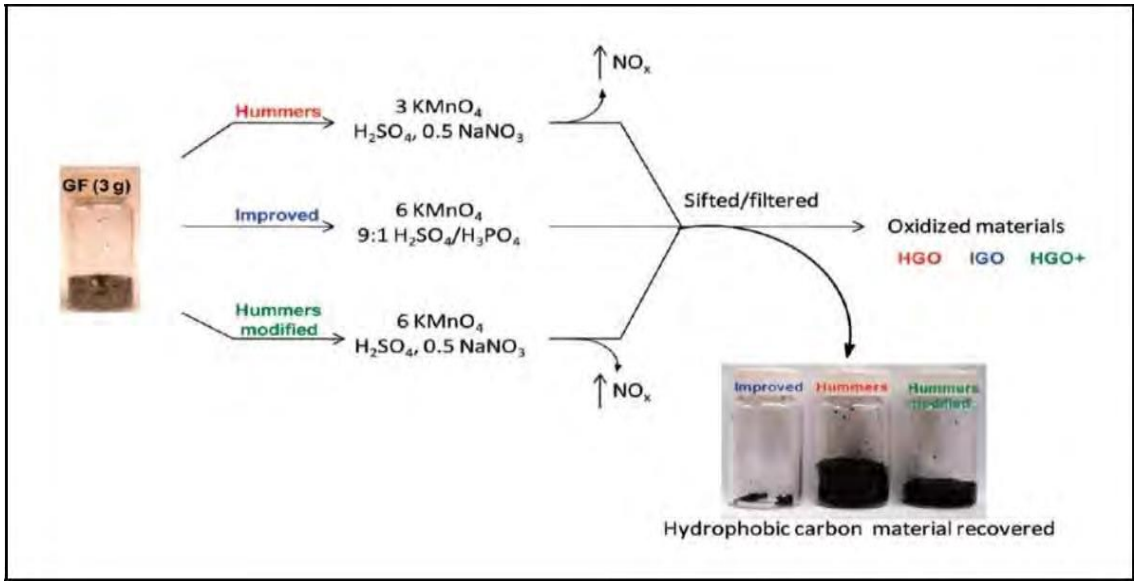

Figure: 2.2: Procedure comparisons of different methods to produce GO.

The very small amount of under-oxidized graphite retained on the sieve indicates the increased efficiency of the improved GO method (Chen *et al.*, 2019).

The preparation process of reduced graphene oxide (rGO) consists of three steps: oxidation or intercalation, exfoliation, and reduction (Habte & Ayele 2019).

(i) Oxidation or intercalation: graphite oxide (GTO) was prepared from graphite powder by reacting with a strong oxidizing agent called potassium permanganate mixed with H_2SO_4/H_3PO_4 (9:1) (v/ v) at 50°C for 12 hours in a water bath. H_2SO_4 is the most common intercalating agent.

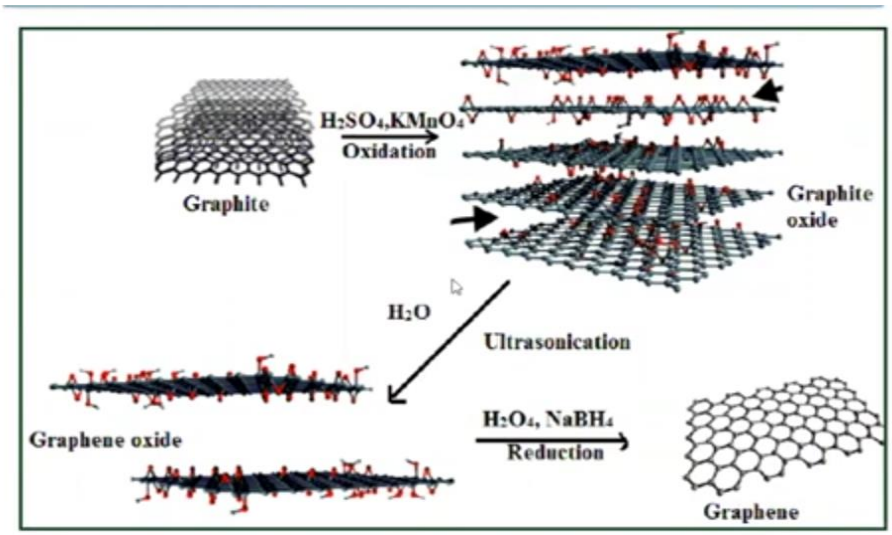

Figure: 2.3: synthesis of GO & rGO.

(ii) Exfoliation: in this step, the oxidized form of graphite was dispersed into distilled water to form single-layer graphene oxide (GO), and then it was heated with a magnetic stirrer for 12 hours at 60°C in a water bath, the black paste was collected by filtration followed by centrifugation and dried at 60°C for 24 hours.

(iii) Reduction: it is the last stage in synthesizing reduced graphene oxide (rGO). In this stage, the GO obtained from the stage (ii) was dispersed and ascorbic acid was added as the reducing agent, followed by heating it at 60°C for 30 min. Reduced product was collected using filtration followed by centrifugation. Lastly, the black product was washed with ethanol and distilled water three times, respectively, followed by centrifugation; then, the product was collected and dried in an oven at 120°C for 24 hours.

The chemical reduction process is carried out using dimethylhydrazine or hydrazine in the presence of a polymer or surfactant to produce homogeneous colloidal suspensions of graphene. The process flow chart of the chemical synthesis of graphene is shown in a schematic in Fig. 2.4 (a) and (b).

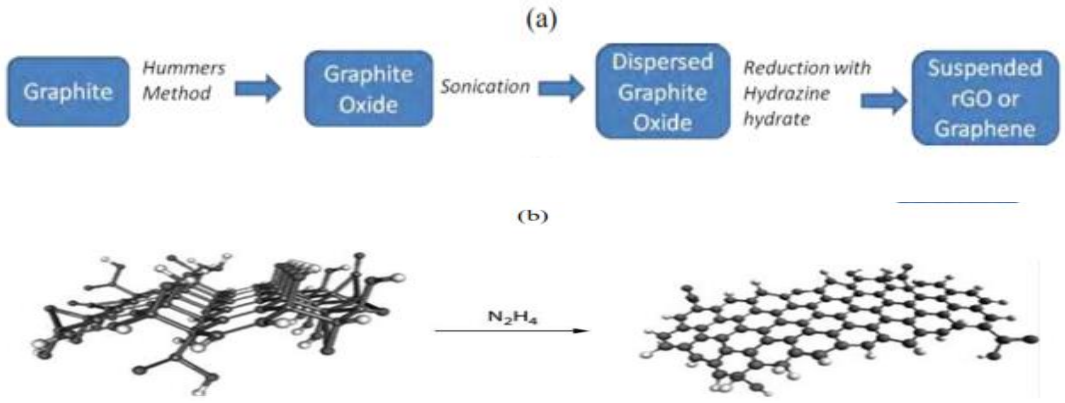

Figure: 2.4: (a) The process flow chart of graphene synthesis derived from graphite oxide, (b) Schematic showing that the 3-D GO (carbon in grey, oxygen in dark grey, and hydrogen in white) restores its planar structure when reduced and dispersed with hydrazine.

In contrast, the chemical syntheses of graphene have several disadvantages such as small yield, defective graphene, and partially reduced GO, which readily deteriorates the properties of graphene.

2.3 Synthesis of Metal-Graphene Composite

Research on metal-graphene composites is still in its infancy with very few studies as compared to metal oxide-graphene composites. The metal-based composite systems, which have explored the potential of graphene as a second phase, include gold, platinum, silver, copper, and silicon. The projected application of these composites is found in energy devices such as Li-ion batteries, supercapacitors, electrocatalysts, and biosensors (Khan *et al.,* 2017). The challenge in synthesizing metal-graphene composites remains similar to that for metal oxide-graphene systems. An additional challenge for metal-graphene composites could be the reaction at the interface because metals are much more reactive than metal oxide. The basic principles adopted for synthesizing metal-graphene composites are classified into the following categories.

2.3.1 Reduction of GO to rGO after Chemical Mixing with Metals

This class of processing route involves the mixing of metal particles with GO to form the composite structure, after which GO is reduced to graphene. Composites containing gold, palladium, platinum, and cobalt are fabricated through this route. (Lai *et al.,* 2013) used a water-ethylene glycol system to disperse GO and metal nanoparticles. The metal nanoparticles absorbed on GO sheets play a major role in the reduction reaction of GO with ethylene glycol and form the metal-graphene composite. Homogeneous dispersion of GO in water-ethylene glycol systems confirms even the distribution of metallic nanoparticles on them. On the other hand, metallic nanoparticles sitting on the graphene sheets prevent their restacking and agglomeration. This class of fabrication route assures uniform distribution of phases in a metal-graphene composite.

2.3.2 Chemical Mixing of Graphene with Metals

This class of processing route uses graphene and metallic salt as the starting materials. The metallic salts are reduced in dispersion and deposited on graphene sheets to form the composite. The aim of fabricating these composite structures is mainly to prevent the aggregation of graphene layers by introducing nanosized metallic particles between the layers deposited platinum nanoparticles on graphene sheets by the chemical reduction of H_2PtCl_6 with methanol (Morales-Torres *et al*., 2012). Considering the agglomeration tendency of graphene, Gong *et al.* used chitosan to form a stable dispersion of graphene in water. After casting and drying this dispersion on a glassy carbon electrode, a cyclic voltammetry scan of the electrode is done in $KAuCl_4$ solution to form an Au-graphene composite film on the electrode to be used as a sensor (Gong *et al*., 2016)

2.3.3 Electrodeposition

Electrodeposition of metallic nanoparticles is performed on graphene film-casted electrodes to fabricate the metal-graphene composite film. Available in this category report is the synthesis of a gold-graphene composite (Hussain *et al.,* 2020). Graphene produced by different methods was dispersed in an aqueous solvent and cast on a glassy carbon electrode. Au nanoparticles were deposited from a $HAuCl_4$-containing bath to fabricate the Au-graphene composite film. These composite films are mostly used as biosensors.

2.4 Green synthesis of graphene supported metal nanocomposite

Recently, biological approaches for synthesizing NPs have been increasingly considered. These methods represent a green technology aimed at minimizing negative environmental impacts. The synthesis of NPs using a chemical approach requires three main ingredients: a metal salt, a reducing agent, and a stabilizer or capping agent. One possible way to develop a "green" process is to adapt benign synthesis approaches involving the utilization of nontoxic capping agents, less hazardous reducing agents, and the selection of environmentally benign solvents. Biosynthetic routes provide nanostructures with better-defined sizes and morphologies than some of the physicochemical techniques of production (Nasrollahzadeh *et al.,* 2019).

In the biological and green approach, many interesting biological tools, such as bacteria, yeasts, fungi, algae, and plants, offer accessible alternatives to chemical procedures and physical methods for the large-scale production of green NPs having dual functions (reducing and capping agents). However, the preparation of microorganisms is generally more expensive than the preparation of plant extracts. Among the organisms reported viable for the green synthesis of NPs, the best candidates are plants, owing to their diversity and sustainability. Plants can be used as an economic and valuable alternative for the large-scale biosynthesis of NPs. Among the existing biological methods for NP synthesis, methods based on plant extracts have been widely reported in the literature (Sabouri *et al.,* 2020).

Although the precise mechanisms underlying the green synthesis of MNPs using plant extracts have not been thoroughly investigated yet, a bottom-up mechanism has been proposed (El-Seedi *et al*., 2019). This proposed mechanism involves four major steps; (i) the initial activation step (bio-reduction) where the metal ions are reduced into their zero-oxidation states, and (ii) subsequent growth and agglomeration of the small nanoparticles

into more substantial and more thermodynamically stable particles, (iii) termination, where stabilization and capping of the MNPs are performed to form nanoparticles of diverse morphologies and average sizes and (iv) purification and washing of the MNPs usually by centrifugation (Fahmy *et al*., 2020).

2.4.1 Green synthesis of graphene-silver nanocomposite

Green chemistry methods involve the use of simple, economic, environmental-friendly materials and processes that reduce the generation of hazardous waste and harsh reaction conditions. The use of leaf extract as stabilizing and reducing agent is the most attractive approach for this purpose owing to its ease of preparation, simple handling, and low-cost availability. A variety of these reducing agents such as ascorbic acid, tea polyphenols, amino acids, carbohydrates, fenugreek extract, and aloe vera extract have been utilized for the reduction of GO (Bhattacharya *et al.*, 2017).

According to Chandu B. *et al.* research of photocatalytic materials, custard apple leaf extract-reduced graphene oxide-silver (CRG-Ag) nanocomposite was synthesized successfully and reported as follows.

Figure 2.5: Schematic illustration of CRG-Ag nanocomposite formation (Chandu *et al*., 2019).

Graphene oxide (GO) was prepared using the Hummers' method. To synthesize CRG-Ag nanocomposite, 40 mg of GO was dispersed in 100 mL of water using sonication for 4 hr and then 10 wt% of $AgNO_3$ was added and further sonicated for 5 min to get a uniform solution. To this precursor solution, 100 mL of freshly prepared CLE was added and refluxed at 100 °C for 12 hr. The air-cooled solution was then centrifuged at 10,000 rpm for 15 min and vacuum dried at room temperature for 1 hr to fetch the final nanocomposite. A general schematic depiction of reaction methodology is shown in Fig. 2.5.

Additionally, Maryami *et al.* have synthesized Ag/RGO nanocomposite using *Abutilon hirtum* leaf extract (Maryami *et al.,* 2016). Vizuete *et al.* have reported Ag/RGO photocatalyst with Mortino berry extract. Maham *et al.* have reported the synthesis of Ag/RGO/Fe_3O_4 nanocomposite using *Lotus garcinii* leaf extract (Maham *et al.,* 2017).

2.4.2 Plant sources used in the synthesis of nanostructures

Plants have long been known to demonstrate the ability to absorb, hyper accumulate and degrade inorganic metallic and metallic oxide ions from their nearby environment. More recently, it has been shown that many organic entities present in plants can act as effective biological factories to remarkably reduce environmental contamination as well as being capable of retrieving metals from industrial waste. On the other hand, the true challenge to synthesizing MNPs is finding the balance between price, scalability, and applicability. In addition, reagent suitability plays an important role in the large-scale synthesis of NPs. Plants are the best candidates for use in the large-scale biosynthesis of NPs. Plant extracts can be used as reducing agents in the production of NPs and provide a cost-effective and environmentally friendly alternative production source (Nasrollahzadeh *et al*., 2019).

Extracts from various parts of plants including their stems, gum, leaves, seeds, and fruits are efficaciously used for the preparation of NPs (Amiri *et al.,* 2021). This is because various extracts include different concentrations and combinations of organic reducing agents. Reducing agents include various water-soluble plant metabolites (e.g., alkaloids, terpenoids, and phenolic compounds) and coenzymes. Phytochemicals that exist in plant extracts can be used as reducing and stabilizing agents for NPs synthesis. Because of the number of different chemicals involved, the biogenic reduction process is comparatively complex. Phenolic compounds possess hydroxyl and ketone groups that are capable of binding to metals and showing chelation. The preparation of NPs using these approaches is environmentally friendly and provides NPs with better-defined sizes, morphologies, and stability (Gao *et al.,* 2016).

2.4.3 Cinnamon plant

Cinnamon is a mid-brown bark used as a spice and flavouring additive in various cuisines and is obtained from the inner bark of the tree in the family Lauraceae of the genus Cinnamomum. Cinnamon has been used and praised for its medicinal qualities and health benefits since ancient times. It is enriched with cinnamaldehyde, eugenol, cinnamic acid, L-borneol, linalool, and methyl chavicol (Premkumar *et al.,* 2018). Owning strong

antioxidant, anti-inflammation, anticancer, lipid-lowering, and antimicrobial properties, cinnamon is widely studied for pharmacological purposes and is often referred to as a multifaceted medicinal plant. Considering its strong oxygen absorption and reducing properties (due to the presence of a high concentration of cinnamaldehyde and eugenol), many researchers unfold the role of cinnamon and other plants with similar compositions (clove, cumin, piper nigrum, etc) as bio reductants to produce metal nanoparticles (Singh *et al.,* 2010) used cinnamon bark extract to synthesize palladium nanoparticles and studied the effect of bark extract concentration, temperature, and reaction pH on particle size and shape.

Cinnamon camphora leaf extracts into the synthesis of silver and gold nanoparticles, finding it effective at modifying the size and shape of the particles. (Premkumar *et al.,* 2018) studied the antimicrobial properties of silver nanoparticles synthesized using cinnamon extract. (Kamran *et al.,* 2019) in their recent study successfully synthesized manganese nanoparticles using cinnamon extract and explored both the photocatalytic and antimicrobial properties. Copper nanoparticles remain of significant interest to scientists due to their abundant availability, cost-effectiveness, superior conductivity, catalytic, antimicrobial, and bactericidal properties. This work uses the cinnamon plant bark extract for the removal of methylene blue in a nanocomposite form rGO/Ag by adsorption process. Cinnamon plant bark extract does not use in the past year in stabilization & reducing agents of these nanocomposites, silver & reduced graphene oxide.

2.5 Nanocomposite

A nanocomposite is a composite material, in which one of the components has at least one dimension in nanoscopic size. Nature has mastered the synthesis of nanocomposites using natural reagents and polymers such as carbohydrates, lipids, and proteins to create strong composites such as wood (cellulose/lignin), bone (apatite/collagen), nacre (mother-of-pearl) (aragonite/protein),granite (quartz, feldspar), and a myriad of other materials (Peppas et al., 2006).

Nanocomposite particles are spherical or random shaped nanometer size particles reinforced with even smaller particles to obtained desirable set of properties at nanoscale. In nanocomposites, two or more phases are involved in the fabrication of spherically or intricate layered particles having more complicated nanohetero structures as compared to single phase nanoparticle. Basically nanocomposite can be classified as core-shell NCs and

random shaped NCs. In core-shell NCs each individual particle ideally forms a concentric sphere of filler-core and matrix- shell. Whereas the random shaped nanocomposite have morphology of random distribution of fillers in spherical or any geometrical shaped matrix (Kumar & Kumbhat, 2016).

2.5.1 Applications of Graphene-Based Nanocomposites

Graphene has a great number of applications encompassing engineering, electronics, medicine, energy, industrial, household design, environmental and many more (Avouris & Dimitrakopoulos, 2012). A previous review search yielded several review papers that examined fieldoriented and specific applications of graphene. Majority of the papers dealt with electronic/sensor-oriented applications, to generalize the broad applications of graphene and graphenebased nanocomposite into their respective disciplines. The biomedical applications of graphene including drug delivery, gene delivery, cancer therapy, biosensing and bioimaging, GO-based antibacterial materials, and scaffolds for tissue/cell culturing (Shen et al., 2012). Let us see some examples below, application of graphene in environmental application, like an adsorbent for different pollutants.

1) Adsorption of inorganic (cationic and anionic) contaminants

Many kinds of graphene-based materials were used for the removal of toxic inorganic (cationic and anionic) pollutants from aqueous media. Graphene-based materials have great potential to adsorb variety of inorganic contaminants via electrostatic attraction, various p-interactions, and functional groups present in the graphene surfaces. This section, overview the various graphene-based materials reported for the removal of cationic and anionic heavy metal pollutants. The fabricated graphene nanosheets (GNSs) from graphite oxide using an exfoliation process. The sorption of Pb(II) ions from aqueous solutions on pristine GNSs and thermally modified GNSs was studied. The adsorption of lead ions was better enhanced by heat treatment than pristine GNSs. They concluded that the heat treatment of graphene favors adsorption through lead ions (Lewis acid), which increases the Lewis basicity and electrostatic attraction of graphene (Huang et al., 2011). The drawback of the prepared graphene nanosheets is that it requires ultrasonication for a good dispersion of graphene in metal solutions and after sorption it also requires filtration through microsyringe to separate the GNS/solution mixture.

Graphene oxide nanosheets and studied their Cd(II) and Co(II) adsorption from aqueous solutions. They prepared graphene oxide nanosheets showing sorption efficiencies

of 106.3 mg/g for Cd(II) and 68.2 mg/g for Co(II). After the metal adsorption experiments, graphene oxide nanosheets were recovered by membrane filters. (Zhao et al., 2011).

2) Adsorption of organic pollutants

Graphene-based materials act as an excellent adsorbent material for the removal of various organics dyes, pharmaceutical drugs, toxic chemicals, pesticides, solvents, and oils (vegetable oil, paraffin oil, gasoline etc.). The major mechanisms of removal of organic pollutants on the graphene-based materials were π-π interaction, anion-π interaction and cation-π interaction and functional group interactions.

The fabricated magnetic chitosan and graphene oxide (MCGO) composite for the sorption of anionic dye methyl blue from aqueous solution. The maximum methyl blue sorption ability was found to be 95.16 mg/g for MCGO, 43.5 mg/g for graphene oxide, 60.4 mg/g for magnetic chitosan, and 46.23 mg/g for natural chitosan membranes. At acidic pH, anionic dye methyl blue was adsorbed via protonated amino groups of MCGO by ionic interactions. The dye desorption values of H_2O, HCl, and NaOH were 1.4, 5.1, and 95.0%, respectively. The advantages of MCGO include stability, magnetic separation, and easy regeneration, and its high methyl blue dye sorption efficiency is about 90–80% even after five cycles. (Fan et al., 2012).

Graphene oxide and reduced graphene oxide (rGO) for the sorption of cationic dyes, i. e., methyl violet, rhodamine B, methylene blue, and Orange G (anionic dye) from aqueous media. They reported that graphene oxide contains many oxygen functional groups (epoxy, carboxyl, hydroxyl groups, and ketone) and it is hydrophilic in nature with a large negatively charged surface that helps in the effective adsorption of cationic dyes (methylene blue (17.3 mg/g), methyl violet (2.47 mg/g), rhodamine B (1.24 mg/g). Graphene oxide showed negligible adsorption capacity for Orange G (anionic dye). In contrast, the reduced graphene oxide with a large surface area and less negatively charged surface removed 95% of Orange G (5.98 mg/g) and about 50% of cationic dyes. (Ramesha et al., 2011).

3) Catalytic oxidative degradation of organic contaminants

Graphene and graphene-based materials were wieldy used as catalyst for the degradation of organic contaminations from water. The graphene based materials act as an adsorbent material for organic contamination and activates the oxidizing agent (H_2O_2, KIO_4, and Oxone) for the successful degradation. In the presence of graphene based materials, the

degradation performances of oxidizing agent many fold increases. Graphene/$CoFe_2O_4$ (G/ $CoFe_2O_4$) composite to activate the oxidizing agent, peroxymonosulfate (PMS), for the degradation of dimethyl phthalate (DMP). G-$CoFe_2O_4$ was found to be an efficient and better activating agent for PMS than $CoFe_2O_4$. A graphene content of 22% showed optimum degradation of DMP and excess graphene percentage led to very high sorption of DMP as well as inadequate degradation. G-$CoFe_2O_4$ was found to be a good activator for PMS at pH 4.0- 8.3, (Xu et al., 2015).

Graphene oxide-Fe^{3+} hybrid nanosheets (GO-$Fe^{3+)}$ and used for the effective oxidation of Reactive Red 120 using a sonocatalytic method. The commercial oxidants, such as potassium periodate (KIO_4), peroxodisulfate (PDS), hydrogen peroxide (H_2O_2), and peroxymonosulfate (PMS), were used as catalyst to enhance the sonocatalytic degradation (Thangavel et al., 2015).

2.5.2 Nanoparticle

Nanotechnology is a known field of research since last century. Since ‘‘nanotechnology” was presented by Nobel laureate Richard P. Feynman during his well famous 1959 lecture ‘‘There’s Plenty of Room at the Bottom there have been made various revolutionary developments in the field of nanotechnology. Nanotechnology produced materials of various types at nanoscale level. Nanoparticles (NPs) are wide class of materials that include particulate substances, which have one dimension less than 100 nm at least (Laurent et al., 2010). Depending on the overall shape these materials can be 0D, 1D, 2D or 3D. The importance of these materials realized when researchers found that size can influence the physiochemical properties of a substance e.g. the optical properties. A 20- nm gold (Au), platinum (Pt), silver (Ag), and palladium (Pd) NPs have characteristic wine red color, yellowish gray, black and dark black colors, respectively

The field of nanotechnology has gained lately a tremendous development especially due to the remarkable properties of the nanoscale materials, which significantly differ from those of bulk material. These impressive properties led to various applications in many fields of science such as biomedicine, pharmaceutics, cosmetics, catalysis, textiles and optics (Filip et al., 2019). Among metal nanoparticles, silver and gold nanoparticles are widely used because of their applications. The synthesis of nanoscale silver can be easily achieved by various methods, such as physical, photochemical, electrochemical and many

others. Most of the synthetic approaches used to convert silver ions into elemental silver involve the use of hazardous chemicals as reducing agents such as hydrazine, sodium borohydride, sodium sulfide, the use of surfactants, polymers and dendrimers as capping agents or imply severe reaction conditions and might generate toxic byproducts, leading to environmental pollution.

1) Silver nanoparticles

Nowadays, NPs made from noble metals, particularly Ag, Au, Pd and Pt are most effectively studied. Silver ions or silver based compounds are excellent choice in medicinal field. Silver is generally used in the nitrate form to induce antimicrobial effect, while silver nanoparticles (Ag NPs) increase the surface area. Ag NPs are used in the development of new technologies in the areas of electronics, material sciences and medicine and because of their extensive applications in various areas more research is being conducted on the Ag NPs by the scientists throughout the world (Shahverdi et al., 2007).

Ag NPs are unique in nanoscale system due to the ease in its synthesis and chemical modifications. NPs can be fabricated by various synthesizing methods such as biological, chemical, physical and other photochemical, electrochemical, and sonolytic methods. Ag NPs can be synthesized by both top down (physical and chemical methods) and 'bottom-up (via green pathway) approaches. These methods of synthesis can be divided into intra and extracellular. Extracellular nanoparticle synthesis using plant leaf extracts rather than whole plants would be more economical owing to easier downstream processing (Arunachalam & Annamalai, 2013). The non-biodegradable organic dyes resulting from textile, plastic, paper and food industries are usually released in water without any previous treatment, leading to significant environmental pollution.

Many of these dyes can cause substantially damages to the aquatic organisms and they are also highly toxic to human life, possessing mutagenic and carcinogenic effects (Rawat et al., 2018). Therefore, dye effluents should be treated to remove these compounds from waste waters. Various techniques such as absorption, chemical, photochemical and biodegradative methods are conventionally applied for this purpose (Robinson et al., 2001). Dye pollutants are rather resistant to these physical–chemical methods due to their high chemical stability. The removal of these toxic pollutants from these wastewaters is a complex concern and, to this end, a variety of treatments has been designed and developed such as physicochemical and biological methods, as international environmental safety

regulations are becoming more and more stringent (Katheresan et al., 2018). Efforts are made to find an ideal dye removal method able to efficiently remove a large amount of dye in a short time, without generating further pollution by producing more hazardous by-products. To this end, the using of green synthesized metallic nanoparticles as efficient catalysts for the reduction of organic dyes has been largely explored (Rupa et al., 2019). The unique physical, chemical and electronic properties of metal nanoparticles (silver NPs) recommend these nanomaterials as good catalysts, suitable for the reductive degradation of organic dyes, being an efficient alternative to conventional methods used for the removal of dye contaminants (Jyoti & Singh, 2016).

2.6 Dyes

Dyes are toxic, colored, and aromatic organic compounds, which show special compatibility toward a given substrate. The color of dyes is due to the particular absorption of a wavelength of light and the atoms that exist in the dye. A group of atoms called Chromophores or Auxochromes is responsible for the colorant of dyes. Dyes have various applications such as textile, paint, paper, dyeing, leather, plastic, etc, the application of dyes is consistent in our day-to-day activities and it is difficult to avoid them in most areas of human movement. On the other hand, they also have an effect on the environment during their application. One thing they cause a risk to the environment like toxicity, water coloration, carcinogenetic, and mutagenicity which causes water pollution and eutrophication in an ecosystem.

The discharge of dye effluent from the various industries into river waters, lakes, and water reservoirs leads to severe environmental problems and increases BOD content and decreased oxygen level in an aquatic ecosystem. Even the very less amount of concentration of some of the dyes is highly toxic, which is difficult to degrade and causes skin allergies, and leads to carcinogenic problems (Robinson *et al.,* 2001). Thus, dye pollution is not only a source of water pollution but also affects human health and thus it is very important to degrade the dye contaminants to decrease their effect on the environment. Discharged industrial wastewater containing a high concentration of colored toxic compounds results risk of harm to the health of the population as a whole to the environment.

The existence of dye in wastewater:

- Obstruct light penetration

- ❖ Highly visible and unacceptable
- ❖ Stable to light irradiation and heat
- ❖ Become a toxic to microorganisms
- ❖ Difficult to remove due to their complex structure and synthetic origins in which they synthesized.

2.6.1 Classification of Dyes

One of the difficult problems that are challenged in the wastewater treatment of textile industries is the removal of dye from textile dye effluents that originates from many types of dyes used in textile dyeing and printing operations. Commonly Textile dyes can be classified under the categories of anionic, cationic, and nonionic types (Finch, 2004). Anionic dyes contain direct, acid, and reactive dyes. Basic dyes are the only class of cationic dyes used in the textile industry operations. Nonionic dyes rise to disperse dyes, which do not ionize in an aqueous medium. Further dyes may be grouped based on two main classifications. These are based on their chemical structure and dyeing applications or practice. The easier way of dye classification for textile industries is by dyeing application. Under this classification, dyes can be grouped as acid dyes, disperse dyes, basic dyes, direct dyes, reactive dyes, chrome dyes, and vat dyes. Let's see the classification of dyes based on their usage or applications one by one.

i) Direct Dyes

Direct dyes are water-soluble anionic dyes that are functional on cotton, cellulose, paper, leather, and nylon. Direct or substantive dyeing is usually carried out in a neutral or somewhat alkaline dye bath, at or near boiling point, with the accumulation of either sodium chloride (NaCl) or sodium sulfate (Na_2SO_4). Examples of direct dyes are azo, phthalocyanines, stilbene, and oxazine.

ii) Acid Dyes

These are water-soluble anionic dyes and are being convened according to the lines of being colored and also the aromatic compounds contain in the structure that can be ionized. Acid dyes are useful to fibers such as silk, wool, nylon, and modified acrylic fibers using neutral to acid dye baths. Attachment to the fiber is attributed, at least partially, to salt formation between anionic groups in the dyes and cationic groups in the fiber. They are continually used in an acidic solution. Some of the examples of acid dyes include picric acid and Martius yellow.

iii) Reactive Dyes

Reactive dyes employ a chromophore attached to a substituent that is capable of directly reacting with the fiber substrate. These dyes form a covalent chemical bond with fiber is ether or ester linkage under appropriate conditions. The main chemical classes of reactive dyes are azo dyes. Typically, these chemical classes are used for dyeing and printing cotton and wool.

iv) Basic Dyes

These dyes are cationic dyes and water-soluble. Frequently acetic acid is added to the dye bath to help the uptake of the dye onto the fiber. They are functional on paper, polyacrylonitrile, modified nylons, and modified polyesters. In addition, they are used to apply with silk, wool, and tannin-mordant cotton when brightness shade was more required than fastness to light and washing. Generally, the chemical classes are diazahemicyanine, triarylmethane, cyanine, hemicyanine, thiazine, oxazine, and acridine.

v) Disperse Dye

These are significantly water-insoluble nonionic dyes for application to hydrophobic fibers from a microfine aqueous dispersion. They are used mainly on polyester, polyamide, polyacrylonitrile, and polypropylene fibers, and a lesser on nylon, cellulose acetate, and acrylic Fibers. Chemical classes of dyes mostly belong to azo and anthraquinonoid.

vi) Mordant dyes

These dyes have mordant dyeing property that simplifies the fixing of dye to fiber by good quality of the presence of certain groupings in the dye molecule which are capable to hold metal residuals by the formation of covalent and coordinate bonds involving a chelate compound. Most natural dyes are mordant dyes and there is a large literature base telling dyeing techniques. The most significant mordant dyes are the synthetic mordant dyes, or chrome dyes, used for wool.

vii) Vat dyes

Vat dyes are insoluble in water that can apply mainly for dyeing fiber by changing them to their leuco compounds by reduction and solubilization with sodium hydrosulphite and sodium hydroxide solution which is called a vatting process. The main chemical classes of vat dyes are anthraquinone and indigoid.

2.6.2 Methylene blue dye

Methylene blue dye is known as methyl thioninium chloride which is a heterocyclic aromatic chemical compound. It is a basic cationic thiazine dye with the molecular formula $C_{16}H_{18}N_3SCl$ with a molecular mass of 319.87g/mol. This dye gives a net positive charge

when introduced to an aqueous solution because of the presence of chemical groups like amine or sulfur. At room temperature, methylene blue is solid, odorless, dark green powder and gives a blue solution if dissolved in water (Laysandra *et al.*, 2017). This dye is used in several applications like the coating and coloring of paper, hair, cotton, and wool; it is also used as an indicator of oxidation-reduction and as a disinfectant, besides its many other medical usages in medicine, pharmaceutical formulations, in pesticide production, varnish, and lacquer manufacturing, among others (Zaghbani *et al.*, 2007). The IUPAC name of MB dye is 3, 7-bis (Dimethylamino) - phenazathionium chloride, or Tetra methylene blue, the chemical structure is present in Figure 2.6. MB in commercial purity was used without further purification.

Table 2.1: physical and chemical properties of MB.

Physical and chemical properties	Value
Solubility in water	35.5g/L
Melting temperature	180
PH value	3
Molecular weight	319.87 g/mol
Colour	Dark blue-green in oxidized form, colorless in reduced form
Chemical formula	$C_{16}H_{18}N_3SCl$

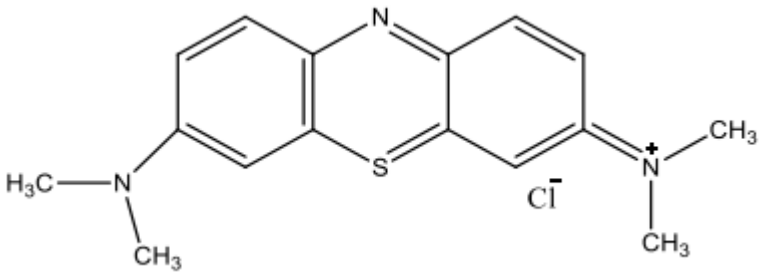

Figure 2.6: chemical structure of methylene blue

2.6.3 Environmental problems of textile dye effluents

Wastewater containing dye effluents represents enormous water pollution which is damaging to humans, fish, and aquatic plants (Divya & Loonker, 2021). Dyes in water give out a bad color and can cause diseases like haemorrhage, ulceration of the skin, nausea, severe irritation of the skin, and dermatitis. They can block the penetration of sunlight from the water surface stopping photosynthesis (Luken & Komendantova-Amann, 2017). Dyes also enhance the biochemical oxygen demand of the receiving water and decrease the re-

oxygenation process and hence hinder the growth of photoautotrophic organisms. Discharging wastewater containing dye compounds into water sources has significantly reduced the quality of water. Since they have a synthetic origin and complex aromatic molecular structures, azo dyes are usually inert and problematic to biodegrade in waste streams (Khan *et al.,* 2013). They also affect the photosynthetic activities of aquatic lives because dyeing effluents will deplete the dissolved oxygen contents in water and prevent sunlight from reaching the water sources (Kadam *et al.,* 2015). In addition to this dye wastewater and its degradation products are usually toxic, mutagenic, teratogenic, and carcinogenic, which are undoubtedly harmful to aquatic organisms and human beings.

Figure 2.7: Dye containing wastewater from textile industries

Therefore, appropriate techniques and processes must apply in industries for efficient removal of these toxic chemicals from water bodies. Many Physico-chemical processes have been projected and applied for the treatment of textile wastewater (Rakibuddin et al., 2015). Among the different recent dye removal methods, Adsorption, ion exchange, membrane filtration, ozonation, electrokinetic coagulation, Fenton reagent, and photocatalyst are the most commonly used. Adsorption technologies for wastewater treatment are becoming more common in recent years due to flexibility and simplicity of design, ease of operation, insensitivity to toxic pollutants, and the harmless nature of involved substances.

2.6.4 Dyes used in Ethiopia's textile industries

In Ethiopia, the textile industry is among the major manufacturing industries, in which the government has given special care to make good for the growth and transformation plan (GTP-II). Most of them are involved in processing natural fibers, particularly cotton. There are diverse classes of dyes used in Ethiopia's textile dyeing and printing operations. The most commonly used dyes are reactive and direct dyes for coloring cotton. Worldwide Synthetic textile dyes used each year are gone during manufacture and processing operation and 20% of these dyes discharge into the environment through effluents that result from the treatment of residual industrial waters (Yusuf, 2019). Among the various classes of dyes, Reactive dyes are the brightest class of soluble dyes used by the Ethiopian textile industry as their pigment value is very high. It is used commonly in textiles industries regarding favorable characteristics of bright color, water-fast, simple application techniques with low energy consumption (Nimkar, 2018).

2.6.5 Methods of dye removal from textile wastewater

Currently, numerous methods are developing for removing dyes from textile wastewater containing dye effluents. Generally, technology can be divided into three main classes: biological, chemical, and physical methods (Rytwo *et al.*, 2002). All of them have their advantages and drawbacks. Because of high cost and final disposal problems, many of these conventional methods for treating textile wastewater containing dye effluents have not been usually applied on a large scale in the textile and paper Industries (Hasan *et al.,* 2008). The methods applied for the removal of dyes from textile wastewater containing dye effluents include adsorption, membrane filtration, ozonation, chemical precipitation, ion exchange, flocculation, membrane separation, etc. Among the adsorption method is an advantageous over the other methods, because of its simple design with a sludge free environment, concerning their efficiency in the removal of contaminants and it involves low investment costs. Adsorption does not have an adverse environmental effect on the treatment of textile wastewater containing dye that's why in developing countries like Ethiopia it is a good study area where it becomes interesting.

Physical methods

There are many physical methods available for textile wastewater treatment. One of the classes of such methods is the membrane process and they are being increasingly used in the dye removal process for the recovery of valuable compounds from the wastewater and the recycling of the water. The membrane technology mainly revolved around trapping or

filtering the pollutant through physical means and thus, separating them with the effluent. The factors that determine the type and porosity of the filter are the specific temperature and chemical composition of the wastewaters. There are also additional different physical methods that are used for the removal of dyes from wastewater, Coagulation and flocculation are physical methods that are used for the decolorization of wastewater comprising disperse dyes. These methods have low decolorization efficiency and a high generation of sludge. (Aksu & Kabasakal, 2004).

Chemical methods

Chemical methods for removal of dyes are taken place by the addition of chemicals like lime aided with aluminum sulfate which has a disadvantage of the additional cost of a chemical, but they are the most common methods for decolorization of textile wastewater due to their ease to use. These treatment methods include coagulation or flocculation combined with flotation and filtration, precipitation, flocculation with Fe (II)/Calcium hydro oxide, electro flotation, electrokinetic coagulation, conventional oxidation methods by oxidizing agents (ozone), irradiation or electrochemical developments. These treatment techniques are often expensive, and even if the dyes are removed, the accumulation of concentrated sludge creates a disposal problem. During the application of this method for dye removal, the probability of a secondary pollution problem occurring is high because of excessive chemical use. (Marandi & Bakhtiar Sepehr, 2012). Now a day, other developing technologies (techniques), known as advanced oxidation processes, which are based on the generation of very powerful oxidizing agents such as hydroxyl radicals, have been applied with success for pollutant degradation.

Biological methods

Biological treatment methods for removal of textile wastewater are dependent on the amount of dissolved matter (waste) and their efficiency is affected by micro-organisms load, temperature and the amount of organic loading rate, etc. This treatment is carried out in activated sludge and a rotating biological contactor. As compared to physical and chemical methods biological systems for the treatment of wastewater is an alternative and most economical method because of their low-cost method. Biodegradation methods such as adsorption by (living or dead) microbial biomass, fungal decolorization, bioremediation systems, and microbial degradation are commonly used in the treatment of manufacturing and industrial effluents. Microorganisms such as yeasts, bacteria, fungi, and algae can accumulate and degrade different pollutants. (Joutey *et al.,* 2014) In this method, the selected microorganisms familiarize themselves with the pollutant and eventually develop

new resistant strains. The strains can let the microorganisms transform the toxic wastes into less harmful forms. Microorganisms such as bacteria, fungi, algae, yeasts, and the plant can decolorize the dye effluent. (Khan *et al.*, 2012)

However, their application is often restricted because of technical constraints. Biological treatment requires a large land area and is constrained by sensitivity near diurnal variation as well as the toxicity of some chemicals and less flexibility in design and process operation. (P.E.Kumar, 2015). This method of treatment is unable to obtain satisfactory color elimination with current conventional biodegradation processes.

2.7 Adsorption Phenomena: Surface Process

Adsorption is a process that occurs when a gas or liquid solute accumulates on the surface of a solid or a liquid (adsorbent), forming a molecular or atomic film (the adsorbate). Adsorption is a surface phenomenon. Formally adsorption may be defined as a process in which the concentration of a chemical species is greater on the surface than in the bulk resulting from inelastic collision suffered by molecules on the surface. In industrial, activated charcoal, synthetic resins are used as adsorbents for water purification. The species that are adsorbed are called adsorbate and the material of the surface on which adsorption takes place is called adsorbent. Adsorption strictly refers to the accumulation of adsorbate on the surface only due to the residual field of force. It is different from absorption, in which a substance diffuses into a liquid or solid to form a solution. The term sorption encompasses both processes, while desorption is the reverse process. Various physical, chemical, and biological treatment techniques can be employed to adsorb color from dye-containing wastewaters (Zietzschmann, 2021).

2.7.1 Properties of adsorbate: organic ionic dyes

A dye can generally be described as an organic colorant that has an affinity to the substrate to which it is being applied and consists of a color-producing structure. Dyes can be firmly fixed to the fabrics and other supporting materials used in textile, food, and other industries for imparting different shades of colors. Methylene blue (MB), is the typical organic cationic dye (Sanusi, 2020) and also its maximum absorbance wavelength is 664 nm. Methylene blue is a heterocyclic aromatic chemical compound with the molecular formula $C_{16}H_{18}N_3SCl$ and its IUPAC name is 3, 7-bis (Dimethylamino)-phenothiazin-5-ium chloride. It has many uses in a range of different fields, such as biology and chemistry. At room temperature, it appears as a solid, odorless, dark green powder that yields a blue solution when dissolved in water. Methylene blue is widely used as a redox indicator in

analytical chemistry. Solutions of this substance are blue when in an oxidizing environment but will turn colorless if exposed to a reducing agent. The methylene blue is unable to penetrate viable cells leaving them unstained. In the human body, methylene blue is highly stable; if ingested, Methylene blue has some other adverse effects on the human body (Karaghool, 2021).

2.7.2 Adsorption isotherms

Adsorption is usually described through isotherms. Many different types of isotherms have been observed in the literature (Al-Ghouti & Da'ana, 2020). These isotherms can have very different shapes depending on the type of adsorbent, the type of adsorbate, and intermolecular interactions between the solute and the surface. The variation of surface coverage (Θ) with equilibrium pressure (or concentration in the case of solution) at a given temperature is called adsorption isotherm. According to the IUPAC classification, there are different types of adsorption isotherm as follows (Al-Ghouti & Da'ana, 2020).

a) Type 1: This shape of the isotherm is characterized by the asymptotic approach of a monolayer of adsorbate on the surface.

b) Type 2: This is the most common type of isotherm corresponding to the multi-layer formation on a surface of high adsorption potential.

c) Type 3: This pattern of isotherm is comparatively uncommon, corresponding to multilayer formation on the solid.

d) Type 4 & 5: These are analogous to types 2 & 3 on porous adsorbents where the adsorption is limited by the volume of mesopore, causing the adsorption to level off at a pressure less than the saturation pressure of adsorbate. They reflect capillary condensation and may show a hysteresis effect.

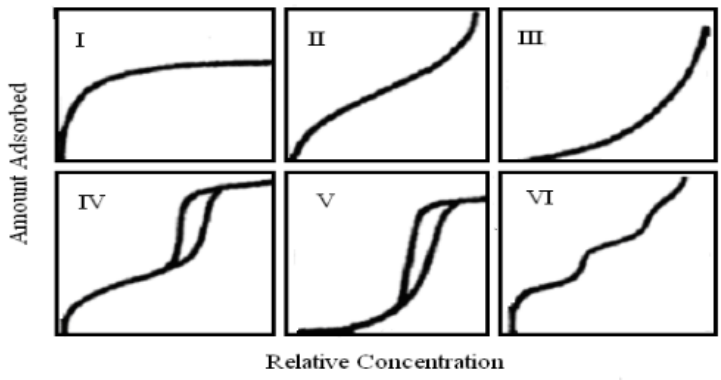

Figure: 2.8: IUPAC Classification of adsorption isotherms.

2.7.3 Model of adsorption isotherms

Several theoretical models were proposed to explain the experimental adsorption isotherms (Saadi et al., 2015). (a) Langmuir isotherm. (b) Freundlich isotherm. (c) BET isotherm. (d) Temkin isotherms etc.

(a) Langmuir Isotherm: Characteristics feature of Langmuir isotherm equation:

1. Adsorption is limited to monolayer formation.

2. In the case of physisorption, this equation satisfactorily explains adsorption behavior only at low surface coverage and at low adsorbate pressure.

3. In the case of chemisorptions that are associated with monolayer coverage Langmuir equation is quite consistent.

The model of the Langmuir isotherm is reported as follows:

$$qe = \frac{qm\ \ Kl\ \ Ce}{1 + Kl\ \ Ce} \quad \text{.....(Eq1)}$$

Where q_m ($mg * g^{-1}$) is the maximum adsorption capacity of the bioadsorbent and KL ($L * mg^{-1}$) is the Langmuir equilibrium counter related to bioadsorption energy.

(b) Freundlich adsorption isotherm: Freundlich model is described by an empirical equation used for systems with a high degree of heterogeneity. In this model, it is assumed that adsorption occurs at different sites and the formation of multilayer occurs with different adsorption energies. It leads to an exponential decrease in energy as the coverage of the surface originates.

The model of the Freundlich isotherm is reported as follows:

$$q_e = K_f\, C_e^{(1/nf)} \quad \text{.....(Eq2)}$$

where qe ($mg * g^{-1}$) is the capacity of bioadsorption of the metal, Ce ($mg * L^{-1}$) is the concentration of the metal in the equilibrium, and K_f($mg * g^{-1}$($L * mg^{-1}$) ($1/n_f$)) and n_f (dimensionless) are the constants of the Freundlich isotherm and are related to the capacity of biosorption and intensity, respectively; Freundlich constant (n_f) depends on the adsorption capacity, and it is used to evaluate the favorability of adsorption. The values of n_f between 2 and 10 indicate a high adsorption capacity, while values between 1 and 2

indicate a moderate adsorption capacity, and values less than 1 indicate a small adsorption capacity.

2.7.4 Factors affecting adsorption of dyes

There are many factors affecting dye adsorption such as pH, temperature, amount of adsorbent dosage, initial dye concentration, etc (Aboelfetoh *et al.,* 2020).

1) PH of the Solution: One of the most important factors affecting the capacity of adsorbents in wastewater treatment is solution pH. The effect of pH solution on the adsorption can be determined by preparing adsorbent–adsorbate solution with fixed dye concentration and adsorbent dose but with different pH by adding NaOH (1 M) or HCl (1 M) solutions to adjust pH and then shaken until equilibrium.

2) Effect of amount of adsorbent

Adsorbent dosage is another important process parameter because this determines the capacity of an adsorbent for a given amount of the adsorbent at any operating condition. The effect of the amount of adsorbent on the adsorption process can be determined by preparing adsorbent adsorbate solution with different amounts of adsorbents added to fix initial dye concentration and fixed initial solution pH then shaken together until equilibrium is achieved.

3) Effect of contact time

Adsorption of dyes found to extend with a rise of your time over adsorbent. The quantity of dye adsorbed on clay was found to be fast at the initial period of contact time then become slow and stagnant with the rise in contact time; the mechanism of adsorbate removal is often described within the migration of the dye molecule from the solution to the adsorbent particle and diffusion through the surface.

4) Effect of initial dye concentration

Adsorption capacity with the adsorbent increases with the rise of dye concentration till saturation is reached. Initial dye concentration generates a big driving gradient force to overwhelm mass transfer resistance to the dyes between solid and aqueous phases.

CHAPTER THREE

MATERIAL AND METHODS

3.1 Materials and Chemicals

The major equipment's and apparatus used during this thesis work were analytical balance, mortar, and pestle, 250ml plastic bottles, Sieves (200-250mm size), pH meter, 50-250ml size beaker, measuring cylinder, conical flask, digital oven, UV-DRS (UV-Vis NIR CLB, Model V-770), ATR-FTIR (Perkin Elmer spectrum 65 model FTIR), P-XRD (XRD-7000, SHIMADZU Corporation, Japan), SEM (JCM-6000plus SEM, SHIMADZU Corporation, Japan), crucible, volumetric flasks (50-250 ml), test tubes, glove, and Whatman filter paper, etc

Most of the chemicals used in this thesis work were analytical grades obtained from different chemical suppliers. The cinnamon plant bark was purchased from Adama town local market. The chemicals used include $AgNO_3$, methylene blue, $NaNO_3$, $KMnO_4$, 98% H_2SO_4, 36% HCl, 30% H_2O_2, NaOH, NH_3, chloroform, graphite powder, distilled water, and tap water.

3.1.1 Experimental site

The synthesis of Ag NPs, rGO, and rGO/Ag NCs biosorbent and all batch adsorption experiments were carried out at the Applied Chemistry Department Laboratory of Adama sciences and Technology University and Wolkite University. The synthesized samples were characterized at Addis Ababa science and Technology University Central Laboratory and Adama science Technology University Department of Material Engineering.

3.2 Experimental Design and Procedures

3.2.1 Preparation of cinnamon bark extract

The preparation of the extract was done using the reported procedure with minor modification. The bark of the cinnamon plant was ground by using a mortar and pestle to a fine powder. Then 5gm of cinnamon powder was dispersed in 100 mL deionized water in a conical flask and boiled for 45 minutes and later cooled to room temperature. The dispersion was filtered to obtain a clear solution of cinnamon extract and stored in a refrigerator at 4°C until further use (Moosavi *et al*., 2015).

3.2.2 Preparation of graphene oxide (GO)

The graphene oxide was prepared by using the Hummer method with little modification. Accordingly, 5gm graphite powder and 2.5gm sodium nitrate were mixed with 120 mL of 98% sulfuric acid in 1000 mL of the conical flask (Suresh *et al.,* 2015). The mixture was stirred for 30 min in an ice bath followed by the addition of 12gm potassium permanganate with vigorous stirring at a temperature of below 20°C. The stirring continued overnight and 150 mL of distilled water was slowly added. The reaction temperature was rapidly increased to 98°C and 50 mL of 30% H_2O_2 was added. Then the product sample was washed with 5% HCl, deionized water, and then finally dried.

3.2.3 Reduction of graphene oxide (GO) to reduced graphene oxide (rGO)

To reduce the prepared graphene oxide into reduced form, 3gm of GO was dispersed in 100 mL distilled water by stirring for a period of 3 h. The suspension was mixed with 50 mL Cinnamon extract and refluxed for 45 min at 90℃. The product was also washed with distilled water, dried, and stored (Suresh *et al.*, 2015).

3.2.4 Green synthesis of Ag NPs

The Ag NPs were synthesized by using cinnamon bark extract as the green reducing agent. 50 mL of a clear filtered solution of cinnamon bark extract was added to 100 mL of 0.3M $AgNO_3$ solution stirred at room temperature for 4 h and heated for 30 min at 40-45ºC. The solution color changed from yellow to dark brown were indicating the formation of Ag NPs. The final product was centrifuged at 2000 rpm for 20 min and washed twice with deionized water then finally dried (Supritha, 2021).

3.2.5 Synthesis of reduced graphene oxide-silver nanoparticle nanocomposite (rGO/Ag NP)

Cinnamon bark aqueous extract plays a dual role as a reducing agent for both the graphene oxide (GO) suspension to rGO and silver nitrate ($AgNO_3$) to Ag NP, simultaneously. The GO suspensions are prepared from graphite powder using Hummer's method (Suresh *et al.,* 2015). 5 gm of the prepared GO and 5 gm of $AgNO_3$ were added in a conical flask, then 100 ml of distilled water was added with continuous stirring on a magnetic stirrer for 2 h at 90 °C, and also 50 ml of cinnamon bark aqueous extract was added which act as a reducing agent and the suspension was stirred continuously for 3 h. UV–vis spectrophotometric measurements were carried out to confirm the synthesis of the

nanocomposite. Later, the sample was centrifuged at 2000 rpm for 10 min and the product powder was dried and stored for further analysis (Supritha, 2021).

3.3 Phytochemicals tests of cinnamon bark extract

The cinnamon bark extracts were screened for flavonoids, tannins, coumarins, saponosid, glycosides, anthocyanin, terpenoids, and phenols test. The aqueous solution of the sample was prepared according to the method described (Ghareeb et al., 2018) with little modification and the result clear filtered extract solution was used in tests.

3.3.1 Test of coumarins (Alkaline reagent test)

In a test tube, 2 mL of NaOH was added to 2 mL of the cinnamon extract solution. The development of a greenish-yellow or blue fluorescence indicated a positive test for Coumarins (IK & Uthman ISAH, 2015)

3.3.2 Test of Tannins

2 mL of cinnamon extract solution was added to 2 mL of water followed by drops of dilute ferric chloride solution (0.1%). A green to blue-green (cathechic tannins) or a blue-black (gallic tannins) coloration were positive indicators (Dandjesso, 2012).

3.3.3 Test of flavonoids

Flavonoids were tested by adding drops of Lead acetate solution (10%) to 1 mL of cinnamon extract. The formation of a yellow precipitate showed the presence of flavonoids (IK & Uthman ISAH, 2015).

3.3.4 Test of glycosides

Glycoside test was performed by adding 2ml of cinnamon solution into 4ml of glacial acetic acid containing one drop of 5% ferric chloride solution which was under laid with 1 ml of concentrated H_2SO_4. A brown ring obtained at the interface indicates the presence of glycosides (Dandjesso, 2012).

3.3.5 Test of phenols

A positive test for the phenol group was obtained when 1 mL of cinnamon extract solution was treated with drops of ferric chloride (5%) and observed for the production of deep blue or black color (Sofowora, 1996).

3.3.6 Test of anthocyanin

1 mL of the mixture contained HCl (2M) and ammonia (4M, 1mL) were added to 1 mL of cinnamon extract solution. The color change from pink-red to blue-violet indicates the presence of anthocyanins (Dandjesso, 2012).

3.3.7 Test of terpenoids (Chloroform test)

The terpenoids test was performed by mixing 2 mL chloroform with 2 mL cinnamon extract solutions. Then 2 mL of concentrated H_2SO_4 was added to this mixture and heated in a water bath (65°C) for 120 seconds. The presence of terpenoids was indicated by a reddish-brown tint at the interface (Sofowora, 1996).

3.3.8 Test of saponosids (frothing test)

About 2 mL of cinnamon extract solution were introduced into a test tube containing 2 mL of distilled water. The tube was stopped and shaken vigorously for about 15 seconds. Allowed to stand for 15 min, persistent frothing indicated the presence of saponosids (Sofowora, 1996).

3.4 Characterization studies

The synthesized reduced graphene oxide, silver nanoparticles, and the reduced graphene oxide-silver nanocomposite were characterized using various instrumental techniques to confirm the success of the synthetic procedure and to determine the morphologies, particle size, and functional group and other properties required for the material to be used as adsorbent are meeting. In this regard, UV-DRS, FTIR, Powder XRD, and SEM were employed to characterize the synthesized sample.

3.4.1 P-XRD analysis

The crystal structure and phase of rGO, Ag NPs, and rGO/Ag NPs nanocomposite, analysis was done by taking a small amount of the powder and grounded to fine particle and analyzed by P-XRD (XRD-7000, SHIMADZU Corporation, Japan) equipped with a Cu target for generating a Cu Kα radiation with λ = 0.15406 nm. The 2θ record ranges from 10^0-80^0 while the accelerating voltage and applied current are held at 40 kV and 50 mA, respectively. The particle size (D) of the powders was calculated by using Scherer's Formula;

$$D = \frac{k\lambda}{B\cos\theta} \quad \text{..... (Eq3)}$$

3.4.2 UV-DRS analysis

The synthesized rGO, Ag NPs, and rGO/Ag NP NCs were analyzed by using UV–Vis DRS a Perkin Elmer Lamda-2 spectrophotometer (UV-Vis NIR CLB, Model V-770), with a spectral range of 200–800 nm to study optical properties, and calculate the bandgap energy of each prepared samples by using Kubelka-Munk(K-M) function.

3.4.3 Fourier Transform Infrared Spectroscopy (FTIR-ATR) analysis

FTIR-ATR characterization was performed to identify the functional groups existing on the cinnamon plant extract, reduced graphene oxide, silver NPs, and rGO-Ag NCs. FTIR within ATR analysis was conducted for each of the prepared samples by using a Perkin Elmer spectrum 65 model FTIR spectrometer in average wavelength from 4000 to 400cm^{-1} with a resolution of 2.0 $cm^{-1}$to observe the changes in functional groups.

3.4.4 Scanning electron microscopy (SEM) analysis

Scanning electron microscopy (SEM) was used to study the surface morphology of the three synthesized samples. In this study morphology analysis of the samples was investigated by using SEM (JCM-6000plus BENCHTOP SEM, SHIMADZU Corporation, Japan). The SEM images were noted from different areas of samples at 15.0KV at varying resolutions from 500x to10,000x and the instrument operated at constant beam energy.

3.5 Removal of methylene blue (MB) using Ag NPs, rGO, and rGO/Ag NCs by sorption

3.5.1 Preparation of working standard solutions

In this study, MB powder was used as the adsorbate molecule in adsorption experiments. Preparation of stock solution of MB was carried out by dissolving 1 g of MB in 1000 mL distilled water to get 1000 mg/L. Further 10, 15, 20, and 25 mg/L of working standard solutions of MB were prepared from the standard 1000 mg/L dye solution by using dilution law (Mulushewa *et al*., 2021).

3.5.2 Batch sorption experiment

A batch mode sorption study for individual parameters was carried out using a 250 mL conical flask. The effects of different parameters such as pH, adsorbent dose, adsorbate concentration, and contact time are investigated by varying any one of the parameters and keeping the other parameters constant, and study adsorption isotherms, adsorption kinetics to determine how the change in removal capacity induced by these factors. For each

measurement, samples should be periodically taken out of the flask then shaken and filtered using a Whatman filter paper. The investigate ranges of the experimental variables was as follows: pH of solutions (2, 4, 6, 8, & 10), adsorbent dosage (40, 60, 80, 100, 120 mg), initial concentrations (10, 15, 20 & 25 mg/L), and contact time (30, 50, 70, 90 & 110 minutes). The absorbance of the filtrate solutions was determined by using a UV-visible Spectrophotometer at the maximum wavelength of 664 nm and it is possible to calculate the removal efficiency of Ag NPs, rGO, and rGO/Ag NCs by using the Equation 4.

$$Removal\ efficiency\ (\%) = \frac{Co - Ce}{Co}\ x\ 100 \quad \text{..... (Eq4)}$$

Where C_0 is the initial concentration (mg/L) and Ce is the residual (equilibrium) concentration (mg/L) of the MB being studied.

The removal capacity of rGO/Ag nanocomposite is the amount of MB adsorbed per unit mass of adsorbent was calculated based on the mass balance principle Equation 5.

$$Removal\ capacity\ (qe) = \frac{Co - Ce}{M}\ x\ v \quad \text{..... (Eq5)}$$

3.5.3 Reusability test of rGO/Ag NPs nanocomposite

80 mg of rGO/Ag nanocomposite was added into 50 ml of MB solution with a concentration of 10 mg/L and then stirred for 50 min. Then the dye adsorbed nanocomposite was separated by centrifugation and desorption carried out by the addition of distilled water. The desorbed nanocomposite was separated and used for the second cycle of adsorption (Markandeya *et al.,* 2017). The same procedure was repeated at least five times to estimate the efficiency of methylene blue dye removal.

3.5.4 Sorption isotherms

Adsorption isotherms were investigated to evaluate the applicability of the adsorption process for the removal of MB from industrial wastewater. The interactions between the adsorbate and adsorbents also are described by several models for the adsorption isotherms, based on a set of assumptions that are mainly related to the heterogeneity/homogeneity of adsorbents, the type of coverage, and the possibility of interaction between the adsorbate species. The most commonly used equilibrium models are Langmuir and Freundlich isotherms (Yuan *et al.,* 2019). Therefore, adsorption isotherm experiments were conducted to examine the relationship between the solid phase and the solution phase concentration of the adsorbate at an equilibrium condition.

Langmuir isotherm determined by the following equation (6)

$$\frac{1}{\text{qe}} = \frac{1}{KL\ qmax} * \frac{1}{Ce} + \frac{1}{qmax} \ldots\ldots\ldots\ldots\ldots\ldots\ldots\ldots\ldots\ldots\ldots\ldots\ldots\ldots\ldots\ldots \text{(Eq6)}$$

Freundlich isotherm determined under the following equation (7)

$$\ln \text{qe} = \ln Kf + \frac{1}{n} * \ln Ce \ldots\ldots\ldots\ldots\ldots\ldots\ldots\ldots\ldots\ldots\ldots\ldots\ldots\ldots\ldots\ldots \text{(Eq7)}$$

3.5.5 Sorption kinetic studies

To investigate the adsorption rate processes, the most common models used to fit the kinetic adsorption experiments are pseudo-first-order and pseudo-second-order. The kinetics of adsorption describes the solute uptake rate, which in turn governs the residence time of adsorption reaction (Mulushewa *et al*., 2021). It is one of the important characteristics in defining the efficiency of adsorption.

Pseudo-first order kinetics determined under the following equation (8)

$$\ln(\text{qe} - \text{qt}) = lnqe - K1 * t \ldots\ldots\ldots\ldots\ldots\ldots\ldots\ldots\ldots\ldots\ldots\ldots\ldots\ldots\ldots\ldots \text{(Eq8)}$$

Pseudo-second order kinetics are determined by the following equation (9)

$$\frac{\text{t}}{\text{qt}} = \frac{1}{K2\ \text{qe}^2} + \frac{1}{qe} * t \ldots\ldots\ldots\ldots\ldots\ldots\ldots\ldots\ldots\ldots\ldots\ldots\ldots\ldots\ldots\ldots \text{(Eq9)}$$

CHAPTER FOUR

RESULT AND DISCUSSION

4.1 Phytochemical screening results

The presence or absence of different phytoconstituents viz. carbohydrate, glycoside, protein, tannins, saponins, flavonoids, and terpenoids were detected by the phytochemical screening methods with different chemical reagents. Phytochemical components are responsible for both pharmacological and toxic activities in plants. These metabolites are said to be useful to a plant itself but can be toxic to animals, including man (Paliwal *et al*., 2011; Sharma *et al*., 2011). The presence of these chemical constituents in this plant is an indication that the plant if properly screened the reducing and capping agent for synthesis of nanoparticles and could yield drugs of pharmaceutical significance.

Flavonoids, tannins, terpenoids, saponin, glycoside, and phenolic compounds were found in cinnamon bark extracts as a good positive result. The coumarins test was slightly positive but anthocyanin was a negative result indicative of its absence in the cinnamon extract. The images showing various color changes during the Phytochemicals screening tests were presented in Fig. 4.1 and the summary of the result was tabulated in Table 4.1. This result is consistent with previous literature reports (Dandjesso, 2012). Another previous study conducted on an aqueous extract of cinnamon bark reported that tannins, saponins, phenolic, and terpenoids were present, and hence the result of our study was in strong agreement with the reported results of phytochemical screening as shown in Table 4.1 and Fig. 4.1 (Ebana et al., 2016).

Table 4.1: Qualitative Phytochemical screening of successive extracts of cinnamon bark

Plant constituents	Results
Phenolic/ferric chloride test	++
Saponins/frothing test	++
Tannins/ferric chloride test	++
Flavonoids	++
Coumarins/alkaline reagent test	+
Glycoside test	++

Terpenoids/salowski test	++
Anthrocyanin/ammonia test	_

++ High content + moderate content − not found/No content

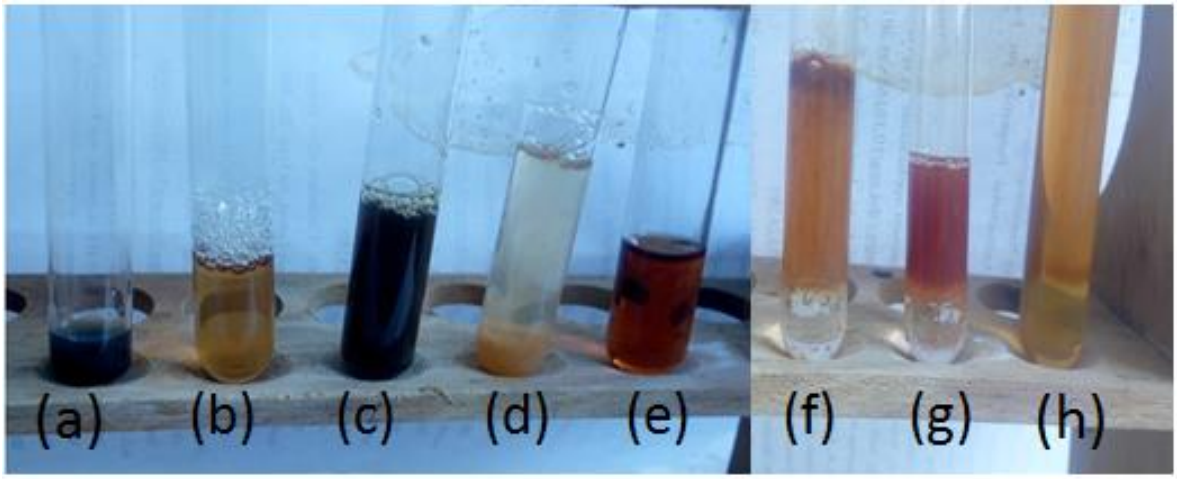

Figure 4.1: Phytochemical test result of cinnamon bark extract for (a) phenolic, (b) saponins, (c) tannins, (d) flavonoids, (e) coumarins, (f) glycoside, (g) terpenoids, and (h) anthrocyanin plant constituent metabolites.

4.2 Characterization of synthesized adsorbent

4.2.1 X-ray Diffraction analysis (P-XRD)

The crystalline phase structure and orientation of the rGO, Ag NP, and rGO/Ag nanocomposites were studied by XRD analysis at room temperature. Figure 4.2 shows a comparison of the XRD patterns of the rGO, Ag NP, and rGO/Ag nanocomposite samples recorded at a diffraction angle in the range 10º–80º. For rGO nanosheets showed a characteristic peak at an angle of 24.73º for the (002) crystal plane. As seen from the figure, the XRD pattern of rGO is not smooth and small peaks were observed. The reason seems to be that there were residual functional groups on the rGO sheets that affected the structure of the rGO sheet. For Ag NPs synthesized (Fig. 4.5), the diffraction profile had an intense peak at 2θ of 38.29°, 44.30°, 64.25°, and 77.12°, corresponding to (111), (200), (220), and (311) planes in Ag NPs reduced by cinnamon bark extract (JCPDS No. 04-0783) (Ibrahim, 2015).

The crystallinity and phase structure of the rGO/Ag NPs nanocomposite also were investigated via XRD analysis. Fig.4.2 illustrates the single-phase diffractogram of the material, which signifies that Ag NPs are perfectly embedded over rGO and behave as a

single entity. It represents the four significant sharp diffraction peaks at 2θ = 38.32°, 44.27°, 64.23°, and 77.03°, attributed to diffraction over (1 1 1), (2 0 0), (2 2 0), and (3 1 1) planes of the face center cube Ag crystalline phases (JCPDS No. 04-0783). The broad region at 2θ = 20–25° (002) corresponds to the amorphous nature of the rGO moiety (JCPDS No. 84-0713). These obtained results were in good agreement with previously reported literature (Hemmati et al., 2020).

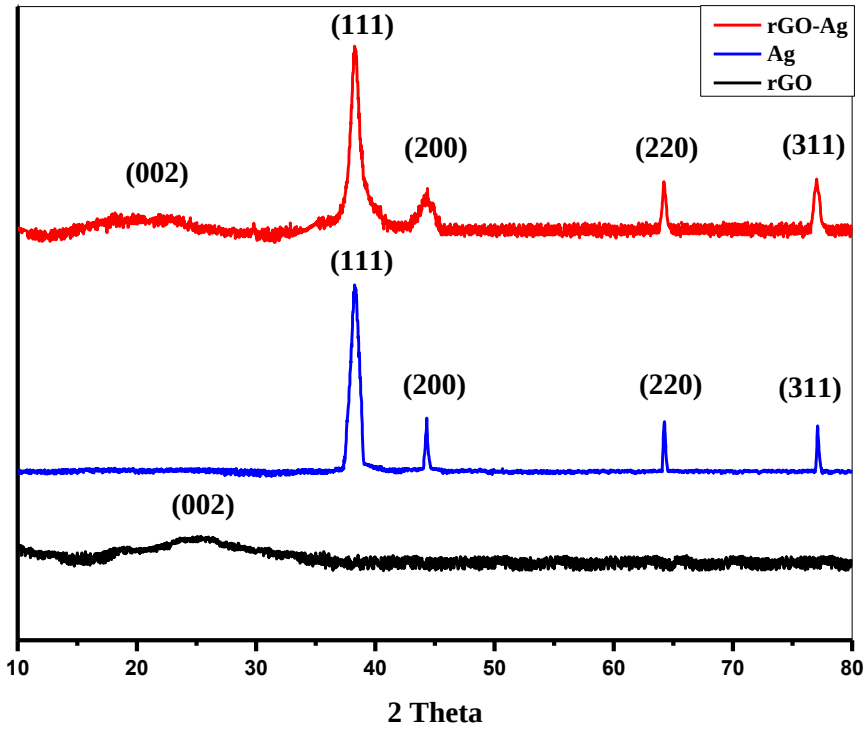

Figure 4.2 XRD patterns of rGO, Ag NPs, and rGO/Ag NPs nanocomposite.

Generally, from XRD analysis, Scherer's equation was applied to calculate each peak crystal size, interlayer distance (d-spacing), and average crystallite size of Ag NPs and rGO/Ag NPs nanocomposite (Gawade et al., 2017).

$$D = \frac{k\lambda}{\beta cos\theta} \quad \text{.....(Eq10)}$$

Where D is crystallite size, k is Scherer's constant, which is 0.9, λ is the wavelength of the X-ray radiation, which is 0.15406 nm, ß is peak width at half maximum (radians), and θ is Bragg's angle. Hence, the average crystallite size and inter-layer distance (d-spacing) for all samples were calculated and reported in Table 4.2.

Table 4.2 calculated crystallite sizes and interlayer distance (d-spacing) of rGO, Ag NPs, and rGO/Ag NPs nanocomposite from XRD data.

Sample name	2 theta	Theta	d (Aº)	FWHS	D (nm)	D average (nm)
Ag NPs	38.29035	19.14518	2.348742	0.87791	10.00461	
	44.30179	22.1509	2.042981	0.30389	28.9024	
	64.25056	32.12528	1.448552	0.21858	40.18277	
	77.12647	38.56324	1.235687	0.21671	40.52951	29.9nm
rGO/Ag NPs NCs	38.32	19.16	2.346993	1.15552	7.603208	
	44.27	22.135	2.044374	1.36506	6.436098	
	64.23	32.115	1.448966	0.37974	23.13599	
	77.03	38.515	1.236994	0.53607	16.38902	13.35nm
rGO	24.7318	12.3659	3.5969	12.5817	0.67415	0.67415nm

The XRD results revealed that the average particle sizes were 29.9 nm, 0.67 nm, and 13.35 nm for Ag NPs, rGO, and rGO/Ag NPs nanocomposite respectively.

4.2.2 UV-DRS Analysis

UV-diffuse reflectance spectroscopy is one of the most widely used techniques for the structural characterization of metal nanoparticles. Due to the unique optical properties of the Ag NPs, a great deal of information about the physical state of the nanoparticles can be obtained by analyzing the optical characterization of Ag NPs. It is known that the size and shape of the Ag NPs considerably change their optical properties since the surface-to-volume ratio increases with a decrease in the size of the particle. Ultraviolet-visible spectroscopy of the silver nanocrystals was performed in a Perkin Elmer Lamda-2 spectrophotometer and is shown in Fig. 4.3 the surface plasmon resonance band was detected for a peak at 341 nm confirming that the Ag NPs are shown different shape and particle size due to non-homogeneity (Singaravelan & Bangaru Sudarsan Alwar, 2015).

The reduction of GO to rGO was confirmed as the solution changed from brown to black color. In addition, the rGO exhibited a peak at 279 nm, which is a red-shift from the characteristic peak of GO at 230–240 nm shown in Fig. 4.3 supplements the success of the reduction process (Geetha Bai et al., 2016).

The UV-vis spectrum was used to monitor the formation of Ag nanoparticles on the surface of graphene. The rGO/Ag nanocomposites showed an obvious blue shift with a sharp peak positioned at 334 nm corresponding to the Ag NPs, where the rGO peak was moved to 272 nm due to the high intense peak arising from the deposition of Ag NPs on the rGO sheets. The blue shift of the plasmonic nanomaterials is associated with the structure, size as well as properties of the substrate. In addition the observed peak shift could be either due to a decrease in the size of the Ag NPs or due to the presence of rGO, the matrix on which the Ag NPs were deposited (Geetha Bai *et al*., 2016).

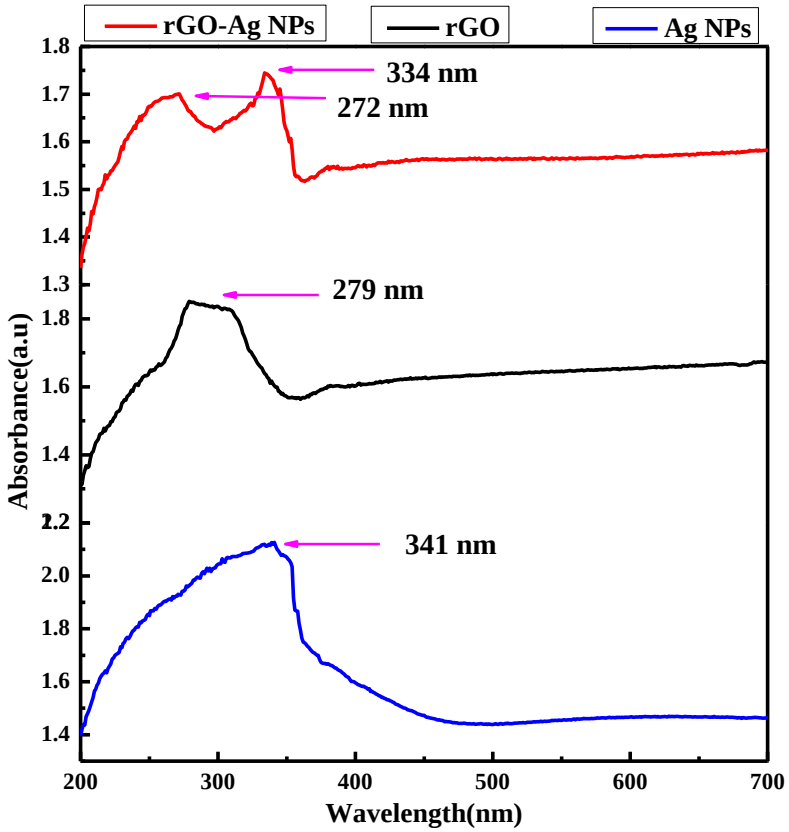

Figure 4.3: UV-Vis DRS spectrum of Ag NPs, rGO, and rGO-Ag NCs

Bandgap energy

The diffuse reflectance spectra were translated into the absorption spectra by the Kubelka-Munk method. Kubelka-Munk's equation is described as follows: $\alpha = 2(1-R)/2R$, where α is the absorption coefficient and R is the reflectivity at a particular wavelength (Suzuki & Kijima, 2005).

The bandgap energy can be determined using the Tauc relation. According to the Tauc relation, the absorption coefficient α for material is given by $\alpha = A(hv - Eg)n$. Where Eg is the bandgap, constant, A is different for different transitions, (hv) is the energy of a photon

in eV and n denotes the nature of the sample transition. The 'n' in the equation has values 1/2, 2, 3/2, and 3 for allowed direct, allowed indirect, forbidden direct, and forbidden indirect transitions respectively (Jeon et al., 2011). The tauc plot of the sample synthesized is given in Fig 4.4. It is reported that the optical gap energy of nano-sized crystals depends on their crystallite size; it increases with decreasing crystallite size in the nano-size range (Lu et al., 1996).

The absorption coefficient value is calculated from the diffuse reflectance using Kubelka–Munk equation,

$$F(R) = \frac{2(1-R)}{2R} = K/S \quad \text{.....(Eq11)}$$

Where, R is the absolute reflectance of the Ag NPs, rGO, rGO-Ag NPs nanocomposite, K, is the molar absorption coefficient, and S, is the scattering coefficient. The acquired diffuse reflectance spectrum is converted to Kubelka-Munk function F(R), which is equivalent to the absorption coefficient (α). Thus the vertical axis is converted into the quantity $(F(R)hv)^{½}$ and plotted against photon energy (hv). The indirect allowed $(F(R)hv)^2$ ploted graph result is does not used because its linearity is not fitted with straight line for the curve. In this study the bandgap value is obtained by the intercept of the fitted straight line of the linear part of the curve from $(F(R)hv)^{1/2}$direct allowed transition. The value of optical band gap energy was found to be 2.95 eV, 3.04 eV, and 3.24 eV for rGO, Ag NPs, and rGO-Ag NPs nanocomposite respectively shown in Fig. 4.4.

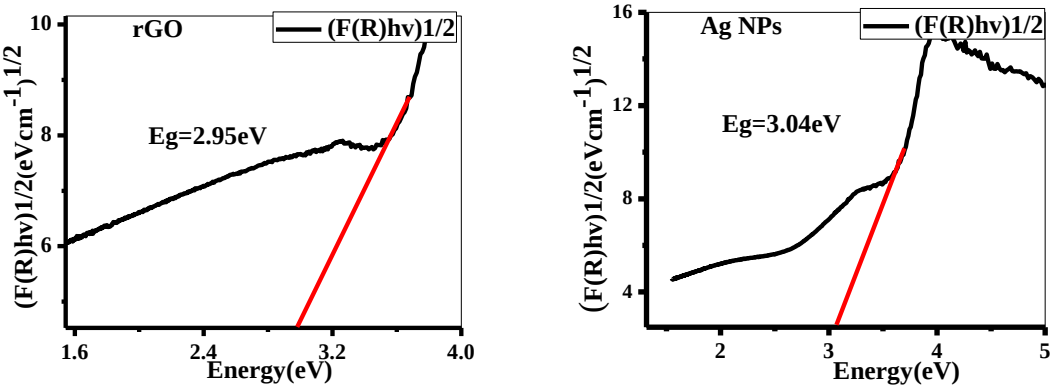

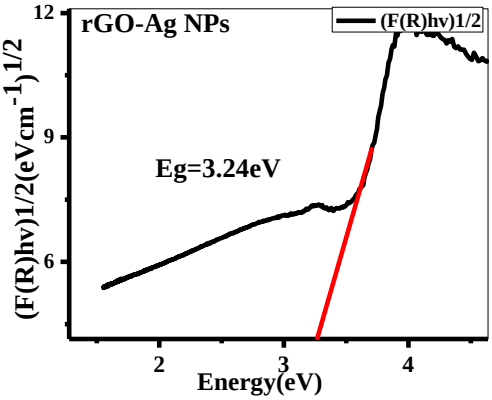

Figure 4.4: Band gap energy of rGO, Ag NPs, and rGO-Ag NPs nanocomposite.

4.2.3 Fourier transform infrared spectroscopy (FTIR-ATR) analysis

FTIR-ATR analysis was employed to evaluate the functional group present in rGO, Ag NPs, rGO/Ag nanocomposite, and cinnamon bark plant extract (PE) as shown in Fig. 4.5. Accordingly, due to the water-mediated green synthesis process in cinnamon plant extract, peaks were observed located at around 3314 cm^{-1} (O-H stretch of alcohol), 2984 cm^{-1}, (C-H stretch of alkanes), 2445 and 2148 confirms (C≡C stretch of alkynes), 1642 cm^{-1} are attributed to the vibration stretching of aldehyde carbonyl (C=O) groups, representing a high concentration of cinnamaldehyde. Other significant peaks were observed at 647 cm^{-1} (vibration of alkanes), 751 cm^{-1} (benzene rings =CH), 1059 cm^{-1} (C-O), 1260 cm^{-1} (C-O-C bond of aromatic acid ester), 1342 cm^{-1} (C-N stretch, aromatic amines), and 1488 cm^{-1} (C=C bond). All these characteristic peaks confirm that the plant extract is rich in phenolic and aromatic compounds, especially cinnamaldehyde and alcohol.

The dual role of the plant extract as a reducing and capping agent of the functional groups on the NP's surface was confirmed by FTIR analysis as shown in Fig. 4.5. The FTIR spectrum of Ag NPs showed reflectance bands located at 3170, 1730, 1597, 1284, and 1004 cm^{-1} respectively, which correspond to the O-H stretching, C=O stretching, C=C stretching, C−N stretching, C−C stretching, with different functional group adsorbed on the surface of NPs (Kim *et al.*, 2014). Since rGO was synthesized by the reduction of GO, similar peaks were also observed due to the residues of oxy-carboxyl functional groups. It observed that the peaks in reduced graphene oxide (rGO) were weak intensity peaks than graphene oxide at 1025, 1217, 1586, 1717, and 3166 cm^{-1} which indicates the C−C, C−O−C, C=C, C=O, and O-H stretching respectively. When compared to the cinnamon bark

extract, the intensity of these peaks was smaller in the other three spectra i.e. rGO, Ag NPs, and the rGO/Ag nanocomposite. The involvement of cinnamon bark extract as a green reducing agent during the reduction could be the source of these hydroxyl groups in rGO and rGO/Ag. In the spectrum obtained from rGO/Ag nanocomposite, the peaks at 3274, 1732, 1595, 1224 and 1030 cm^{-1} show the same pattern of reduced graphene oxide and silver nanoparticles, which exhibited the peak were present O-H stretching, C=O, C=C, C-O-C and C−C stretching respectively by using cinnamon bark extract as reducing and capping agent.

The overall FTIR spectra analysis revealed that the synthesis of reduced GO, Ag NPs and rGO/Ag nanocomposite using the cinnamon plant part extract was successful.

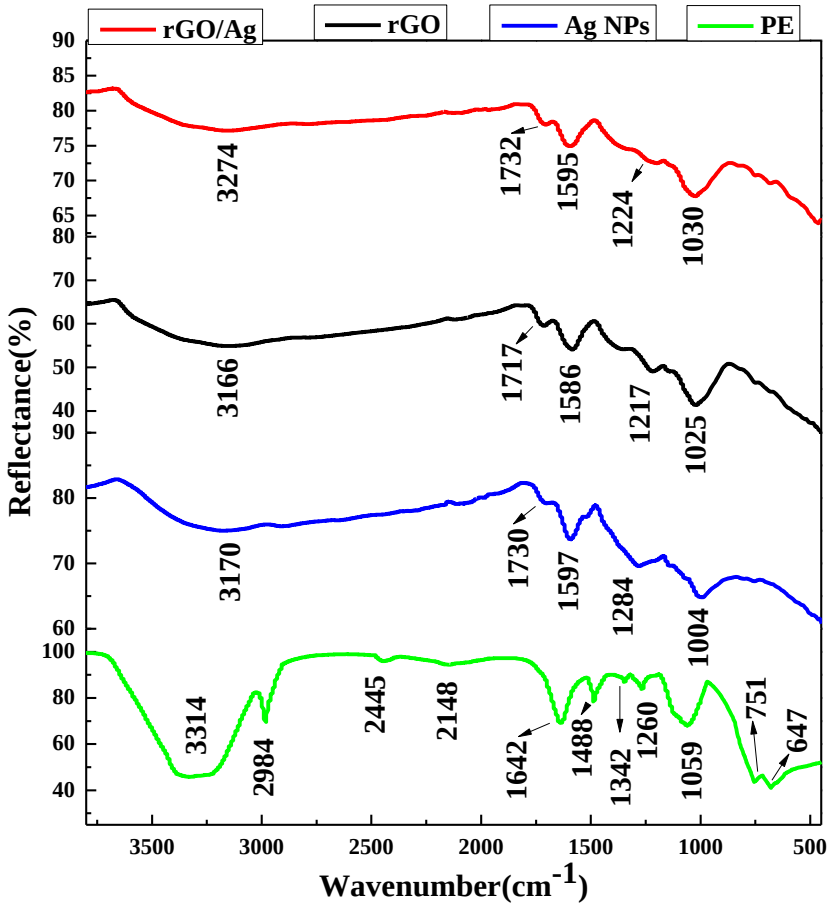

Figure 4.5: ATR-FTIR spectrum data of PE, Ag NPs, rGO, and rGO/Ag NPs NCs.

4.2.4 Scanning electron microscopy (SEM) analysis

The surface morphology of the synthesized rGO, Ag NPs, and rGO/Ag NP was characterized by using SEM (JEOL, JCM-6000Plus) at different magnification. As shown in Fig. 4.6 ($a_{1\&2}$), the synthesized silver nanoparticles indicate that mono-dispersive and

demonstrated the non-homogeneity of the particles in terms of their shape and size. It also shows different shapes like spherical, and triangular of Ag NPs with varying particle sizes found in the micrograph which is a good agreement previously reported literature (Lee & Jun, 2019). The observation of some larger nanoparticles may be attributed to the fact that silver nanoparticles have the tendency to agglomerate due to their high surface energy and high surface tension of ultrafine nanoparticles (Theivasanthi & Alagar, 2012). The fine particle size results in a large surface area that, in turn, enhances the nanoparticles' catalytic activity.

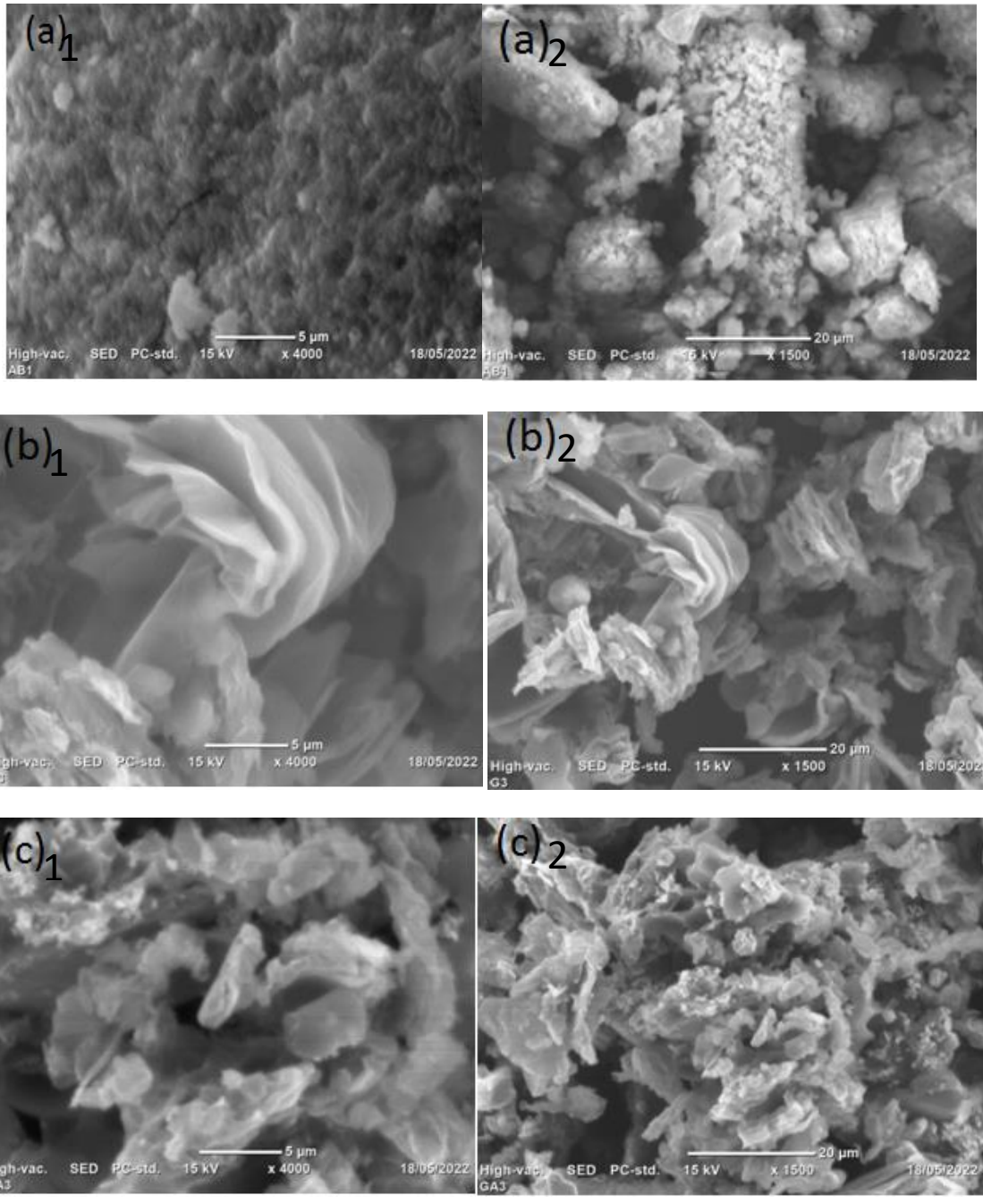

Figure 4.6 the SEM analysis of ($a_{1\&2}$) Ag NPs, ($b_{1\&2}$) rGO, and ($c_{1\&2}$) rGO/Ag NPs at different magnification.

Fig 4.6 ($b_{1\&2}$) shows that the formed rGO nanosheets were arranged together in stacked sheets, which confirms the reduction of GO. The image revealed an ultra-thin feature of rGO with wrinkles, which suggests the few layers are close together and form an interlinked structure (Singh et al., 2017).

For the rGO/Ag nanocomposite, as shown in Fig. 4.6 ($c_{1\&2}$), it was found that Ag nanoparticles are deposited on rGO nanosheets in the form of clusters. The Ag nanoparticles were deposited on rGO nanosheets due to the strong electrostatic and electronic interaction between rGO nanosheets and Ag nanoparticles (Mangalam et al., 2019).

4.3 Optimization of adsorbent for removal efficiency of methylene blue from aqueous solution

In this study we optimize the three synthesized adsorbent rGO, Ag NPs, and rGO/Ag NCs for the removal of methylene blue dye from aqueous solution. The need to optimize the precursor synthesized adsorbent were especially for silver nanoparticles there is a few previous study for removal of dyes, so I need to optimize this synthesized adsorbent to know in detail and as general to compare the optimized data from the composite data for removal efficiency because the composites to be expected enhance the removal capability c ompared to the parent material.

4.3.1 UV-Vis analysis of methylene blue dye solution

The chemical structure and UV-Vis absorption spectrum of MB in the aqueous solution are shown in Fig. 4.7. Four characteristic peaks at (246, 292, 614, and 664 nm) of MB are observed and they are similar to those reported previously (Yu et al., 2015). As indicated in Figure 4.7, methylene blue has two absorbance peaks at 614 and 664 nm in the visible region.

- The absorption band at high energy (π*-π* transition of the benzene ring) and a band at low energy around 660-670 nm (moving according to the pH of the solution) and

- n- π* transitions (n is the free doublet on the nitrogen atom of the C=N bond and the free doublet of the S atom on the S=C bond). The peak at 614 nm is not a band but a shoulder and it corresponds to a vibronic transition 0-1 (level 0 of the ground state to level 1 of the excited state).

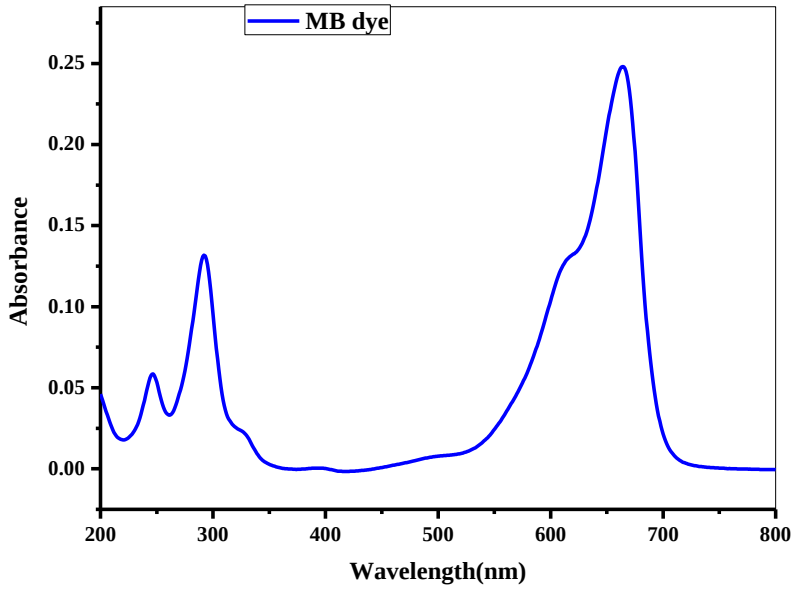

Figure 4.7: UV-Vis spectrum of methylene blue dye

4.3.2 Calibration plot of working methylene blue standard solution

The calibration plot for MB dye at 664 nm was used to determine the residual concentration in the filtrate after adsorption of MB dye using three different adsorbents from an aqueous solution. The obtained data from the calibration plot is given in Table 4.3 and figure 4.8.

Table 4.3: Methylene blue dye working standard solution calibration data

The initial concentration of MB(mg/L)	Absorbance
10	1.468
15	2.180
20	2.837
25	3.588

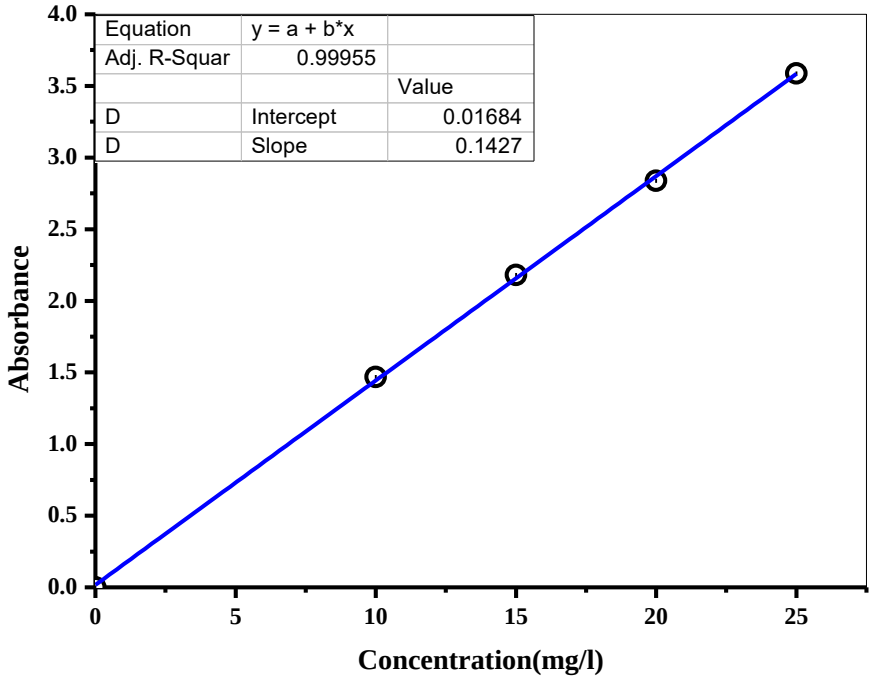

Figure 4.8: Calibration plot of working methylene blue standards solution.

4.4 MB dye adsorption by using Ag NPs, rGO, and rGO/Ag NPs nanocomposite

4.4.1 Effect of pH

The pH of dye solutions plays an important role in the adsorption process and especially in the adsorption efficiency, which is due to the charge of the adsorbent surface, degree of ionization of materials in solution, and also the separation of functional groups in the activated sites of the adsorbent. The influence of pH on the adsorption of dye was studied for three adsorbents separately by adding 80 mg of Ag NPs, rGO, and rGO/Ag NPs to 10 mg/L of methylene blue solution with pH values ranging from 2 to 10 for a contact time of 50 min. As shown in Fig. 4.9(a), dye uptake by Ag NPs increased as the pH of the solution increased because for cationic dyes such as MB, adsorption decreases in pHs lower than pHpzc due to the cationic nature of the adsorbent surface and increases in pHs higher than pHpzc due to the anionic nature of the adsorbent surface (Das et al., 2013). In this study, the adsorption of MB was increased to 10 by increasing pH, and its removal efficiency increased from pH 2 = (86.04%) to pH 10 = (90.03%).

The adsorption of methylene blue dye by rGO and rGO/Ag NPs nanocomposite was found to decrease with an increasing pH value of a solution, as shown in fig. 4.9 (b) and (c). This

shows that in an acidic medium, the efficiency of adsorption is greater than in a basic medium. The electrostatic attraction between positively charged H^+ ions that are present in lower pH and cationic charges on the dye is the main reason for the electrostatic adsorption. Thus, the optimum pH value for the adsorption of dye using rGO and rGO/Ag nanocomposite is found to be pH 2. The removal efficiency of rGO adsorbent increases from pH 10 = (94.31%) to pH 2 = (96.97%), but the removal efficiency of the two precursor adsorbents is lower than from rGO/Ag nanocomposite. In this nanocomposite, the removal efficiency also increased from pH 10 = (97.39%) to pH 2 = (99.98%).

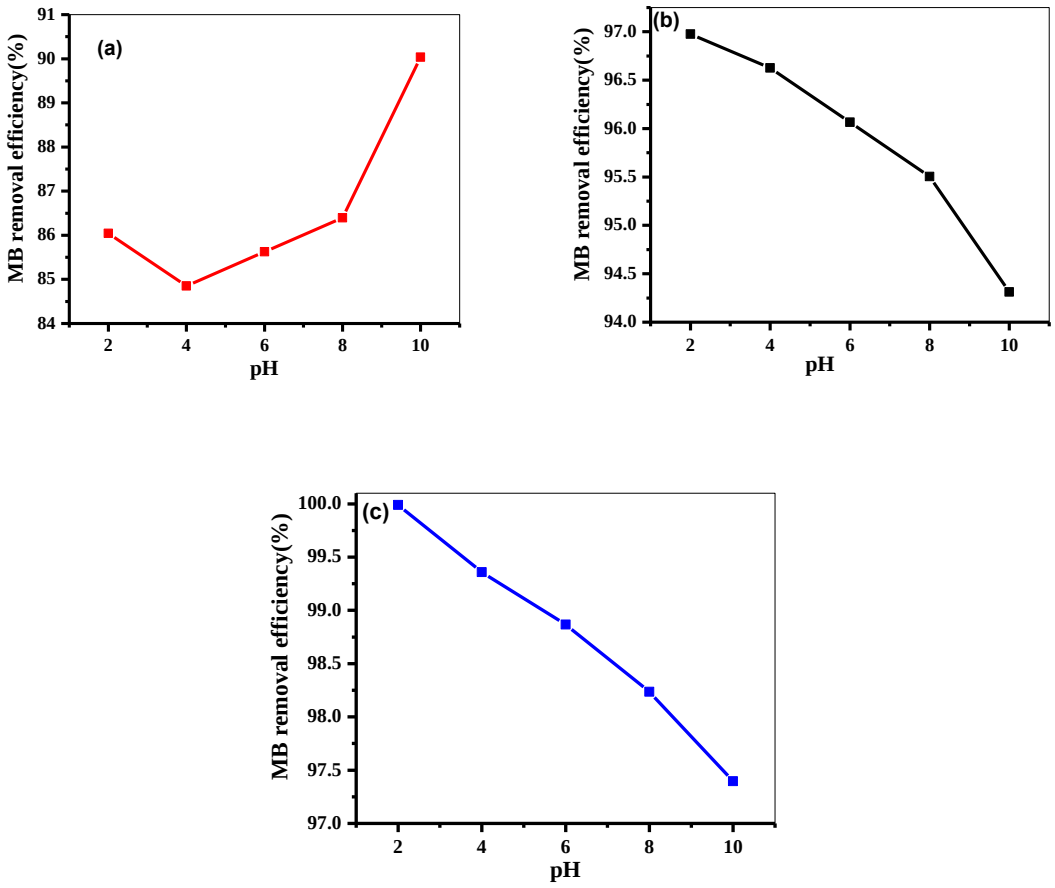

Figure 4.9: Effect of pH on MB dye removal by (a) Ag NPs, (b) rGO, and (c) rGO/Ag NP nanocomposite adsorbent at 80 mg adsorbent dose, 10 mg/L initial concentration, 50 minute contact time and 310 rpm.

4.4.2 Effect of adsorbent dosage

To study the effect of adsorbent dosage of Ag NPs, at PH 10, rGO at pH 2, and rGO/Ag NPs nanocomposite at pH 2 with time of 50 minutes, and 10 mg/L fixed concentration of MB dye was used. The adsorbent with different doses for each of the three synthesized

samples separately (40–120 mg) was used for this experiment. The impact of the adsorbent doses on the elimination effectiveness of MB by the selected Ag NPs, rGO, and rGO/Ag nanocomposite was shown in Fig. 4.10 (a), (b), and (c) respectively. In all three adsorbents, the results indicate that the percentage removal of MB dye increased from 88.89% to 90.03% for Ag NPs, 96.27% to 96.97% for rGO, and 98.79% to 99.98% for rGO/Ag NPs nanocomposite with an increase of adsorbent amount up to 80 mg. This was due to an increase in adsorption sites. Further increases in the adsorbent dosage did not affect dye removal; it is due to the formation of aggregation and lack of dye molecules for the adsorption (Wu et al., 2013). Thus, the optimum concentration of nanocomposite was found to be 80 mg, and this amount was used for further experimental analysis.

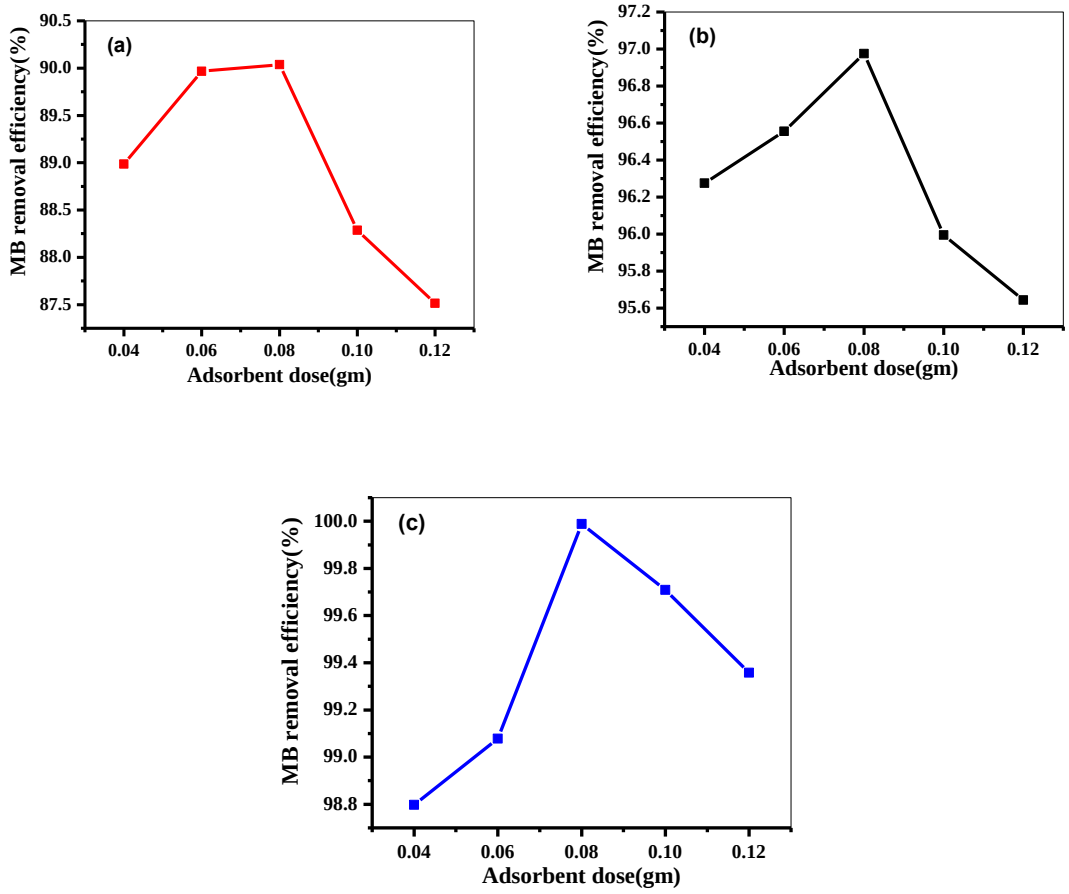

Figure 4.10: Effect of adsorbent dose on the removal of MB dye by (a) Ag NPs, (b) rGO, and (c) rGO/Ag NP nanocomposite adsorbent at pH 10 for Ag NPs, pH 2 for rGO and rGO/Ag NPs, 10 mg/L initial concentration, 50 min contact time, and 310 rpm.

4.4.3 Effect of contact time

Equilibrium time is one of the most important variables in designing cost-effective systems for wastewater refinement. As shown in Figures 4.11 (a), (b), and (c), the adsorption of methylene blue dye at an initial concentration of 10 mg/L was studied at different contact times (30–110 min) with an adsorbent dose of 80 mg for three synthesized adsorbents, Ag NPs at pH 10, rGO and rGO/Ag NCs at pH 2. Data showed that 50 minutes is sufficient to reach equilibrium conditions. The high adsorption rate in early contact times is due to several activated adsorption sites available for dye molecules that increase dye penetration to the adsorption surface. The concentration gradient decreases over time because of saturation of the adsorbent surface, and the removal percentage approximately remains constant.

At an initial 30 min up to the equilibrium time of 50 min of adsorption, the dye removal percentage was 88% to 90% for Ag NPs, 96.41% to 96.97% for rGO, and 98.86% to 99.98% for rGO/Ag NPs nanocomposite. As the time increases, the adsorption keeps on increasing and reaches equilibrium at 50 min with an adsorption efficiency of 99.98% for the nanocomposite adsorbent. This is due to the presence of a huge number of free adsorption sites during the initial stage of reaction, which then reduces as an increase in time and finally reaches equilibrium (Elmorsi, 2011).

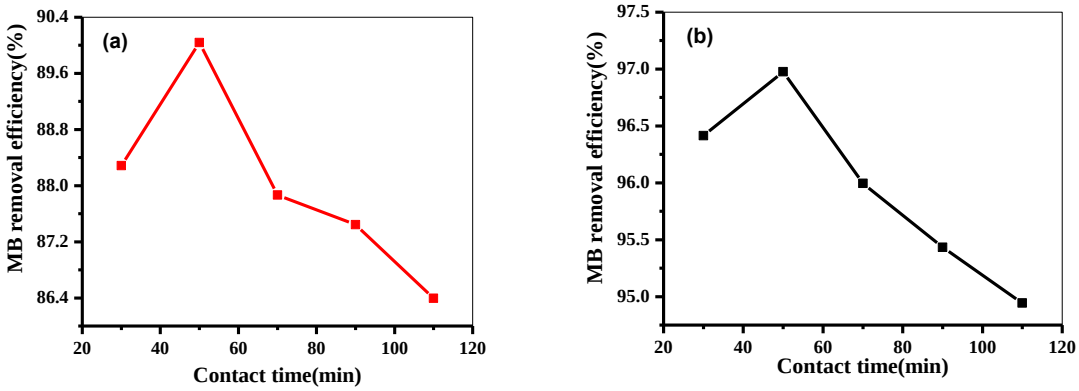

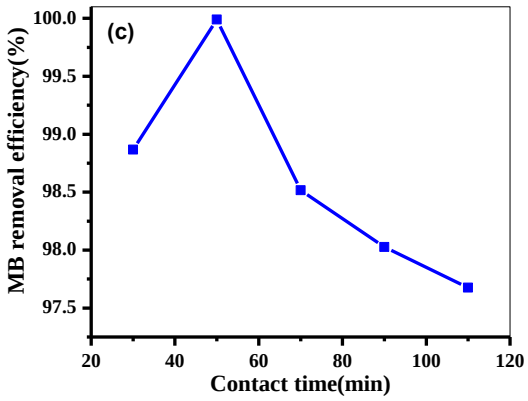

Figure 4.11: Effect of contact time on the removal of MB dye by (a) Ag NPs, (b) rGO, and (c) rGO/Ag NP nanocomposite adsorbent at pH 10 for Ag NPs, pH 2 for rGO and rGO/Ag NPs, 10 mg/L initial concentration, and 310 rpm.

4.4.4 Effect of initial concentration

To investigate the effect of initial dye concentration on adsorption properties, a series of experiments were conducted using different concentrations of MB solution (10, 15, 20, and 25 mg/L) with an 80 mg adsorbent dose of Ag NPs, rGO, and rGO/Ag NPs nanocomposite at pH 10 for silver NPs and pH 2 for rGO and rGO/Ag nanocomposite within 50 min of contact time. As shown in Fig. 4.12, the adsorption is very fast at a lower initial concentration of MB solution.

The result shows that removal efficiency was decreased with an increase in initial concentrations, although the amount of total MB accumulation increased. From this experiment, it was observed that about 90.03%, 96.97%, and 99.98% of MB were removed at an initial concentration of 10 mg/L by using Ag NPs, rGO, and rGO/Ag NPs nanocomposite adsorbents, respectively, at the same operating conditions shown in (Figure 4.12 (a), (b), (c)). The percentage of MB removal decreases with an increase in the initial dye concentration, which may be due to the saturation of adsorption sites on the adsorbent surface. At a low initial concentration, there are unoccupied active sites on the adsorbent surface, so most of the MB solution might contact the active sites of adsorbents. However, at a higher concentration, most of the dye was not able to contact the active surfaces because the active sites might have been occupied by the MB solution, which is consistent with the results obtained (Rahman et al., 2012).

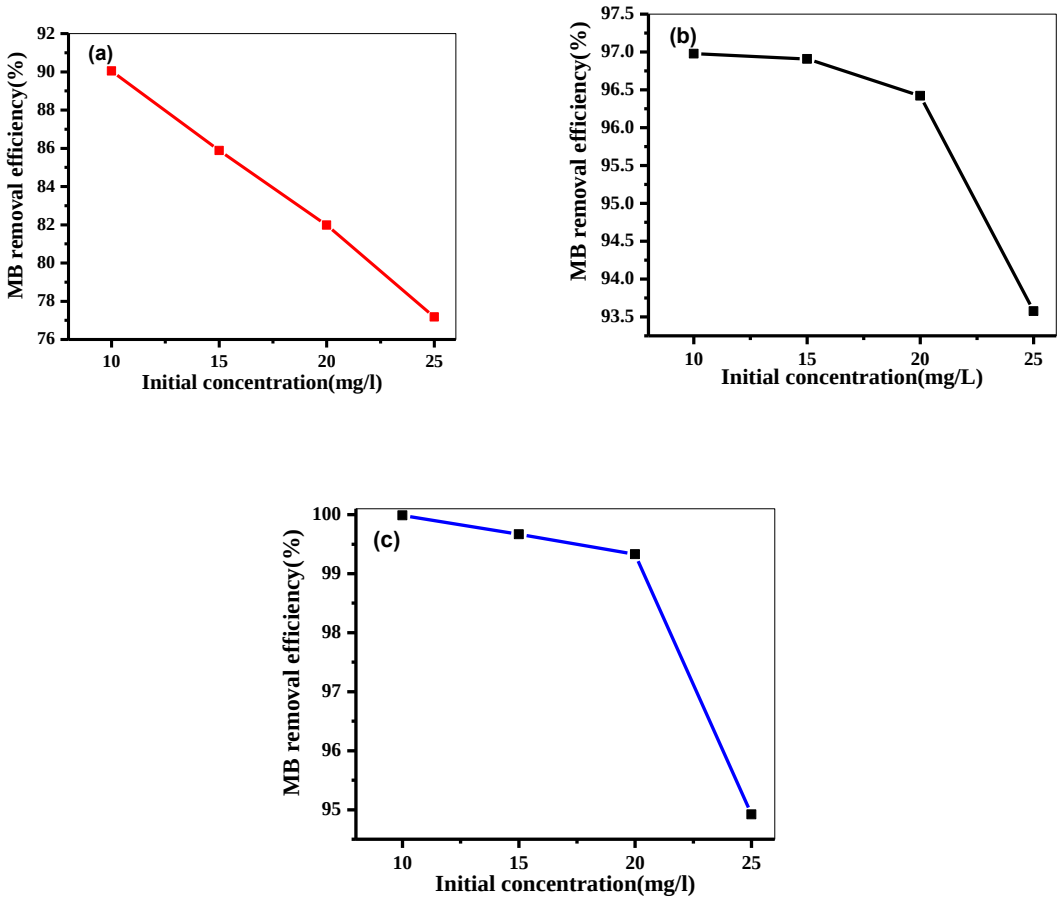

Figure 4.12: Effect of initial concentration on MB dye removal by (a) Ag NPs, (b) rGO, and (c) rGO/Ag NP nanocomposite adsorbent at pH 10 for Ag NPs and pH 2 for rGO and rGO/Ag NPs, 80 mg adsorbent dose, 50 min contact time, and 310 rpm.

4.4.5 Reusability test of rGO/Ag NP nanocomposite

The characteristic of a good adsorbent is to have both adsorptions as well as desorption capability that is of high efficiency. Fig. 4.13 shows the adsorption efficiency of rGO/Ag NPs nanocomposite at pH 2, time of 50 min and initial concentration of 10 mg/L was 99.98%, 96.55%, 92.35%, 87.79%, and 82.11% for first up to fifth cycle reusability, respectively. After five cycles, the adsorption efficiency of the nanocomposite remains more than 80%, which confirms that the synthesized rGO/Ag NP can act as a stable, efficient, and environmentally friendly adsorbent (Sun et al., 2011).

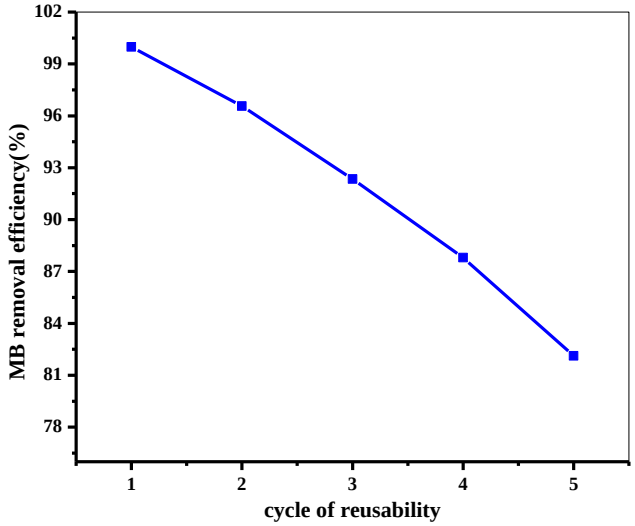

Figure 4.13: Reusability test of rGO/Ag NP nanocomposite adsorbent for the removal of methylene blue dye.

4.5 Adsorption isotherm

The adsorption isotherm indicates how retained particles diffuse between the liquid phase and the solid surface when equilibrium is achieved during adsorption. The examination of the isotherm information by fitting them to various isotherm models is a vital step in finding an appropriate model. The adsorption isotherm model was limited to the synthesized Ag NPs, rGO, and rGO/Ag NPs nanocomposites adsorbents were explored with Freundlich and Langmuir adsorption isotherms.

4.5.1 Langmuir adsorption isotherm model

The Langmuir adsorption isotherm is based on the formation of homogeneous monolayer coverage on the adsorbent surface, uniform energy of adsorption, and no interaction between molecules adsorbed on neighboring sites (Gemeay et al., 2017). The adsorption isotherms can be studied by determining the amount of dye adsorbed per unit mass of adsorbent (qe) and the concentration of dye in solution at equilibrium (Ce). In this, the Langmuir constant (K_L) and the maximum adsorption capacity (q_{max}) were obtained from the slope and the intercept of a linear form of the Langmuir equation, respectively (Md. Sandollah et al., 2020).

$$\frac{Ce}{qe} = \frac{Ce}{q_{max}} + \frac{1}{q_{max}\, K_L} \quad \text{.....(Eq13)}$$

The values of q_{max} (mg/g) and K_L (L/mg) was determined from the plot of Ce vs Ce/qe. The adsorption capacity is often correlated with the variation in the area and porosity of the adsorbent. Higher surface area and pore volume resulted in higher adsorption capacity (Kavitha & Namasivayam, 2007). The essential characteristics of the Langmuir isotherm model are often expressed by a dimensionless constant called the equilibrium parameter, R_L.

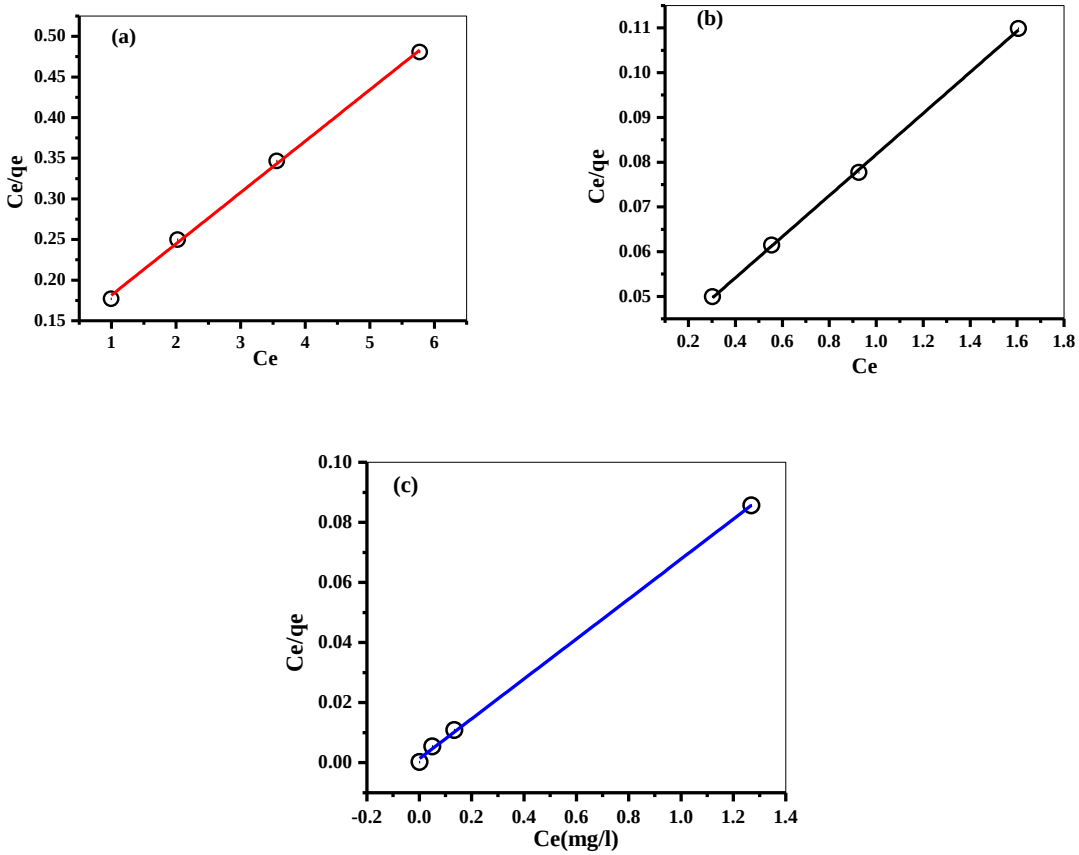

Figure 4.14: Langmuir adsorption isotherm model (a) for Ag NPs, (b) for rGO, and (c) for rGO/Ag NPs NCs.

The Langmuir adsorption was indicated by the maximum adsorption capacity (qmax), which represents the saturated monolayer adsorption at equilibrium. The result shown in Table 4.4 indicates the Langmuir adsorption isotherm parameters q_{max} (8.44 mg/g) and R^2 were 0.998 for silver nanoparticles, q_{max} (27.92 mg/g) and R^2 was 0.999 for reduced graphene oxide nanosheets, and q_{max} (763.35 mg/g) and R^2 was 0.999 for the rGO/Ag NPs nanocomposite. It indicates the correlation coefficient (R^2) and the q_{max} value of the nanocomposite was better than the single precursor surface area by adsorption of methylene blue dye.

From the correlation coefficient R^2 of Langmuir, the adsorption isotherm indicates the adsorption study of MB dye on Ag NPs, rGO, and rGO/Ag NPs NCs was best fitted linearly by the Langmuir isotherm model. The calculated energy of adsorption constant a (K_L) values are 1.87 L/mg, 0.11 L/mg, and 0.01 L/mg for Ag NPs, rGO, and rGO/Ag NPs nanocomposite, respectively. This indicated that the adsorption efficiency of the three adsorbents was good, but the nanocomposite was better than the other two because its K_L value was smaller. According to the Langmuir model, the R_L values calculated as 0.05, 0.11, and 0.833 were obtained between 0 and 1 for Ag NPs, rGO, and rGO/Ag NPs nanocomposite, respectively, which confirmed that the adsorbents adsorbing MB from aqueous solution are favorable under the conditions applied in this study.

Table 4.4: Parameters of Langmuir isotherm models for synthesized samples

Langmuir isotherm model	synthesized samples		
	Ag NPs	rGO	rGO/Ag NPs NCs
q_{max} (mg/g)	8.44	27.92	763.35
R_L	0.05	0.11	0.83
K_L (L/mg)	1.87	0.11	0.01
R^2	0.998	0.999	0.999

4.5.2 Freundlich adsorption isotherm model

The Freundlich adsorption isotherm is based on the formation of a heterogeneous surface or surfaces supporting sites of varied affinities, and it is assumed that the stronger binding sites are occupied first and that the binding strength decreases with an increasing degree of site occupation. The Freundlich isotherm model is the earliest known relationship describing non-ideal and reversible adsorption, not restricted to the formation of a monolayer. This empirical model can be applied to multilayer adsorption with a non-uniform distribution of adsorption heat and affinities over the heterogeneous surface (Wang et al., 2014). The linear form of the Freundlich isotherm equation is as follows:

$$\ln \mathrm{qe} = \ln Kf + \frac{1}{n} * \ln Ce \quad \text{.....(Eq14)}$$

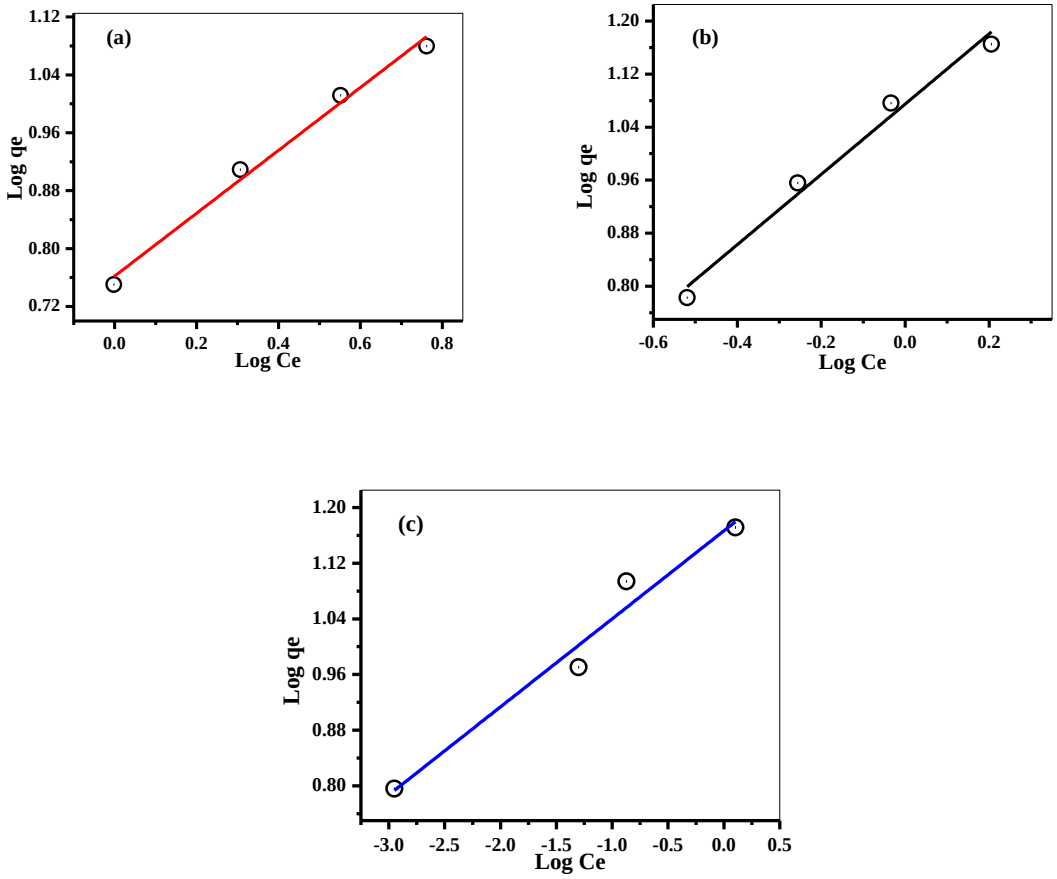

Figure 4.15: Freundlich adsorption isotherm models for Ag NPs (a), rGO (b), and rGO/Ag NPs NCs (c).

A smaller value of the Freundlich equation coefficient 1/n points to a better adsorption mechanism and the formation of a relatively stronger bond between adsorbate and absorbent. Bond energies increase with surface density if 1/n = 1, decrease with surface density if 1/n > 1, and all surface sites are equivalent if 1/n = 1. The n values lie in the range of 1–10 for classification as favorable adsorption (Salifu, 2017).

The isotherm parameters result is presented in Table 4.5 as the Freundlich parameter, of 1/n value, was between 0 & 1, which indicates the favorability of MB dye adsorption on Ag NPs, rGO, and rGO/Ag NPs nanocomposite adsorbent. This means the value of (n) is greater than 1, which indicates the bond between the MB dye and the three synthesized adsorbents was strong. In this study, the calculated values of Freundlich equation coefficient n (n = 2.30 for Ag NPs, 1.88 for rGO nanosheets, and 7.90 for rGO/Ag NPs nanocomposite adsorbent) were greater than 1, which indicates that the adsorption process

is favorable. From the Freundlich constant (K_F) values of rGO/Ag, NPs nanocomposite adsorbent is better adsorption than Ag NPs and rGO. This is because the high value of K_F shows that the high adsorption rGO/Ag NPs NCs (14.67) is greater than Ag NPs (5.78) and rGO (11.87). In addition, the correlation coefficient R^2 of Freundlich was 0.985, 0.976, and 0.955 for Ag NPs, rGO, and rGO/Ag NPs nanocomposite adsorbents, respectively. This indicates the Freundlich isotherm correlation coefficient R^2 was lower than the Langmuir isotherm correlation coefficient of the three adsorbents. So this indicates the Langmuir isotherm model is better fitted for methylene blue dye adsorption for the three synthesized samples. The values of the constants and calculated parameters of the Freundlich isotherm are shown below in Table 4.5.

Table 4.5: Freundlich isotherm model parameters for synthesized samples

Freundlich isotherm model	synthesized samples		
	Ag NPs	rGO	rGO/Ag NPs NCs
K_F (mg/g)	5.78	11.87	14.67
(n)	2.30	1.88	7.90
1/n	0.43	0.53	0.12
R^2	0.985	0.976	0.955

4.6 Adsorption kinetic studies

Several kinetics models can be employed to evaluate the rate and mechanism of mass transfer of MB from the liquid phase to the surface of adsorbents. In the present study, the pseudo-first-order and pseudo-second-order kinetic models were adopted to understand the adsorption mechanism of MB to the three different adsorbents. The pseudo-first-order model was described by Lagergren (1898) in a linear form as displayed in the equation, and the linear form of the pseudo-second-order model was summarized by Ho and McKay (1999) as written in the equation below.

$$\ln(\mathrm{qe} - \mathrm{qt}) = lnqe + K_1 t \quad \text{(Eq15)}$$

$$\frac{\mathrm{t}}{\mathrm{qt}} = \frac{1}{K_2 qe^2} + \frac{t}{qe} \quad \text{(Eq16)}$$

Where qe and qt represent the adsorption capacities (mg/g) at equilibrium and at time t, respectively, and k_1 (min^{-1}) and k_2 (gmg^{-1} min^{-1}) are the corresponding rate constants.

4.6.1 Pseudo-first order kinetics

The linear curves plotted based on pseudo-first-order and pseudo-second-order kinetics models are given in Figure 4.16, and the values of qe, k_1, k_2, and R^2 are summarized in Table 4.6. The kinetics of MB adsorption onto Ag NPs, rGO, and rGO/Ag NPs nanocomposite were analyzed using a pseudo-first-order kinetic model. The conformity between experimental data of Ag NPs was (5.62) and the calculated value (0.08), for rGO q_{exp} (6.06), q_{cal} (0.001), and for rGO/Ag NPs nanocomposite q_{exp} (6.24), q_{cal} (0.09) shows disagreement and also that the correlation coefficient R^2 was not close to unity, therefore it is not a favorable model for the adsorption of MB onto the adsorbents as shown in Table 4.6 (Hermawan et al., 2015).

4.6.2 Pseudo-second order kinetics

A pseudo-second-order kinetic model explains the adsorption mechanism over the entire contact time range. As shown in Table 4.6, the calculated adsorption capacity from the pseudo-second-order model (5.40 mg/g) is closer to experimental data (5.62 mg/g) for Ag NPs, q_{cal} (5.93 mg/g) is closer to q_{exp} (6.06 mg/g) for rGO nanosheets, and q_{cal} (6.10 mg/g) was closer to q_{exp} (6.24 mg/g) for rGO/Ag NPs nanocomposite adsorbent than that of the pseudo-first-order model. Furthermore, the comparison of the two kinetics correlation coefficients (R^2) also demonstrates that the adsorption process of MB from an aqueous solution fits the pseudo-second-order model better. The R^2 value comes closer to unity in the case of the pseudo-second-order kinetic model (0.9994, 0.9998, and 0.9998), which is higher than that of the pseudo-first-order kinetic model (0.331, 0.324, and 0.319) for Ag NPs, rGO, and rGO/Ag NPs NCs, respectively. As shown below in table 4.6, the resultant pseudo-second-order kinetic model has a higher value of correlation coefficient, which confirms that it better fits the experimental adsorption data than the pseudo-first-order kinetic model (Jaseela et al., 2019).

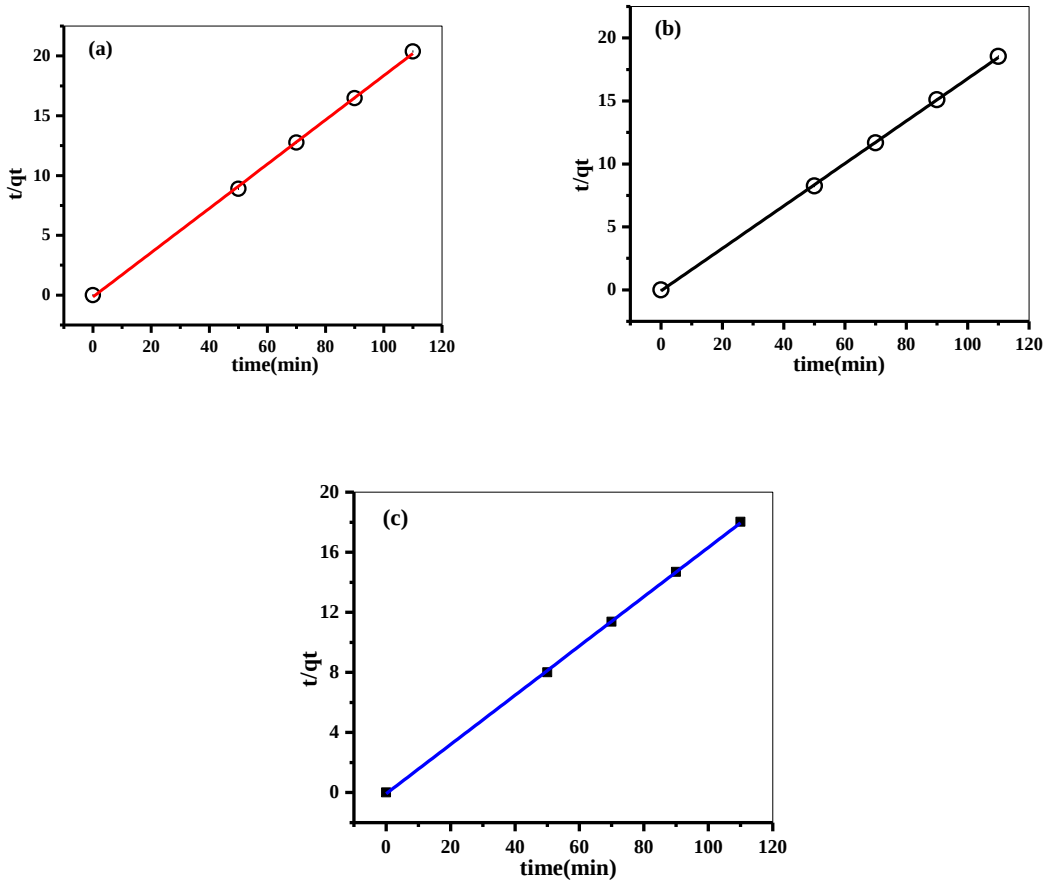

Figure 4.16: pseudo second-order models of (a) Ag NPs, (b) rGO, and (c) rGO/Ag NPs NCs.

Table 4.6: Parameters of pseudo-1st order and pseudo-2nd order for synthesized samples

	Ag NPs		rGO		rGO/Ag NPs NCs	
	Pseudo-1st order	Pseudo-2nd order	Pseudo-1st order	Pseudo 2nd-order	Pseudo -1st order	Pseudo-2nd order
qe(experimental)	5.62	5.62	6.06	6.06	6.24	6.24
qe(calculated)	0.08	5.40	0.001	5.93	0.0921	6.10
K	-0.00024	-0.233	0.00014	-0.384	-0.000063	-0.3618
R^2	0.3314	0.9994	0.3249	0.9998	0.3196	0.9998

5 CONCLUSION AND RECOMMENDATION

5.1 Conclusion

The current study provides a feasible immobilization of green synthesized Ag NPs, rGO, and rGO/Ag NCs using a reduction process using cinnamon bark aqueous extract as a reductant and stabilizer. Diverse techniques (UV-DRS, FTIR-ATR, SEM, and XRD) have been used to characterize the three synthesized adsorbents.

The XRD results showed that the average particle sizes were 29.9 nm, 0.67 nm, and 13.35 nm for Ag NPs, rGO, and rGO/Ag NPs nanocomposite respectively. The synthesized rGO/Ag nanocomposite solid samples used for the removal of MB dye from the aqueous solution better than Ag NPs, and rGO. The removal efficiency of rGO/Ag nanocomposite was 99.98%, while Ag NP and rGO nanosheets removal efficiency were 90.03% and 96.97% respectively. The adsorption results indicate that rGO/Ag nanocomposites are highly capable of removing MB and displaying a high adsorption potential of up to 763.35 mg/g but in the case of Ag NPs, q_{max} was 8.44, for rGO, q_{max} was 27.42 mg/g. In the adsorption process, different parameters affect the efficiency like pH, adsorbent dose, contact time, and initial MB concentration. These parameters were optimized for the three different adsorbent methylene blue removals from an aqueous solution.

The adsorption data was largely compatible with the Langmuir model because their R^2 values were close to unity than the Freundlich isotherm model. From the kinetic study, the adsorption process pursued a pseudo-second-order model because their R^2 value was close to unity and the graph line touched all points. The rGO/Ag NPs nanocomposite also had good reusability efficiency for a five consecutive adsorption process; its removal efficiency was greater than 82%. Thus, this study confirms that the rGO/Ag NP composite is an effective adsorbent for the removal of dye pollutants.

5.2 Recommendation

Based on the present findings, rGO/Ag nanocomposite could be synthesized by using a green method cinnamon bark aqueous extract as a good adsorbent for methylene blue dye. For future study, there are a few recommendations on the characterization of rGO/Ag NPs nanocomposites that will give full information. To determine the elemental composition of the synthesized samples should be characterized by an energy depressive X-ray (EDX) and determine the desorption efficiency for reusability use of composite. In order to investigate the shape of particles, more detailed morphology and surface area of nanocomposite the samples should be characterized by TEM and BET instruments respectively.

REFERENCES

Aboelfetoh, E. F., Gemeay, A. H., & El-Sharkawy, R. G. (2020). Effective disposal of methylene blue using green immobilized silver nanoparticles on graphene oxide and reduced graphene oxide sheets through one pot synthesis. *Environmental Monit oring and Assessment*, *192*(6). https://doi.org/10.1007/s10661-020-08278-2.

Aboubaraka, A. E., Aboelfetoh, E. F., & Ebeid, E. Z. M. (2017). Coagulation effectiveness of graphene oxide for the removal of turbidity from raw surface water. *Chemosphere*, *181*, 738–746. https://doi.org/10.1016/j.chemosphere.2017.04.137.

Aksu, Z., & Kabasakal, E. (2004). Batch adsorption of 2,4-dichlorophenoxy-acetic acid (2,4-D) from aqueous solution by granular activated carbon. *Separation and Purification Technology*, *35*(3), 223–240. https://doi.org/10.1016/s1383-5866(03)00144-8

Al-Ghouti, M. A., & Daana, D. A. (2020). Guidelines for the use and interpretation of adsorption isotherm models: A review. *Journal of Hazardous Materials*, *393*, 1223 83. https://doi.org/10.1016/j.jhazmat.2020.122383.

Amiri, M. S., Mohammadzadeh, V., Yazdi, M. E. T., Barani, M., Rahdar, A., & Kyzas, G. Z. (2021). Plant-Based Gums and Mucilages Applications in Pharmacology and Nanomedicine: A Review. *Molecules*, *26*(6), 1770. https://doi.org/10.3390/molecul es26061770.

Arunachalam, K., & Annamalai, S. (2013). Chrysopogon zizanioides aqueous extract mediated synthesis characterization of crystalline silver and gold nanoparticles for biomedical applications. *International Journal of Nanomedicine*, 2375. https://doi.org/10.2147/ijn.s44076

Avouris, P., & Dimitrakopoulos, C. (2012). Graphene: Synthesis and applications. *Materials Today*, *15*(3), 86–97. https://doi.org/10.1016/s1369-7021(12)70044-5

Azeez, L., Lateef, A., Adebisi, S. A., & Oyedeji, A. O. (2018). Novel biosynthesized silver nanoparticles from Cobweb as adsorbent for rhodamine B: Equilibrium Isotherm, kinetic and thermodynamic studies. *Applied Water Science*, *8*(1). https://doi.org/10.1007/s13201-018-0676-z

Azizi Lalabadi, M., Hashemi, H., Feng, J., & Jafari, S. M. (2020). Carbon nanomaterial against pathogens; the antimicrobial activity of carbon nanotubes, graphene/graphe ne oxide, fullerenes, and their nanocomposites. *Advances in Colloid and Interface Science*, *284*, 102250. https://doi.org/10.1016/j.cis.2020.102250.

Bhattacharya, G., Sas, S., Wadhwa, S., Mathur, A., McLaughlin, J., & Roy, S. S. (2017). Aloe vera assisted facile green synthesis of reduced graphene oxide for electrochemical and dye removal applications. *RSC Advances*, *7*(43), 26680 to 2668 8. https://doi.org/10.1039/c7ra02828h

Bhuyan, M. S. A., Uddin, M. N., Islam, M. M., Bipasha, F. A., & Hossain, S. S. (2016). Sy nthesis of graphene. *International Nano Letters*, *6*(2), 65 to 83. https://doi.org/10.10 07/s40089/015-0176-1

Chandu, B., Kurmarayuni, C. M., Kurapati, S., & Bollikolla, H. B. (2019). Green and econ omical synthesis of graphene silver nanocomposite exhibiting excellent photocataly tic efficiency. *Carbon Letters*, *30*(2), 225–233. https://doi.org/10.1007/s42823-019-000913.

Chen, F., Jin, X., Cao, Y., Jia, D., Liu, A., Wu, R., & Long, M. (2019). Effects of the synthesis conditions on the photocatalytic activities of sulfide-graphene oxide composites. *Dyes and Pigments*, *162*, 177 188. https://doi.org/10.1016/j.dyepig.201 8.09.054.

Choi, B.-hee, Lee, H.-H., Jin, S., Chun, S., & Kim, S.-H. (2007). Characterization of the optical properties of silver nanoparticle films. *Nanotechnology*, *18*(7), 075706. http s://doi.org/10.1088/0957-4484/18/7/075706

Choi, W., Lahiri, I., Seelaboyina, R., & Kang, Y. S. (2010). Synthesis of Graphene and Its Applications: A Review. *Critical Reviews in Solid State and Materials Sciences*, *35*(1), 52–71. https://doi.org/10.1080/10408430903505036

Crini, G., Lichtfouse, E., Chanet, G., & Morin-Crini, N. (2020). Applications of hemp in textiles, paper industry, insulation and building materials, horticulture, animal nutrition, food and beverages, nutraceuticals, cosmetics and hygiene, medicine, agrochemistry, energy production and environment: a review. *Environmental Chemistry Letters*, *18*(5), 1451–1476. https://doi.org/10.1007/s10311-020-01029-2

Dandjesso, C. (2012). Phytochemistry and hemostatic properties of some medicinal plants sold as anti-hemorrhagic in Cotonou Markets (Benin). *Indian Journal of Science and Technology*, *5*(8), 1–5. https://doi.org/10.17485/ijst/2012/v5i8.10

Das, S. K., Khan, M. M., Parandhaman, T., Laffir, F., Guha, A. K., Sekaran, G., & Mandal, A. B. (2013). Nano-silica fabricated with silver nanoparticles: Antifouling adsorbent for efficient dye removal, effective water disinfection and biofouling control. *Nanoscale*, *5*(12), 5549. https://doi.org/10.1039/c3nr00856h

Divya, S., & Loonker, S. (2021). A review study on textile effluent treatments of agricultural soil near textile industry. *SSRN Electronic Journal*. https://doi.org/10.2139/ssrn.3904263

Djeussi, D. E., Noumedem, J. A. K., Seukep, J. A., Fankam, A. G., Voukeng, I. K., Tankeo, S. B., Nkuete, A. H. L., & Kuete, V. (2013). Antibacterial activities of selected edible plants extracts against multidrug-resistant gram-negative bacteria. *BMC Complementary and Alternative Medicine*, *13*(1). https://doi.org/10.1186/1472-6882-13-164

Dresselhaus, M. S., & Araujo, P. T. (2010). Perspectives on the 2010 Nobel Prize in Physics for Graphene. *ACS Nano*, *4*(11), 6297 6302. https://doi.org/10.1021/nn1029789.

Ebana, R., Edet, U., Ekanemesang, U., Etok, C., Ikon, G., & Noble, M. (2016). Phytochemical screening and antimicrobial activity of three medicinal plants against urinary tract infection pathogens. *Asian Journal of Medicine and Health*, *1*(2), 1–7. https://doi.org/10.9734/ajmah/2016/29460

Elmorsi, T. M. (2011). Equilibrium isotherms and kinetic studies of removal of methylene blue dye by adsorption onto Miswak leaves as a natural adsorbent. *Journal of Environmental Protection*, *02*(06), 817 to 827. https://doi.org/10.4236/jep.2011.26093

El-Seedi, H. R., El-Shabasy, R. M., Khalifa, S. A. M., Saeed, A., Shah, A., Shah, R., Iftikhar, F. J., Abdel-Daim, M. M., Omri, A., Hajrahand, N. H., Sabir, J. S. M., Zou, X., Halabi, M. F., Sarhan, W., & Guo, W. (2019). Metal nanoparticles fabricated by green chemistry using natural extracts: biosynthesis, mechanisms, and applications. *RSC Advances*, *9*(42), 24539 to 24559. https://doi.org/10.1039/c9ra02225b.

Fahmy, S. A. Preis, E., Bakowsky, U., & Azzazy, H. M. E. S. (2020). Platinum Nanopartic les: Green Synthesis and Biomedical Applications. *Molecules*, *25*(21), 4981. https://doi.org/10.3390/molecules25214981.

Fan, L., Luo, C., Li, X., Lu, F., Qiu, H., & Sun, M. (2012). Fabrication of novel magnetic chitosan grafted with graphene oxide to enhance adsorption properties for methyl blue. *Journal of Hazardous Materials*, *215/216*, 272/279. https://doi.org/10.1016/j.jhazmat.2012.02.068

Fei, P., Zhong, M., Lei, Z., & Su, B. (2013). One-pot solvothermal synthesized enhanced magnetic zinc ferrite–reduced graphene oxide composite material as adsorbent for

methylene blue removal. *Materials Letters*, *108*, 72/74.https://doi.org/10.1016/j.matlet.2013.06.098

Fereja, W. M., Tagesse, W., & Benti, G. (2020). Treatment of coffee processing wastewater using Moringa stenopetala seed powder: Removal of turbidity and chemical oxygen demand. *Cogent Food & Agriculture*, *6*(1), 1816420. https://doi.org/10.1080/23311932.2020.1816420.

Filip, G. A., Moldovan, B., Baldea, I., Olteanu, D., Suharoschi, R., Decea, N., Cismaru, C. M., Gal, E., Cenariu, M., Clichici, S., & David, L. (2019). UV-light mediated green synthesis of silver and gold nanoparticles using cornelian cherry fruit extract and their comparative effects in experimental inflammation. *Journal of Photochemistry and Photobiology B: Biology*, *191*, 26/37.https://doi.org/10.1016/j.jphotobiol.2018.12.006

Finch, C. A. (2004). Colour chemistry. RM christie. London and Cambridge: Royal Society of Chemistry, 2002. PP VII+ 205, ISBN 0 85404 573 2. *Polymer International*, *53*(2), 233–234. https://doi.org/10.1002/pi.1414

Fu, L., & Fu, Z. (2015). Plectranthus amboinicus leaf extract assisted biosynthesis of ZnO nanoparticles and their photocatalytic activity. *Ceramics International*, *41*(2), 2492–2496. https://doi.org/10.1016/j.ceramint.2014.10.069

Gao, J. F., Li, H. Y., Pan, K. L., & Si, C. Y. (2016). Green syntheses of nanoscale zerovalent iron using a grape seed extract as a stabilizing agent and the application for quick decolorization of azo and anthraquinone dyes. *RSC Advances*, *6*(27), 22526–22537. https://doi.org/10.1039/c5ra26668h.

Gawade, V. V., Gavade, N. L., Shinde, H. M., Babar, S. B., Kadam, A. N., & Garadkar, K. M. (2017). Green synthesis of zno nanoparticles by using Calotropis Procera leaves for the photodegradation of methyl orange. *Journal of Materials Science: Materials in Electronics*, *28*(18), 14033–14039. https://doi.org/10.1007/s10854-017-7254-2

Geetha Bai, R., Muthoosamy, K., Shipton, F. N., Pandikumar, A., Rameshkumar, P., Huang, N. M., & Manickam, S. (2016). The biogenic synthesis of a reduced graphene oxide–silver (RGO–AG) nanocomposite and its dual applications as an antibacterial agent and cancer biomarker sensor. *RSC Advances*, *6*(43), 36576 3658 7. https://doi.org/10.1039/c6ra02928k

Gemeay, A. H., Elsharkawy, R. G., & Aboelfetoh, E. F. (2017). Graphene Oxide/Polyanili ne/Manganese Oxide Ternary Nanocomposites, Facile Synthesis, Characterization, and Application for Indigo Carmine Removal. *Journal of Polymers and the Environment*, *26*(2), 655–669. https://doi.org/10.1007/s10924-017-0947-z.

Ghareeb, M. A., Habib, M. R., Mossalem, H. S., & Abdel-Aziz, M. S. (2018). Phytochemical analysis of eucalyptus camaldulensis leaves extracts and testing its antimicrobial and schistosomicidal activities. *Bulletin of the National Research Centre*, *42*(1). https://doi.org/10.1186/s42269-018-0017-2

Gleditsch, E. (1923). Sur le poids atomique du chlore. *Journal de Chimie Physique*, *21*, 456–460. https://doi.org/10.1051/jcp/19231924200456.

Gong, X., Liu, G., Li, Y., Yu, D. Y. W., & Teoh, W. Y. (2016). Functionalized Graphene Composites: Fabrication and Applications in Sustainable Energy and Environment. *Chemistry of Materials*, *28*(22), 8082 8118. https://doi.org/10.1021/acs.chemmater. 6b01447.

Guarín, J. R., Moreno-Pirajan, J. C., & Giraldo, L. (2018). Kinetic Study of the Bioadsorption of Methylene Blue on the Surface of the Biomass Obtained from the Algae D. Antarctica. *Journal of Chemistry*, *2018*, 1 to12. https://doi.org/10.1155/20 18/2124845.

Habte, A. T., & Ayele, D. W. (2019). Synthesis and characterization of reduced graphene oxide (rGO) started from graphene oxide (GO) using the tour method with different parameters. *Advances in Materials Science and Engineering*, *2019*.

Haldorai, Y., Kim, B. K., Jo, Y. L., & Shim, J. J. (2014). Ag@graphene oxide nanocompos ite as an efficient visible-light plasmonic photocatalyst for the degradation of organic pollutants: A facile green synthetic approach. *Materials Chemistry and Physics*, *143*(3), 1452–1461. https://doi.org/10.1016/j.matchemphys.2013.11.065.

Hasan, M., Ahmad, A. L., & Hameed, B. H. (2008). Adsorption of reactive dye onto cross-linked chitosan/oil palm ash composite beads. *Chemical Engineering Journal*, *136*(2-3), 164–172. https://doi.org/10.1016/j.cej.2007.03.038

Hebeish, A., El Rafie, M., Abdel Mohdy, F., Abdel Halim, E., & Emam, H. (2010). Carbox ymethyl cellulose for green synthesis and stabilization of silver nanoparticles. *Carbohydrate Polymers*, *82*(3), 933 to 941. https://doi.org/10.1016/j.carbpol.2010.0 6.020.

Hemmati, S., Heravi, M. M., Karmakar, B., & Veisi, H. (2020). Green fabrication of reduced graphene oxide decorated with Ag nanoparticles (RGO/AG NPS)

nanocomposite: A reusable catalyst for the degradation of environmental pollutants in aqueous medium. *Journal of Molecular Liquids*, *319*, 114302. https://doi.org/10.1016/j.molliq.2020.114302

Hermawan, A. A., Bing, T. K., & Salamatinia, B. (2015). Application and optimization of using recycled pulp for methylene blue removal from wastewater: A response surface methodology approach. *International Journal of Environmental Science and Development*, *6*(4), 267–274. https://doi.org/10.7763/ijesd.2015.v6.602

Huang, L., Yang, H., Zhang, Y., & Xiao, W. (2016). Study on Synthesis and Antibacterial Properties of Ag NPs/GO Nanocomposites. *Journal of Nanomaterials*, *2016*, 1 to 9. https://doi.org/10.1155/2016/5685967.

Huang, Z.-H., Zheng, X., Lv, W., Wang, M., Yang, Q.-H., & Kang, F. (2011). Adsorption of lead(ii) ions from aqueous solution on low-temperature exfoliated graphene nanosheets. *Langmuir*, *27*(12), 7558–7562. https://doi.org/10.1021/la200606r

Hummers, W. S., & Offeman, R. E. (1958). Preparation of Graphitic Oxide. *Journal of the American Chemical Society*, *80*(6), 1339. https://doi.org/10.1021/ja01539a017.

Hussain, S. Z., Ihrar, M., Hussain, S. B., Oh, W. C., & Ullah, K. (2020). A review on graph ene based transition metal oxide composites and its application towards super capacitor electrodes. *SN Applied Sciences*, *2*(4). https://doi.org/10.1007/s42452-020-2515-8.

Ibrahim, H. M. M. (2015). Green synthesis and characterization of silver nanoparticles using banana peel extract and their antimicrobial activity against representative microorganisms. *Journal of Radiation Research and Applied Sciences*, *8*(3), 265–275. https://doi.org/10.1016/j.jrras.2015.01.007

IK, M., & Uthman ISAH, K. (2015). The effect on extracting solvents using natural dye extracts from hyphaene thebaica for dye-sensitized solar cells. *Journal of Material Science & Engineering*, *05*(01). https://doi.org/10.4172/2169-0022.1000208

Industrial Wastes and Their Management Challenges in Ethiopia. (2019). *Chemistry and Materials Research*. https://doi.org/10.7176/cmr/11-8-01.

Jaseela, P. K., Garvasis, J., & Joseph, A. (2019). Selective adsorption of methylene blue (MB) dye from aqueous mixture of MB and methyl orange (MO) using mesoporous titania (tio2) – poly vinyl alcohol (PVA) nanocomposite. *Journal of Molecular Liquids*, *286*, 110908. https://doi.org/10.1016/j.molliq.2019.110908

Jemal, A. F., Fangnon Firmin, Rejoice, F., & M. (2020). Effectiveness Assessment of Indu strial Effluent Standard Implementation in Addis Ababa City, Ethiopia.

International Journal of Scientific and Research Publications (IJSRP), 10(06), 142 to 148. https://doi.org/10.29322/ijsrp.10.06.2020.p10218

Jeon, J.-W., Jeon, D.-W., Sahoo, T., Kim, M., Baek, J.-H., Hoffman, J. L., Kim, N. S., & Lee, I.-H. (2011). Effect of annealing temperature on optical band-gap of amorphous indium zinc oxide film. *Journal of Alloys and Compounds*, *509*(41), 10062–10065. https://doi.org/10.1016/j.jallcom.2011.08.033

Jiao, L., Wang, X., Diankov, G., Wang, H., & Dai, H. (2010). Facile synthesis of high qual ity graphene nanoribbons. *Nature Nanotechnology*, *5*(5), 321 to 325. https://doi.org/ 10.1038/nnano.2010.54.

Joutey, N. T., Sayel, H., Bahafid, W., & El Ghachtouli, N. (2014). Mechanisms of hexavalent chromium resistance and removal by microorganisms. *Reviews of Environmental Contamination and Toxicology Volume 233*, 45–69. https://doi.org/10.1007/978-3-319-10479-9_2

Jyoti, K., & Singh, A. (2016). Green synthesis of nanostructured silver particles and their catalytic application in dye degradation. *Journal of Genetic Engineering and Biotechnology*, *14*(2), 311–317. https://doi.org/10.1016/j.jgeb.2016.09.005

Kadam, A. A., Lade, H. S., Lee, D. S., & Govindwar, S. P. (2015). Zinc chloride as a coagulant for textile dyes and treatment of generated dye sludge under the solid state fermentation: Hybrid treatment strategy. *Bioresource Technology*, *176*, 38–46. https://doi.org/10.1016/j.biortech.2014.10.137

Kamran, U., Bhatti, H. N., Iqbal, M., Jamil, S., & Zahid, M. (2019). Biogenic synthesis, ch aracterization and investigation of photocatalytic and antimicrobial activity of manganese nanoparticles synthesized from Cinnamomum verum bark extract. *Journal of Molecular Structure*, *1179*, 532 to 539. https://doi.org/10.1016/j.molstru c.2018.11.006.

Karaghool, H. A. K. (2021). Biodecolorization of methylene blue using aspergillus consort ium. *IOP Conference Series: Earth and Environmental Science*, *779*(1), 012111. htt ps://doi.org/10.1088/1755-1315/779/1/012111.

Katheresan, V., Kansedo, J., & Lau, S. Y. (2018). Efficiency of various recent wastewater dye removal methods: A Review. *Journal of Environmental Chemical Engineering*, *6*(4), 4676–4697. https://doi.org/10.1016/j.jece.2018.06.060

Kavithad, D., & Namasivayam, C. (2007). Experimental and kinetic studies on methylene blue adsorption by Coir Pith Carbon. *Bioresource Technology*, *98*(1), 14–21. https://doi.org/10.1016/j.biortech.2005.12.008

Khan, A. H., Ghosh, S., Pradhan, B., Dalui, A., Shrestha, L. K., Acharya, S., & Ariga, K. (2017). Two-Dimensional (2D) Nanomaterial's towards Electrochemical Nanoarchitectonics in Energy-Related Applications. *Bulletin of the Chemical Society of Japan*, *90*(6), 627–648. https://doi.org/10.1246/bcsj.20170043.

Khan, R., Bhawana, P., & Fulekar, M. H. (2012). Microbial decolorization and degradation of synthetic dyes: A Review. *Reviews in Environmental Science and Bio/Technology*, *12*(1), 75–97. https://doi.org/10.1007/s11157-012-9287-6

Khan, T. A., Nazir, M., & Khan, E. A. (2013). Adsorptive removal of rhodamine B from textile wastewater using water chestnut (Trapa Natans L.) peel: Adsorption dynamics and kinetic studies. *Toxicological & Environmental Chemistry*, *95*(6), 919–931. https://doi.org/10.1080/02772248.2013.840369

Kim, B. S., Salunke, B., Sawant, S., & Alkotaini, B. (2014). Biological synthesis of silver nanoparticles using plant leaf extracts and their specific antimicrobial activity. *New Biotechnology*, *31*. https://doi.org/10.1016/j.nbt.2014.05.889

Konicki, W., Aleksandrzak, M., & Mijowska, E. (2017). Equilibrium, kinetic and thermod ynamic studies on adsorption of cationic dyes from aqueous solutions using graphene oxide. *Chemical Engineering Research and Design*, *123*, 35 to 49. https:// doi.org/10.1016/j.cherd.2017.03.036.

Kumar, N., & Kumbhat, S. (2016). Essentials in Nanoscience and nanotechnology. https://doi.org/10.1002/9781119096122

Lai, D., Chen, W., & Jiang, G. (2013). Research Progress of Graphene based Composite M aterials. *Current Physical Chemistry*, *3*(3), 269 to 282. https://doi.org/10.2174/1877 946811303030004.

Laurent, S., Forge, D., Port, M., Roch, A., Robic, C., Vander Elst, L., & Muller, R. N. (2010). Magnetic iron oxide nanoparticles: Synthesis, stabilization, vectorization, physicochemical characterizations, and biological applications. *Chemical Reviews*, *110*(4), 2574–2574. https://doi.org/10.1021/cr900197g

Laysandra, L., Sari, M. W., Soetaredjo, F. E., Foe, K., Putro, J. N., Kurniawan, A., Ju, Y.-H., & Ismadji, S. (2017). Adsorption and photocatalytic performance of bentonite-titanium dioxide composites for methylene blue and rhodamine B decoloration. *Heliyon*, *3*(12). https://doi.org/10.1016/j.heliyon.2017.e00488

Lee, S., & Jun, B.-H. (2019). Silver nanoparticles: Synthesis and application for nanomedicine. *International Journal of Molecular Sciences*, *20*(4), 865. https://doi. org/10.3390/ijms20040865

Luken, R., & Komendantova-Amann, N. (2017). Industry and sustainable development in 18 developing and transition economies. *Sustainable Development Policy and Administration*, 503–532. https://doi.org/10.4324/9781315087535-22

Lu, X. M., Zhu, J. S., Zhang, W. Y., Ma, G. Q., & Wang, Y. N. (1996). The energy gap of r.f.-sputtered batio3 thin films with different grain size. *Thin Solid Films*, *274*(1-2), 165–168. https://doi.org/10.1016/0040-6090(95)08000-7

Lu, Y., Mei, Y., Schrinner, M., Ballauff, M., Möller, M. W., & Breu, J. (2007). In situ formation of Ag nanoparticles in spherical polyacrylic acid brushes by UV irradiation. *The Journal of Physical Chemistry C, 111*(21), 7676 to 7681. https://doi .org/10.1021/jp070973m

Maham, M., Nasrollahzadeh, M., Sajadi, S. M., & Nekoei, M. (2017). Biosynthesis of Ag/r educed graphene oxide/Fe3O4 using Lotus garcinii leaf extract and its application as a recyclable nanocatalyst for the reduction of 4-nitrophenol and organic dyes. *Journal of Colloid and Interface Science*, *497*, 33 to 42. https://doi.org/10.1016/j.jci s.2017.02.064.

Mangalam, J., Kumar, M., Sharma, M., & Joshi, M. (2019). High adsorptivity and visible light assisted photocatalytic activity of silver/reduced graphene oxide (AG/RGO) nanocomposite for wastewater treatment. *Nano-Structures & Nano-Objects*, *17*, 58–66. https://doi.org/10.1016/j.nanoso.2018.11.003

Marandi, R., & Bakhtiar Sepehr, S. M. (2012). Removal of orange 7 dye from wastewater used by natural adsorbent of moringa oleifera seeds. *American Journal of Environmental Engineering*, *1*(1), 1–9. https://doi.org/10.5923/j.ajee.20110101.01

Markandeya, Shukla, S. P., Dhiman, N., Mohan, D., Kisku, G. C., & Roy, S. (2017). An Ef ficient Removal of Disperse Dye from Wastewater Using Zeolite Synthesized from Cenospheres. *Journal of Hazardous, Toxic, and Radioactive Waste*, *21*(4), 04017017. https://doi.org/10.1061/(asce)hz.2153-5515.0000369.

Maryami, M., Nasrollahzadeh, M., Mehdipour, E., & Sajadi, S. M. (2016). Preparation of the Ag/RGO nanocomposite by use of Abutilon hirtum leaf extract: A recoverable catalyst for the reduction of organic dyes in aqueous medium at room temperature. *International Journal of Hydrogen Energy*, *41*(46), 21236 to 21245. https://doi.org/ 10.1016/j.ijhydene.2016.09.130.

Md Sandollah, N. A., Sheikh Mohd Ghazali, S. A., Wan Ibrahim, W. N., & Rusmin, R. (2020). Adsorption-desorption profile of methylene blue dye on raw and acid

activated kaolinite. *Indonesian Journal of Chemistry, 20*(4), 755. https://doi.org/10.22146/ijc.43552

Moosavi, R., Ramanathan, S., Lee, Y. Y., Siew Ling, K. C., Afkhami, A., Archunan, G., Padmanabhan, P., Gulyás, B., Kakran, M., & Selvan, S. T. (2015). Synthesis of antibacterial and magnetic nanocomposites by decorating graphene oxide surface with metal nanoparticles. *RSC Advances, 5*(93), 76442 to 76450. https://doi.org/10.1039/c5ra15578a.

Morales Torres, S., Pastrana Martínez, L. M., Figueiredo, J. L., Faria, J. L., & Silva, A. M. T. (2012). Design of graphene-based TiO_2 photocatalyst a review. *Environmental Science and Pollution Research, 19*(9), 3676-3687. https://doi.org/10.1007/s11356-012-0939-4.

Mulushewa, Z., Dinbore, W. T., & Ayele, Y. (2021). Removal of methylene blue from textile waste water using kaolin and zeolite-x synthesized from Ethiopian kaolin. *Environmental Analysis Health and Toxicology, 36*(1), e2021007. https://doi.org/10.5620/eaht.2021007.

Nabavi, S., di Lorenzo, A., Izadi, M., Sobarzo Sánchez, E., Daglia, M., & Nabavi, S. (2015). Antibacterial Effects of Cinnamon: From Farm to Food, Cosmetic and Pharmaceutical Industries. *Nutrients, 7*(9), 7729 to7748. https://doi.org/10.3390/nu7095359.

Nasrollahzadeh, M., Issaabadi, Z., & Sajadi, S. M. (2019). Green synthesis of Cu/Al_2O_3 nanoparticles as efficient and recyclable catalyst for reduction of 2,4-dinitrophenylhydrazine, Methylene blue and Congo red. *Composites Part B: Engineering, 166*, 112–119. https://doi.org/10.1016/j.compositesb.2018.11.113.

Nimkar, U. (2018). Sustainable chemistry: A solution to the textile industry in a developing world. *Current Opinion in Green and Sustainable Chemistry, 9*, 13 to 17. https://doi.org/10.1016/j.cogsc.2017.11.002.

Paliwal, R., Sharma, V., Pracheta., and Sharma, S., "Elucidation of free radical scavenging and antioxidant activity of aqueous and hydro-ethanolic extracts of Moringaoleifera pods", Research Journal of Pharmacy and Technology, 4, 4, 2011, pp. 566-571.

Palomino, O. (2020). Peer Review #3 of "in vitro anti-diabetic effects and phytochemical profiling of novel varieties of cinnamomum zeylanicum (L.) extracts (v0.1)". https://doi.org/10.7287/peerj.10070v0.1/reviews/3

Pathania, D., Sharma, S., & Singh, P. (2017). Removal of methylene blue by adsorption onto activated carbon developed from Ficus carica bast. *Arabian Journal of Chemistry*, *10*, S1445–S1451. https://doi.org/10.1016/j.arabjc.2013.04.021

P.E.Kumar, M. S. (2015). Adsorption of rhodamine B from an aqueous solution: Kinetic, equilibrium and thermodynamic studies. *International Journal of Innovative Research in Science, Engineering and Technology*, *04*(02), 497 to 510. https://doi.org/10.15680/ijirset.2015.0402039

Pénicaud, A., & Drummond, C. (2012). Deconstructing Graphite: Graphenide Solutions. *Accounts of Chemical Research*, *46*(1), 129–137. https://doi.org/10.1021/ar300141s

Peppas, N. A., Hilt, J. Z., Khademhosseini, A., & Langer, R. (2006). Hydrogels in biology and medicine: From molecular principles to bionanotechnology. *Advanced Materials*, *18*(11), 1345–1360. https://doi.org/10.1002/adma.200501612

Poh, H. L., Sanek F., Ambrosi, A., Zhao, G., Sofer, Z., & Pumera, M. (2012). Graphene prepared by Staudenmaier, Hofmann and Hummers methods with consequent thermal exfoliation exhibit very different electrochemical properties. *Nanoscale*, *4*(11), 3515. https://doi.org/10.1039/c2nr30490b.

Premkumar, J., Sudhakar, T., Dhakal, A., Shrestha, J. B., Krishnakumar, S., & Balashanmugam, P. (2018). Synthesis of silver nanoparticles (AgNPs) from cinnamon against bacterial pathogens. *Biocatalysis and Agricultural Biotechnology*, *15*, 311 to 316. https://doi.org/10.1016/j.bcab.2018.06.005.

Rahman, M. A., Amin, S. M., & Alam, A. M. (2012). Removal of methylene blue from waste water using activated carbon prepared from rice husk. *Dhaka University Journal of Science*, *60*(2), 185–189. https://doi.org/10.3329/dujs.v60i2.11491

Rakibuddin, M., Gazi, S., & Ananthakrishnan, R. (2015). Iron(II) phenanthroline-resin hybrid as a visible light-driven heterogeneous catalyst for green oxidative degradation of organic dye. *Catalysis Communications*, *58*, 53 to 58. https://doi.org/10.1016/j.catcom.2014.08.035

Ramesha, G. K., Vijaya Kumara, A., Muralidhara, H. B., & Sampath, S. (2011). Graphene and graphene oxide as effective adsorbents toward anionic and cationic dyes. *Journal of Colloid and Interface Science*, *361*(1), 270–277. https://doi.org/10.1016/j.jcis.2011.05.050

Rawat, D., Sharma, R. S., Karmakar, S., Arora, L. S., & Mishra, V. (2018). Ecotoxic potential of a presumably non-toxic azo dye. *Ecotoxicology and Environmental Safety*, *148*, 528–537. https://doi.org/10.1016/j.ecoenv.2017.10.049

Robinson, T., McMullan, G., Marchant, R., & Nigam, P. (2001). Remediation of dyes in textile effluent: A critical review on current treatment technologies with a proposed alternative. *Bioresource Technology*, *77*(3), 247 to 255. https://doi.org/10.1016/s0960-8524(00)00080-8

Ruoff, G. E. (1999). Slowing the Initial Titration Rate of Tramadol Improves Tolerability. *Pharmacotherapy*, *19*(1), 88–93. https://doi.org/10.1592/phco.19.1.88.30515.

Rupa, E. J., Kaliraj, L., Abid, S., Yang, D.-C., & Jung, S.-K. (2019). Synthesis of a zinc oxide nanoflower photocatalyst from sea buckthorn fruit for degradation of industrial dyes in wastewater treatment. *Nanomaterials*, *9*(12), 1692. https://doi.org/10.3390/nano9121692

Rytwo, G., Tropp, D., & Serban, C. (2002). Adsorption of diquat, paraquat and methyl green on sepiolite: Experimental results and model calculations. *Applied Clay Science*, *20*(6), 273–282. https://doi.org/10.1016/s0169-1317(01)00068-0

Saadi, R., Saadi, Z., Fazaeli, R., & Fard, N. E. (2015). Monolayer and multilayer adsorption isotherm models for sorption from aqueous media. *Korean Journal of Chemical Engineering*, *32*(5), 787–799. https://doi.org/10.1007/s11814-015-0053-7.

Sabouri, Z., Sabouri, M., Amiri, M. S., Khatami, M., & Darroudi, M. (2020). Plant based synthesis of cerium oxide nanoparticles using rheum turkestanicum extract and evaluation of their Cytotoxicity and photocatalytic properties. *Materials Technology*, 1 to 14. https://doi.org/10.1080/10667857.2020.1863573.

Salifu, A. (2017). Fluoride removal from drinking water using granular aluminum-coated bauxite as adsorbent: Optimization of synthesis process conditions and equilibrium study. *Fluoride Removal from Groundwater by Adsorption Technology*, 161–202. https://doi.org/10.1201/9781351199995-5

Sanusi, A. (2020). Extraction of Dye from Detarium microcarpum and Its Application on Leather. *American Journal of Polymer Science and Technology*, *6*(4), 40. https://doi.org/10.11648/j.ajpst.20200604.12.

Shahverdi, A. R., Minaeian, S., Shahverdi, H. R., Jamalifar, H., & Nohi, A.-A. (2007). Rapid synthesis of silver nanoparticles using culture supernatants of enterobacteria: A novel biological approach. *Process Biochemistry*, *42*(5), 919–923. https://doi.org/10.1016/j.procbio.2007.02.005

Shao, W., Liu, X., Min, H., Dong, G., Feng, Q., & Zuo, S. (2015). Preparation, Characterization, and Antibacterial Activity of Silver Nanoparticle Decorated Graphene Oxide Nanocomposite. *ACS Applied Materials & Interfaces*, *7*(12), 6966 to 6973. https://doi.org/10.1021/acsami.5b00937.

Sharma, V., Paliwal, R., Pracheta., and Sharma, S., "Phytochemical analysis and evaluation of antioxidant activities of hydro-ethanolic extract of Moringaoleifera lam. Pods", Journalof Pharmacy Research, 4, 2, 2011, pp. 553-556

Shen, H., Zhang, L., Liu, M., & Zhang, Z. (2012). Biomedical applications of graphene. *Theranostics*, *2*(3), 283–294. https://doi.org/10.7150/thno.3642

Singaravelan, R., & Bangaru Sudarsan Alwar, S. (2015). Electrochemical synthesis, characterisation and phytogenic properties of silver nanoparticles. *Applied Nanoscience*, *5*(8), 983–991. https://doi.org/10.1007/s13204-014-0396-0

Singh, A. K., Talat, M., Singh, D. P., & Srivastava, O. N. (2010). Biosynthesis of gold and silver nanoparticles by natural precursor clove and their functionalization with amine group. *Journal of Nanoparticle Research*, *12*(5), 1667 to 1675. https://doi.org/10.1007/s11051-009-9835-3.

Singh, S., Joshi, M., Panthari, P., Malhotra, B., Kharkwal, A. C., & Kharkwal, H. (2017). Citrulline rich structurally stable zinc oxide nanostructures for superior photo catalytic and optoelectronic applications: A green synthesis approach. *Nano-Structures & Nano-Objects*, *11*, 1–6. https://doi.org/10.1016/j.nanoso.2017.05.006

Sofowora, A. (1996). Research on medicinal plants and traditional medicine in Africa. *The Journal of Alternative and Complementary Medicine*, *2*(3), 365 372. https://doi.org/10.1089/acm.1996.2.365

Sreeprasad, T. S., Maliyekkal, S. M., Lisha, K. P., & Pradeep, T. (2011). Reduced graphene oxide–metal/metal oxide composites: Facile synthesis and application in water purification. *Journal of Hazardous Materials*, *186*(1), 921–931. https://doi.org/10.1016/j.jhazmat.2010.11.100

Sun, H., Cao, L., & Lu, L. (2011). Magnetite/reduced graphene oxide nanocomposites: One step solvothermal synthesis and use as a novel platform for removal of dye pollutants. *Nano Research*, *4*(6), 550–562. https://doi.org/10.1007/s12274-011-0111-3

Supritha, C. T. (2021). Green Synthesis and Characterization of Silver Nanoparticles using Cinnamomum zeylanicum Bark Extract. *International Journal of Current*

Microbiology and Applied Sciences, *10*(01), 444 to 451. https://doi.org/10.20546/ijcmas.2021.1001.055.

Suresh, D., Udayabhanu, Pavan Kumar, M., Nagabhushana, H., & Sharma, S. (2015). Cinnamon supported facile green reduction of graphene oxide, its dye elimination and antioxidant activities. *Materials Letters*, *151*, 93 to 95. https://doi.org/10.1016/j.matlet.2015.03.035.

Suzuki, K., & Kijima, K. (2005). Optical band gap of barium titanate nanoparticles prepared by RF-plasma chemical vapor deposition. *Japanese Journal of Applied Physics*, *44*(4A), 2081–2082. https://doi.org/10.1143/jjap.44.2081

Thangavel, S., Raghavan, N., Kadarkarai, G., Kim, S.-J., & Venugopal, G. (2015). Graphene-oxide (go)–fe3+ hybrid nanosheets with effective sonocatalytic degradation of reactive red 120 and study of their kinetics mechanism. *Ultrasonics Sonochemistry*, *24*, 123–131. https://doi.org/10.1016/j.ultsonch.2014.11.019

Theivasanthi, T., & Alagar, M. (2012). Electrolytic synthesis and characterization of silver nanopowder. *Nano Biomedicine and Engineering*, *4*(2). https://doi.org/10.5101/nbe.v4i2.p58-65

Vidhu, V. K., & Philip, D. (2014). Catalytic degradation of organic dyes using biosynthesized silver nanoparticles. *Micron*, *56*, 54–62. https://doi.org/10.1016/j.micron.2013.10.006

Vijay Kumar, S., Huang, N., Lim, H., Marlinda, A., Harrison, I., & Chia, C. (2013). One step size-controlled synthesis of functional graphene oxide/silver nanocomposites at room temperature. *Chemical Engineering Journal*, *219*, 217 to 224. https://doi.org/10.1016/j.cej.2012.09.063

Wang, F., Zhang, L., Wang, Y., Liu, X., Rohani, S., & Lu, J. (2017). Fe_3O_4 @SiO_2 @CS-TETA functionalized graphene oxide for the adsorption of methylene blue (MB) and Cu(II). *Applied Surface Science*, *420*, 970 to 981. https://doi.org/10.1016/j.apsusc.2017.05.179.

Wang, H., Yuan, X., Zeng, G., Leng, L., Peng, X., Liao, K., Peng, L., & Xiao, Z. (2014). Removal of malachite green dye from wastewater by different organic acid-modified natural adsorbent: Kinetics, equilibriums, mechanisms, practical application, and disposal of dye-loaded adsorbent. *Environmental Science and Pollution Research*, *21*(19), 11552–11564. https://doi.org/10.1007/s11356-014-3025-2

Wu, Q., Feng, C., Wang, C., & Wang, Z. (2013). A facile one-pot solvothermal method to produce superparamagnetic graphene–fe3o4 nanocomposite and its application in the removal of dye from aqueous solution. *Colloids and Surfaces B: Biointerfaces*, *101*, 210–214. https://doi.org/10.1016/j.colsurfb.2012.05.036

Xu, L. J., Chu, W., & Gan, L. (2015). Environmental application of graphene-based COFE2O4 as an activator of peroxymonosulfate for the degradation of a plasticizer. *Chemical Engineering Journal*, *263*, 435/443. https://doi.org/10.1016/j.cej.2014.11.065

Yuan, N., Cai, H., Liu, T., Huang, Q., & Zhang, X. (2019). Adsorptive removal of methylene blue from aqueous solution using coal fly ash-derived mesoporous silica material. *Adsorption Science & Technology*, *37*(3 to 4), 333 to 348. https://doi.org/10.1177/0263617419827438.

Yusuf, M. (2019). Synthetic dyes: A threat to the environment and water ecosystem. *Textiles and Clothing*, 11–26. https://doi.org/10.1002/9781119526599.ch2

Yu, X., Huang, L., Wei, Y., Zhang, J., Zhao, Z., Dai, W., & Yao, B. (2015). Controllable preparation, characterization and performance of CU2O thin film and photocatalytic degradation of methylene blue using response surface methodology. *Materials Research Bulletin*, *64*, 410 to 417. https://doi.org/10.1016/j.materresbull.2015.01.009

Zaghbani, N., Hafiane, A., & Dhahbi, M. (2007). Separation of methylene blue from aqueous solution by micellar enhanced ultrafiltration. *Separation and Purification Technology*, *55*(1), 117–124. https://doi.org/10.1016/j.seppur.2006.11.008

Zhou, Q., Xia, G., Du, M., Lu, Y., & Xu, H. (2019). Scotch tape like exfoliation effect of g raphene quantum dots for efficient preparation of graphene nanosheets in water. *Applied Surface Science*, *483*, 52–59. https://doi.org/10.1016/j.apsusc.2019.03.290.

Zhao, G., Li, J., Ren, X., Chen, C., & Wang, X. (2011). Few-layered graphene oxide nanosheets as superior sorbents for Heavy Metal Ion Pollution Management. *Environmental Science & Technology*, *45*(24), 10454–10462. https://doi.org/10.1021/es203439v

Zietzschmann, F. (2021). Neuauflage: Adsorption Technology in Water Treatment. *Vom W asser,119*(3), 115. https://doi.org/10.1002/vomw.202170307.

Appendix

Cinnamon bark powder | Cinnamon bark extract | Silver NPs solution



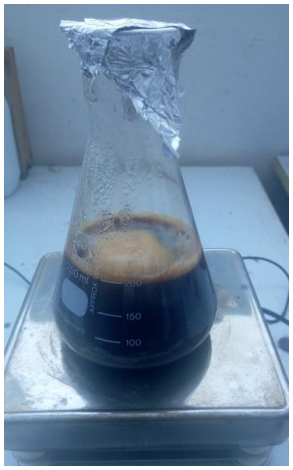
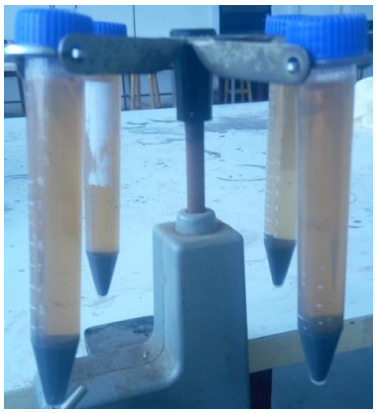

Centrifuged silver NPs solution | Ag NPs crystal | Ag NPs fine powder

Figure 7.1: Pictures of green synthesis silver NPs

Mix of Graphite, $NaNO_3$ & $KMnO_4$ with H_2SO_4 ⇨ addition of H_2O ⇨ addition of H_2O_2

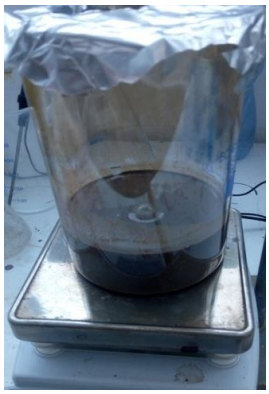

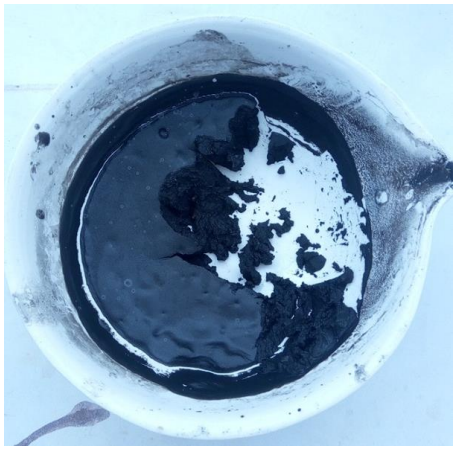

Paste like graphene oxide

Fine powder of graphene oxide

Figure 7.2: pictures of graphene oxide synthesis

GO dispersed in water & plant extract

Centrifuged rGO

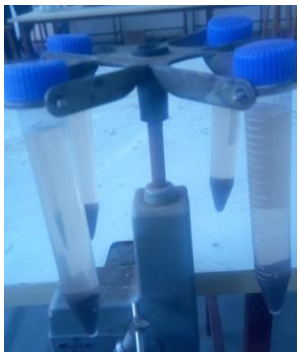

Dried rGO

Figure 7.3: Picture of reduced graphene oxide synthesis

GO & $AgNO_3$ disperse in H_2O & PE ⇨ Centrifuged rGO/Ag ⇨ Fine powder of rGO/Ag

Figure 7.4: Picture of rGO/Ag NPs nanocomposite synthesis

$G_{1,2,3}$ for rGO $AB_{1,2,3}$ for silver NPs $GA_{1,2,3}$ for rGO/Ag NPs NCs

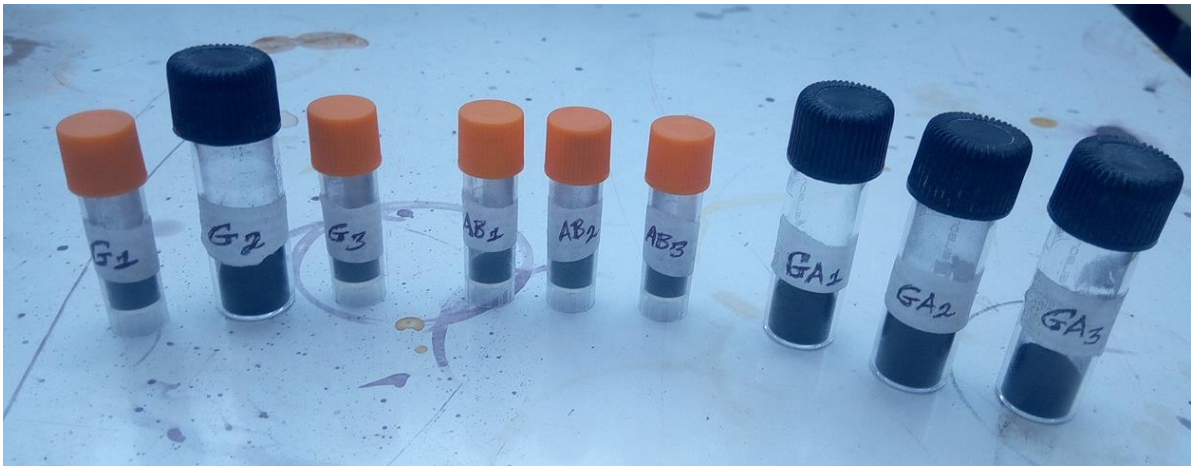

Figure 7.5: Total synthesis samples with its code for characterization

Figure 7.6: weight balance of adsorbent

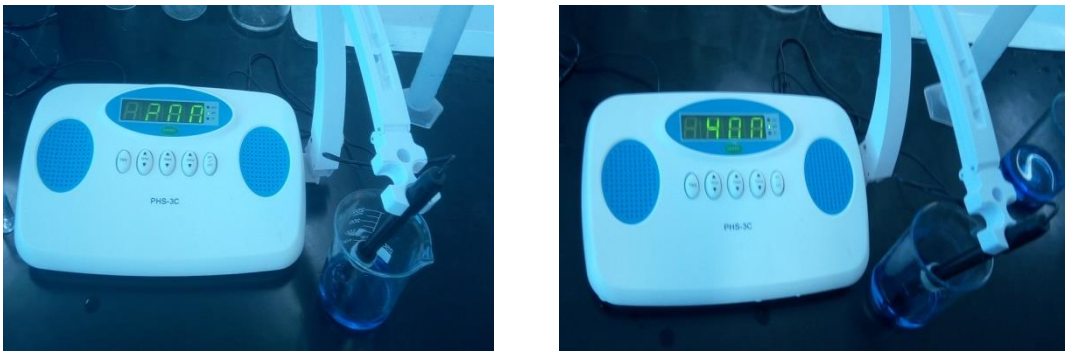

Figure 7.7: picture of pH adjustment in optimization

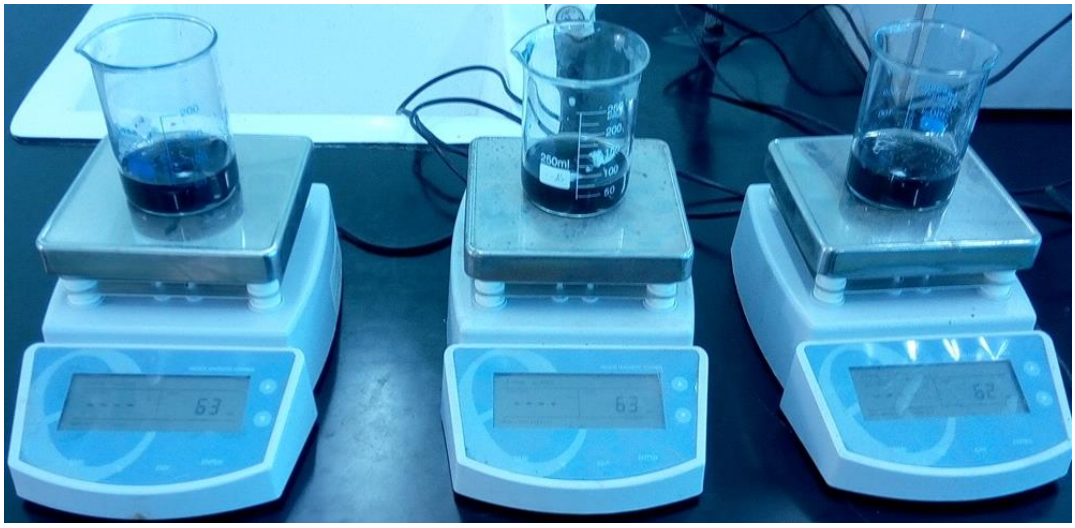

Figure 7.8: adsorption experiment stirring by digital magnetic stirrer for rGO

Figure 7.9: adsorption experiment stirring by digital magnetic stirrer for Ag NPs

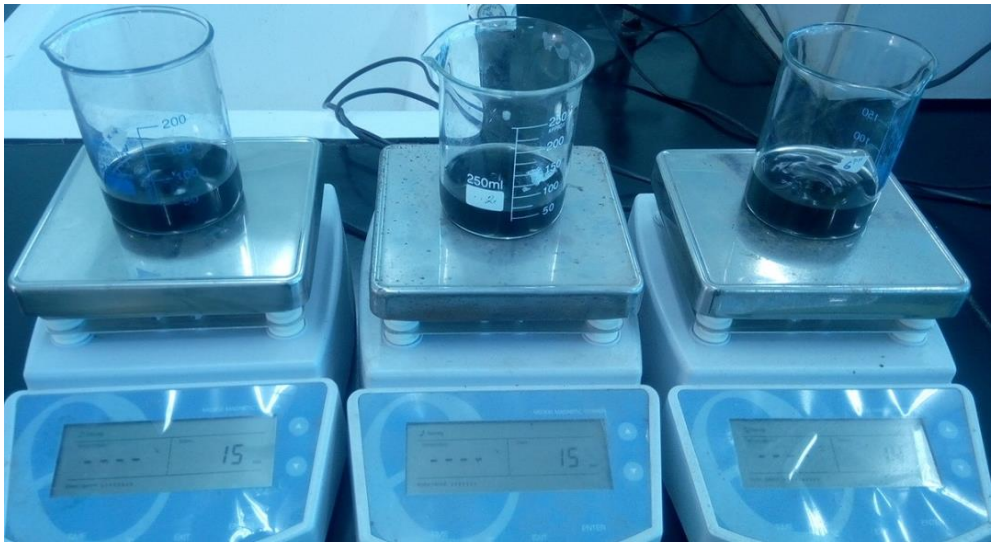

Figure 7.10: adsorption experiment stirring by digital magnetic stirrer for rGO/Ag NCs

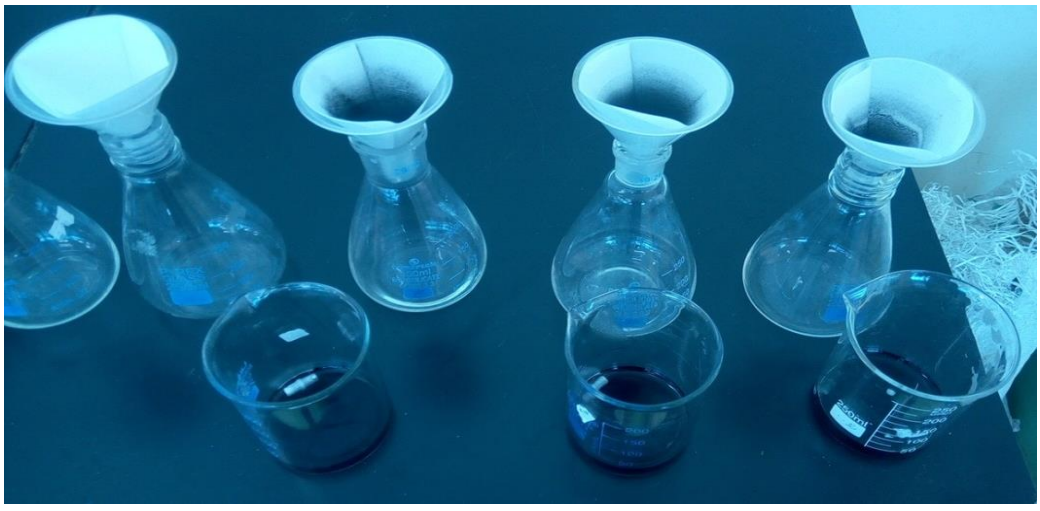

Figure 7.11: Filtration process in adsorption experiment

Figure 7.12: Working standard solution of methylene blue dye